ATTENUATION MECHANISMS FOR MOLYBDENUM IN NEUTRAL ROCK DRAINAGE

by

MICHAEL JOSEPH WILLIAM CONLAN

B.A.Sc., Queen's University, 2006

A THESIS SUBMITTED IN PARTIAL FULFILLMENT OF
THE REQUIREMENTS FOR THE DEGREE OF

MASTER OF APPLIED SCIENCE

in

THE FACULTY OF GRADUATE STUDIES

(Geological Engineering)

THE UNIVERSITY OF BRITISH COLUMBIA

(Vancouver)

May 2009

Abstract

Solubility controls and adsorption of molybdate (MoO_4) were studied to better understand the fate of molybdenum (Mo) in neutral rock drainage. Batch and column experiments predict that MoO_4 mobility is limited by powellite ($CaMoO_4$) and wulfenite ($PbMoO_4$) precipitation under neutral pH conditions and that adsorption of molybdate is relatively limited. Batch experiments demonstrate that wulfenite forms almost immediately and effectively removes Pb and Mo from solution to concentrations below detection limits whereas powellite formation is kinetically limited and reduces Mo concentrations to ~10 mg L^{-1} in systems containing Ca. An initial inhibition of powellite formation is observed, likely due to a lack of available nucleation sites. After the nucleation phase, powellite formation from supersaturated conditions follows a second order rate expression with linear dependence on Ca^{2+} and MoO_4^{2-}. Column experiments provide further evidence of rapid wulfenite formation and kinetically limited powellite formation. Both powellite and wulfenite have also been identified in samples extracted from barrel-sized field experiments designed to study the weathering of carbonate-rich waste rock material, providing direct evidence that these minerals contribute to controlling Mo mobility under field conditions. In contrast to Pb and Ca, both Cu and Zn did not form molybdate precipitates, even under highly supersaturated conditions as predicted by PHREEQC. Additional experiments indicate that Mo attenuation by adsorption under neutral pH conditions is limited and is dependent on the amount of available sorption sites. Desorption experiments on existing waste rock indicate that some Mo has likely been adsorbed to iron hydroxides, but further analyses are required to determine the extent.

Table of Contents

List of Tables

List of Figures

Acknowledgements

I would like to offer my greatest thanks to my advisors Dr. Uli Mayer and Dr. Roger Beckie for the help and support they provided during my degree. Their encouragement and knowledge allowed me to progress at my greatest abilities. The thoughts and ideas of Dr. Leslie Smith were also abundantly helpful throughout my research. I would also like to thank my colleagues, specifically Katie Jones and Scot Ellis, who answered an endless amount of my questions and kept me sane when times were hard. The help in analyses by lab technicians Maureen Soon, Randy Blaskovich, and Jenny Lai was extremely helpful and made the research run smoothly.

The financial support provided by NSERC with a Postgraduate Scholarship (PGS-M) was greatly appreciated. Extra support provided by the Egil H. Lorntzsen Scholarship through Earth and Ocean Sciences was also incredibly helpful. Grants and support towards the research by NSERC, Antamina, and Teck Ltd. were essential in performing the research.

I would especially like to thank my parents and sister for their constant help and support throughout my years of education. I would never have reached this stage without them.

Dedication

This thesis is dedicated to the numerous people that have helped me reach this stage, including my family and friends that have offered nothing but help, encouragement, and support from around the world. Specifically, this thesis is dedicated to my Mom and Dad, Dr. Kathy Conlan and Glenn Conlan, who have been my role models ever since I can remember. They have both shaped who I am, being a research scientist and a civil engineer, and I am eternally grateful for their help with homework, papers, and life in general, which has brought me to where I am today.

Co-Authorship Statement

A version of Chapter 2 will be submitted for publication. This project was initiated by Dr. Ulrich Mayer and Dr. Roger Beckie as part of a larger project analyzing the potential for metal release from waste rock piles at the Antamina mine in Peru. The research approach was developed by Michael Conlan under the guidance of Dr. Mayer and Dr. Beckie. The laboratory research was independently carried out by M. Conlan. Data analyses were also conducted by M. Conlan with the aid of Dr. Mayer and Dr. Beckie; Dr. Mayer aided especially with the modelling of the data. Randy Blaskovich completed mineral liberation analyses on samples from existing field cells containing waste rock. These data are included in Chapter 2. The manuscript was created and edited by M. Conlan under the guidance of Dr. Mayer and Dr. Beckie. A version of Chapter 3 will also be submitted for publication. Similar to Chapter 2, M. Conlan conducted the work independently under the guidance of Dr. Mayer and Dr. Beckie. Through all stages of the research, Dr. Mayer and Dr. Beckie provided helpful discussions that shaped the project.

Chapter 1 – Introduction

1.1 Problem Description

Many previous water quality studies at mine sites have focused on acid rock drainage (ARD) but fewer investigations have studied neutral rock drainage (NRD). NRD will occur if the mine waste provides a significant pH-buffering capacity from calcareous rocks. Although some metals of environmental concern are mobile under these conditions, NRD has received much less attention in the past. The Antamina Mine in Peru is one of the largest mines in the world that has neutral rock drainage, as it is hosted in limestones and marbles.

ARD originates from the discharge of acidic mine effluent that often contains elevated levels of trace metals and sulfate. The oxidation of residual sulfide minerals, such as pyrite (FeS_2), present in waste rock piles and tailings produce these acidic waters:

$$2FeS_{2(s)} + 7O_2 + 2H_2O \rightarrow 4SO_4^{2-} + 2Fe^{2+} + 4H^+ \quad (1.1)$$

Further acidic conditions are created with the oxidation of ferrous iron (Fe^{2+}) to ferric iron (Fe^{3+}), as follows:

$$4Fe^{2+} + O_2 + 10H_2O \rightarrow 4Fe(OH)_{3(s)} + 8H^+ \quad (1.2)$$

However, the majority of waste rock present at Antamina consists of carbonate minerals, which buffer the generated acid:

$$CaCO_3 + H^+ \rightarrow HCO_3^- + Ca^{2+} \quad (1.3)$$

The generalized conditions of neutral rock drainage are therefore groundwaters with near-neutral to slightly basic pH and high sulfate, calcium, and bicarbonate concentrations.

Dissolved metal concentrations differ quite greatly between ARD and NRD, as their mobility is highly dependent on pH. For most metals, attenuation processes such as precipitation and adsorption occur under neutral pH conditions, leading to sequestration of the metals within the mine waste and minimizing the need for long-term water treatment for these constituents. This is because they remain as positively charged cations and will attach readily to OH^- groups on available sorption sites or will form insoluble minerals. Metals present as oxyanions on the other hand will remain fairly

soluble. This provides a problem for molybdenum (Mo), as it is present in drainage waters as molybdate (MoO_4^{2-}).

Mo is the third most abundant metal being mined at Antamina after copper and zinc. Mo is present in the ore and waste rock as the mineral molybdenite (MoS_2), which is unstable under atmospheric conditions and will undergo oxidative dissolution, similar to pyrite. Oxidation occurs more readily with increasing pH of the groundwater (Usataya, 1952; Salminen, 2005). The dissolution of molybdenite to form aqueous molybdate is as follows:

$$2MoS_2 + 9O_2 + 6H_2O \rightarrow 2MoO_4^{2-} + 4SO_4^{2-} + 12H^+ \qquad (1.4)$$

Mo is a required micronutrient for plants and animals (Goldberg et al., 2002) and Mo deficiencies are commonly seen within agricultural soils. At high concentrations, Mo is toxic since it leads to secondary Cu deficiency (Gustafsson, 2003). It also accumulates within plants which ultimately affects grazing animals. Typical Mo levels in the natural environment can be seen in Table 1.1. Existing Canadian environmental water quality guidelines are in place for Mo with respect to aquatic life, agriculture, and soils, of 73 μg L^{-1}, 10-500 μg L^{-1}, and 5-40 ppm, respectively (Canadian Environmental Quality Guidelines, 2002).

The chemistry of Mo has been studied extensively but its environmental fate has not received the same attention (Carroll et al., 2006). Recently, work has been conducted within agricultural soils to determine transport mechanisms in this medium. Limited research of Mo attenuation by precipitation and sorption has been conducted under neutral drainage conditions, and studies within mining waste rock have not been performed. It is therefore important to analyze the potential attenuation mechanisms of Mo to understand its environmental fate in waste rock piles at Antamina.

1.1.1 Research at Antamina

The research in this thesis is a component of a larger project to examine the physical and geochemical processes that control neutral rock drainage from waste rock at Antamina and other similar mine sites. Compared to ARD, there has been relatively little research about NRD, because many metals are relatively immobile under neutral pH conditions. However, some other elements, in particular Mo and As, which are present as

oxyanions, are only weakly attenuated. To understand the long-term fate of such metals within groundwater drainage from waste rock piles at Antamina, extensive research is being conducted both at the field-scale and in a laboratory setting.

Scaled-down instrumented waste rock piles and an extensive array of field cells have been constructed and are being analyzed to determine the potential for metal release from the full-scale waste rock piles (~400 m high). The field cells are open-topped barrels exposed to the atmosphere and contain different types of waste rock. Natural precipitation passes through the waste rock in the barrels and is collected at the bottom. The volume of the drainage water and the geochemical parameters of the effluent are then analyzed. In addition, five experimental waste rock piles (36 m x 36 m x 11 m high) have been constructed to investigate weathering processes affected by physical and geochemical heterogeneities similar to those found in the full scale piles. Each experimental pile contains various types of waste rock, with different percentages of non-reactive and reactive waste rock. Both flow and geochemical parameters are being analyzed within the test piles using an extensive array of in-situ sensors and monitoring equipment. These experiments are suitable to evaluate the potential for metal release and mass loadings under field conditions; however, the mineralogical heterogeneity of the natural waste rock and uncertainties about flow paths through the piles and field cells make it difficult to study the geochemical processes that control Mo mobility in the field. On the other hand, laboratory experiments using either pure-phase materials or carefully characterized waste rock samples from Antamina are most suited for the detailed analyses of such processes.

Laboratory tests are therefore being conducted to analyze the processes controlling dissolved metal concentrations. The research conducted in this thesis specifically addresses molybdenum with an emphasis on understanding the likely attenuation mechanisms that will control aqueous Mo concentrations within the waste rock piles of Antamina.

1.2 Objectives

It will be imperative to understand the mobility and attenuation of Mo within the waste rock piles at Antamina to gauge the potential for future Mo-release and long-term water treatment requirements. Possible attenuation mechanisms such as precipitation and sorption were therefore studied in a laboratory setting to answer the following research questions:

- Is powellite ($CaMoO_4$) precipitation a significant sink for Mo released from waste rock at Antamina? Will competing ions or changing environmental conditions affect Mo removal by powellite? Can powellite formation be adequately modeled?
- What other secondary Mo precipitates are likely to form? If Mo-rich, Cu-rich, Pb-rich, and Zn-rich waste rock is mixed, will precipitates such as wulfenite ($PbMoO_4$), copper molybdate ($CuMoO_4$), or zinc molybdate ($ZnMoO_4$) form? Will Cu, Zn, and Pb preferentially form with other anions, inhibiting MoO_4^{2-} attenuation?
- Will iron molybdate ($FeMoO_4$) be precipitate within the waste rock pile? Are ferrous iron concentrations high enough, or are conditions too oxidizing?
- Is Mo currently being adsorbed onto waste rock? Which material within the waste rock will adsorb Mo most strongly and to what extent?

1.3 Site Description

The Compañia Minera Antamina (CMA) Co-Zn-Mo mine is an open-pit operation that began extraction in 2001. The mine processes between 70 000 and 100 000 tonnes of ore per day and generates about 300 000 tonnes of waste rock daily (Golder, 2007). The majority of this waste rock is placed in waste rock piles on-site that are exposed to the natural environment. Some of the waste rock contains elevated levels of Co, Zn, Mo, Pb, and Bi which could prove to be detrimental to the surrounding environment - if released and not treated adequately. As previously discussed, Mo specifically has a high

potential to be mobilized due to its abundance in the waste rock and the neutral drainage characteristics.

1.3.1 Location

Antamina is located within the Peruvian Andes, approximately 385 km north of Lima and 50 km east of Huaraz (Figure 1.1). The mine is at an elevation between approximately 4200 and 4800 metres above sea level (Lipten, 2003). The mine is currently expected to be in operation until 2021 (Golder, 2007).

1.3.2 Geological Setting

Antamina is located within the eastern portion of the Western Cordillera in the Peruvian Andes. It is a polymetallic skarn deposit hosted in a sequence of limestones and other sediments (Lipten, 2003). It sits at the base of a glacial valley and is surrounded by ridges of limestone that have been strongly folded and thrusted within the Late Eocene (Figure 1.2).

Mo is the third most abundant ore metal within the deposit after Cu and Zn. It is present within the quartz monzonite intrusive core as molybdenite (MoS_2) as well as in endoskarn material surrounding the core (Lipten, 2003) (Figure 1.3). Trace Mo is also found in indeterminate skarn (transition between endoskarn and exoskarn). Mo reaches concentrations of about 0.03 wt% of the quartz monzonite and skarns, but concentrations vary between the differing types of skarn (e.g. white plagioclase endoskarn, pink garnet endoskarn, brown garnet endoskarn). Most of this material is considered ore; however, some of this rock contains Mo and other metals at uneconomic concentrations, which makes it unsuitable for mineral processing. This material ends up in the waste rock piles, where it provides a substantial source for metal release.

1.3.3 Environmental Setting

Antamina experiences similar conditions as most Andean regions. There are two distinct seasons: the summer which is the wet season and winter which is the dry season. The dry season lasts from April to October, when cool temperatures dominate and lesser amounts of precipitation occur. The wet season between November and March is when

the majority of precipitation occurs; annual precipitation falls within a range of 1200 to 1500 mm (Evans et al., 2005). The ample rainfall provides sufficient recharge to promote leaching of metals from the mine waste deposits

1.3.4 Geochemistry

1.3.4.1 Field Cells

Studies performed by Golder Associates (Golder, 2004; Golder, 2007) have been designed to provide information on the chemical composition of the drainage waters expected to leave the waste rock piles. Field cells each containing specific waste rock material in order to determine leachate concentrations with time have been constructed. The field cells are constructed of 205 L drums filled with waste rock and left open to atmosphere and precipitation so that natural weathering can occur. As of 2007, 47 different rock types were being analyzed, which includes waste rock, low grade ore, medium grade ore, and tailings material at Antamina.

The results of the experiments by Golder (2007) show that the composition of the drainage water is strongly dependent on the waste rock type (Table 1.2). Observed concentrations in drainage waters were used to determine elemental concentrations for the laboratory experiments conducted as part of the present study in order to simulate the waste rock piles as closely as possible. It should, however, be noted that many of the parameters within the field cells have not yet stabilized, adding to the difficulties of predicting metal release from waste rock piles. Even once concentrations have stabilized it is unlikely that these concentrations will correspond to the maximum outflow concentrations from the waste rock piles. Field cell tests focus on a single material and do not account for mixing of different materials within the full scale piles. In addition, the field cells are only about 1 m tall whereas the waste rock piles are approximately 400 m high. The scale difference implies additional physical heterogeneity in the full scale piles and activation of other processes that are not captured in the field cells.

Molybdenum concentrations vary by a large amount depending on the waste rock type. Concentrations in less reactive materials (hornfels, marble, limestone) are quite low, mainly being below instrument detection limits. This is expected, as molybdenite is not commonly found within these rock types. The highest concentrations are found

within the endoskarn, intrusives, and low and medium grade ore field cells. The concentrations in field cell leachate range from 7.3 to 45 mg L^{-1} and each of these cells contain a relatively large amount of molybdenite. Alkalinity in drainage from the field cells have remained between 20 and 70 mg L^{-1} as $CaCO_3$ indicating the strong buffering capacity of the waste rock. pH-values are therefore quite high, being near-neutral to slightly basic for all field cells.

1.3.4.2 Solubility Controls

Based on mineralogy and elemental release from weathering, waters passing through the waste rock pile should be saturated with respect to $CaCO_3$ and also contain elevated levels of Na, Al, Si, Mg, Fe, SO_4, F, and Cl. Other prominent dissolved elements should include Cu, Zn, Mo, Pb, Ag, and Bi, based on their abundance in the ore material. However, secondary mineral phases can act as controls for dissolved constituents. Speciation modeling was therefore conducted by Golder (2007) to determine solubility controls. The solubility controls determined were boehmite/gibbsite ($Al(OH)_3$), calcite ($CaCO_3$), fluorite (CaF_2), gypsum ($CaSO_4 \cdot H_2O$), ferrihydrite ($Fe(OH)_3$), manganite (MnOOH), and malachite ($Cu_2(OH)_2CO_3$).

Both malachite and ferrihydrite are important solubility controls for this research. With malachite expected to control Cu concentrations, it is questionable whether a Cu-molybdate will form. Ferrihydrite is also important, as it can provide suitable surface area for sorption of Mo and other metals.

1.4 Literature Review

There has been a thorough investigation of the chemistry of Mo and Mo sorption within the literature, but few studies have researched Mo precipitates under neutral pH conditions. This literature review encompasses the prominent aspects of Mo attenuation investigated within this thesis, including precipitation and sorption.

1.4.1 Mo Release

In the natural environment, Mo is usually found as either Mo(IV) or Mo(VI) (Fox and Doner, 2002). Mo release under neutral and basic conditions is more prominent than under acidic conditions (Salminen, 2005). With neutral or basic conditions, molybdenite (MoS_2) is weathered and oxidized, mobilizing Mo. In acidic environments, molybdenite is stable or Mo in solution is immobilized by precipitation of iron molybdate. Under neutral conditions, Mo is expected to be released into solution, where the oxidation of molybdenite to form molybdate oxyanions occurs (Bostick et al., 2003). MoO_4^{2-} oxyanions predominate in solutions having pH values above 4 (Burclová et al., 1973; Carroll et al., 2006). Mo stability diagrams can be found in Figure 1.4.

1.4.2 Mo Precipitation

Aqueous ion interactions for 2:2 electrolytes are strong, providing belief that many metal molybdates should precipitate with Mo in solution (Felmy et al., 1992). However, specific metal molybdates have not been studied extensively meaning there is little information to determine how prominent they may be within different geochemical conditions. The two most likely precipitates to form at Antamina include powellite ($CaMoO_4$) and wulfenite ($PbMoO_4$), but other metal molybdates such as Fe, Cu, and Zn molybdates may form.

1.4.2.1 Powellite

Calcium can react with molybdate to form the mineral precipitate powellite, although it is moderately soluble under most conditions, with literature log K_{sp}'s ranging from -7.02 to -8.51 (Essington, 1990). Felmy et al. (1992) conducted research for a better understanding of powellite formation and dissolution and determined the log K_{sp} of powellite to be –7.93. However, the log K_{sp} of -8.05 found by Essington (1990) has been used most frequently within literature. Studies have predicted that powellite is the controlling phase for Mo within alkaline waste materials (Essington, 1992; Meima et al., 2002). Few other studies on powellite have been conducted, and none is associated with mine drainage.

1.4.2.2 Wulfenite

The formation of wulfenite could be a sink for Mo if aqueous Pb is available, as it is one of the most stable Mo minerals (Vlek and Lindsay, 1977). Previous modeling has shown wulfenite as being supersaturated within waters containing Mo and Pb. Wang et al. (1994) determined that wulfenite is likely controlling Mo in coal overburden, with both powellite and Fe-molybdate being undersaturated. Vlek and Lindsay (1977) found that one of thirteen soils was in equilibrium with wulfenite, with pH values ranging from 5.5 to 7.7. Reddy and Gloss (1993) found that wulfenite is expected to control Mo solubility in alkaline soils. Wulfenite is also expected to be the controlling phase for Mo at existing mining sites (Rosemeyer, 1990; Bideaux, 1990). Petrunic et al. (2006) found wulfenite within mine tailings with evidence suggesting that it precipitated out of local pore-water after the oxidation of molybdenite.

1.4.2.3 Other Molybdates

In reducing conditions, relatively insoluble ferrous molybdate ($FeMoO_4$) can form with an abundance of iron in solution (Branam, 1999). Iron scavenges Mo in these conditions and therefore acts as a control of Mo solution concentrations. Oxidizing conditions are expected within the waste rock piles, making this an unlikely sink for Mo. Ferrimolybdite ($Fe(III)_2(MoO_4)_3 \cdot 8H_2O$) is a secondary mineral associated with hydrothermal veins and molybdenum porphyry deposits (Mineral Data Publishing, 2005) and has previously been identified as a possible Mo sink downstream of mine tailings (Langedal, 1997). Co-precipitation of Mo with iron sulfide in anoxic conditions has also been identified (Bertine, 1972).

Thermodynamic data is present for both Zn and Cu molybdates, but no research was found on their occurrences in the natural environment. The potential for precipitation of these phases was analyzed within this research to further understand the role of these phases as a sink for Mo and metals.

1.4.3 Mo Sorption

The geochemical composition of groundwater plays a significant role on how much MoO_4^{2-} will be adsorbed (Stollenwerk, 1995). With many competing ions in

solution, attenuation of Mo will be less due to the other species preferentially filling the adsorption sites. Previous Mo sorption studies have focused heavily on adsorption onto Al and Fe oxides, clays, and different soil types (Xie and MacKenzie, 1991; Peinemann and Helmy, 1994; Goldberg et al., 1996), onto pyrite (Bostick et al., 2003), pyrite and goethite (FeO(OH)) (Xu et al., 2006), and anatase (TiO_2) (Saripalli, 2002). The potential sorption sites at Antamina include hydrous ferric oxides (HFO), calcite, pyrite, and any overburden soils present in the waste rock.

1.4.3.1 Adsorption on Hydrous Ferric Oxides (HFO)

Goldberg et al. (1996) determined that iron oxides adsorbed Mo and the maximum occurred within acidic pH conditions up to about pH 4 to 5. Above this limit, adsorption decreased rapidly with little occurring above pH 8. Examples of adsorption envelopes can be seen in Figure 1.5. It is thought that the mechanism of sorption is the formation of inner-sphere complexes (ligand exchange). However, this may switch to outer-sphere complexes as pH increases. Gustafsson (2003) also created batch systems to determine Mo adsorption to HFO's and found similar results to Goldberg et al. (1996).

1.4.3.2 Adsorption on Calcite

Calcite and calcareous arid-zone soil adsorption was analyzed by Goldberg et al. (1996), and results showed that $CaCO_3$ is not a major sink for Mo within soils. Fox and Doner (2002) also conducted experiments and found Mo sorption on calcite to be low.

1.4.3.3 Adsorption on Pyrite and Goethite

Molybdate sorption onto pyrite occurs mainly at lower pH levels and decreases above pH 5 (Bostick et al., 2003). When increasing pH after sorption occurred in acidic conditions, molybdate readily desorbed, indicating that it likely forms weak surface complexes. Results from Bostick et al. (2003) show that MoO_4^{2-} forms a labile bidentate, mononuclear complex on pyrite.

Molybdate sorption on goethite is higher than on pyrite, but otherwise follows similar trends (Xu et al., 2006). Significant amounts can be accumulated on goethite over

months to years (Fox and Doner, 2002). This could be important, as goethite is typically a weathering product of pyrite within waste rock (Dalton et al., 2000).

1.4.3.4 Adsorption in Alkaline Soils

Research performed by Carroll et al. (2006) shows that Mo sorption within alkaline soils is fairly low and is linear with respect to aqueous Mo concentrations. However, by generating breakthrough curves, it was found that rate-limited sorption influenced the transport of Mo. The sorption was also reversible, but attenuation mechanisms were not determined. The addition of organic matter retarded Mo transport by a factor of two, indicating its importance.

1.4.4 Comparison of Attenuation Mechanisms

With precipitation and sorption being the two most likely attenuation mechanisms for Mo at Antamina, an evaluation of the two processes is required. The geochemical characteristics of the waste rock piles indicate that sorption may not be a prominent sink for Mo, since sorption within neutral pH is not strong. The likeliest sorption sites are HFO's, which are not markedly abundant in some of the waste rock types but will likely form as a result of sulfide mineral oxidation. Molybdate precipitates are more likely to form, but depend on aqueous Mo concentrations and the availability of cations in solution. For low concentrations, precipitation may not affect dissolved Mo concentrations significantly due to thermodynamic constraints. In this case, sorption may be a more important process, even though sorption is expected to be relatively limited. However, as concentrations increase, precipitation will likely occur as the solution becomes supersaturated with respect to metal molybdates. These precipitates could prove to be the dominant sink for Mo in waste rock piles.

1.4.5 Experimental Methods

1.4.5.1 Precipitation Batch Experiments

Aoun et al. (1998) performed a review of the literature on precipitation batch experiments and indicated that many of the methods used to determine nucleation and growth rates are inaccurate. They concluded that a stirred system is preferential when

performing precipitation experiments and that the stirring speed does not significantly affect crystallization times. They performed experiments in a single tank rather than a flowthrough reactor, which is another potential batch method. Yang and Steefel (2007) used a stirred flowthrough reactor to analyze kaolinite precipitation and Cubillas et al. (2005) used a mixed flow-reactor to analyze calcite-$CdCO_3$ exchange. Numerous researchers have used a stirred batch system as used by Aoun et al. (Wong et al., 2001; Stanley et al., 2004; Schöll et al., 2006). The current study employs both stirred and unstirred batch reactors.

1.4.5.2 Sorption Experiments

Adsorption and desorption experiments have both been described in the literature. Adsorption batch experiments have been conducted by adding adsorbent and a known amount of Mo solution to vials that were subsequently shaken or centrifuged for some time (Burclová et al., 1973; Zhang and Sparks, 1989; Peinemann and Helmy, 1993; Goldberg et al., 1996; Saripalli et al., 2002; Xu et al., 2005; Carroll et al., 2006). pH of the solutions were typically modified using NaOH.

Desorption batch experiments are performed in the same manner but using a clean solution such as DI water to determine whether the sorption is reversible or not (Peinemann and Helmy, 1993). DI water extraction is a leaching method often used to analyze loosely bonded material on grains (Kelley et al., 2003). A known amount of DI water is added to the material being analyzed and shaken for some time (often 24 hours) and subsequently centrifuged and analyzed for its chemistry.

A novel technique of an ascorbic extraction to analyze Fe concentrations has recently been applied (Amirbahman et al., 1998; Hyacinthe and Cappellen, 2004; Hyacinthe et al., 2005). Typical extraction techniques are acidic and will therefore dissolve highly soluble phases, such as calcite. This may increase background levels dramatically and will make it impossible to determine whether species are adsorbed onto the material or included in the soluble minerals. Ascorbic extraction is a reductive technique under basic pH conditions, therefore reducing iron and making it a soluble phase yet not dissolving other mineral phases (Roychoudhury, 2006). Sediment is added to an anaerobic solution of ascorbic acid, sodium citrate, and sodium bicarbonate.

Suspensions are subsequently stirred or shaken for 24 hours and then filtered and analyzed for the solution chemistry. Any dissolved material is therefore expected to be from adsorbed species onto iron hydroxides.

1.4.5.3 Column Experiments

Column experiments are typically conducted in order to determine attenuation behaviour under active flow conditions that are more representative of the field. Stollenwerk (1995) conducted column experiments to determine MoO_4^{2-} adsorption onto an aquifer material. 30 cm long columns with a diameter of 2.5 cm were filled with sediment with a size fraction of less than 2 mm. A peristaltic pump was used to pass water through the system at a similar rate as the velocity of groundwater in the aquifer. Prior to the addition of MoO_4^{2-}, uncontaminated groundwater from the field was passed through the system until uniform conditions were reached throughout the column. Groundwater containing known quantities of MoO_4^{2-} was then passed through the system until breakthrough. At this point, uncontaminated groundwater was passed through the column again to assess desorption. The amount of adsorption and desorption was calculated by the difference between influent and effluent concentrations.

1.5 Approach and Experimental Setup

Previous research indicates that Mo attenuation under neutral pH conditions will likely be dominated by precipitation reactions, with a lesser contribution of adsorption. Both powellite and wulfenite are proven sinks for Mo at other mine sites (Rosemeyer, 1990; Bideaux, 1990; Petrunic et al., 2006), but further research is required to determine the importance of these phases in NRD systems. It was therefore decided that experiments would be focus on understanding the likelihood of such precipitate formation under conditions similar to those found at Antamina. Other metal molybdates were also targeted to determine if there are additional solubility controls for Mo in the presence of metals such as Cu and Zn that are typically released by the weathering of waste rock. Some sorption experiments were also conducted, but to a much lesser extent than experiments focusing on precipitate formation, due to the extensive research already

conducted on Mo sorption. Sorption experiments were conducted using existing Antamina waste rock, including both adsorption and desorption investigations.

Initially, batch experiments were conducted due to the comparable ease of experimental design and data interpretation. Varying the elemental constituents and geochemical characteristics allow for an understanding of potential sinks. However, batch systems do not effectively simulate field conditions, requiring column experiments to further understand the potential of Mo attenuation. Modeling of the data also aided in understanding aqueous Mo by providing rates of Mo removal that could be extrapolated to the field-scale.

The aqueous solutions for the batch and column experiments were designed based on the observed drainage water compositions from the field cells (Golder, 2007). A Mo concentration of 200 mg L^{-1} was selected for the batch and column experiments performed assuming Mo concentrations may be elevated in field-scale waste rock piles compared to the field cells. The buffering capacity was simulated in most laboratory experiments by including excess calcium carbonate powder to buffer any acid generation. SO_4 concentrations of 1000 mg L^{-1} were used in most of the batch and column experiments, similar to the maximum concentrations observed in the field cells. 20 mg L^{-1} of Cu, Zn, and Pb were used for the competition experiments. Although field-observed concentrations of these metals were lower, these somewhat elevated concentrations were required to identify and quantify attenuation processes in the experiments.

Figure 1.1 – Location of Antamina mine

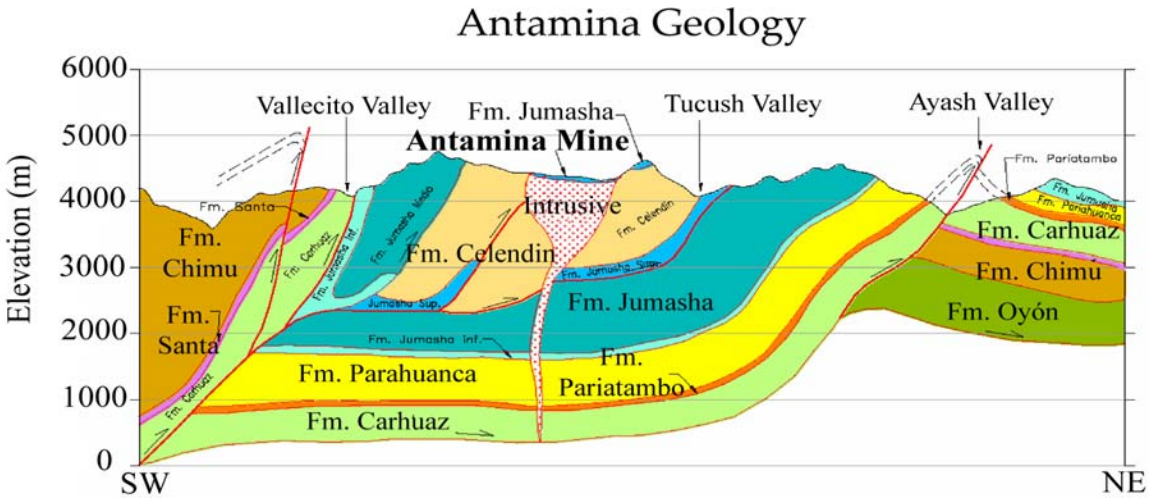

Figure 1.2 – Cross section of the geology at Antamina (modified from Lipten, 2003)

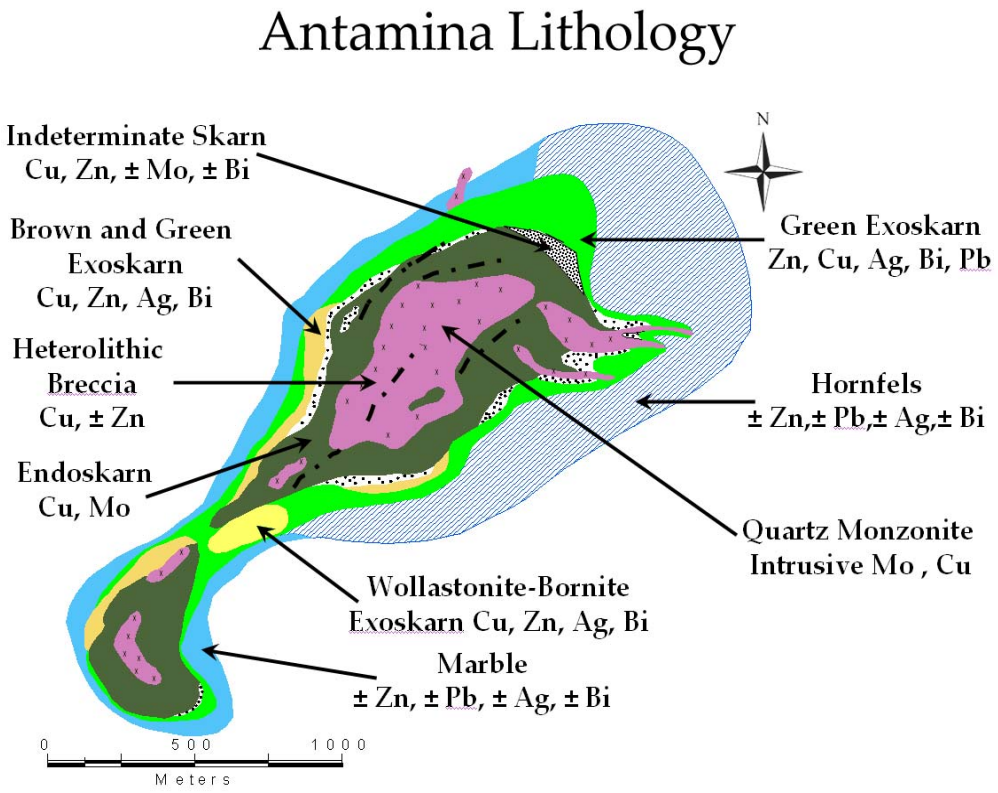

Figure 1.3 – Ore types of Antamina (modified from Lipten, 2003)

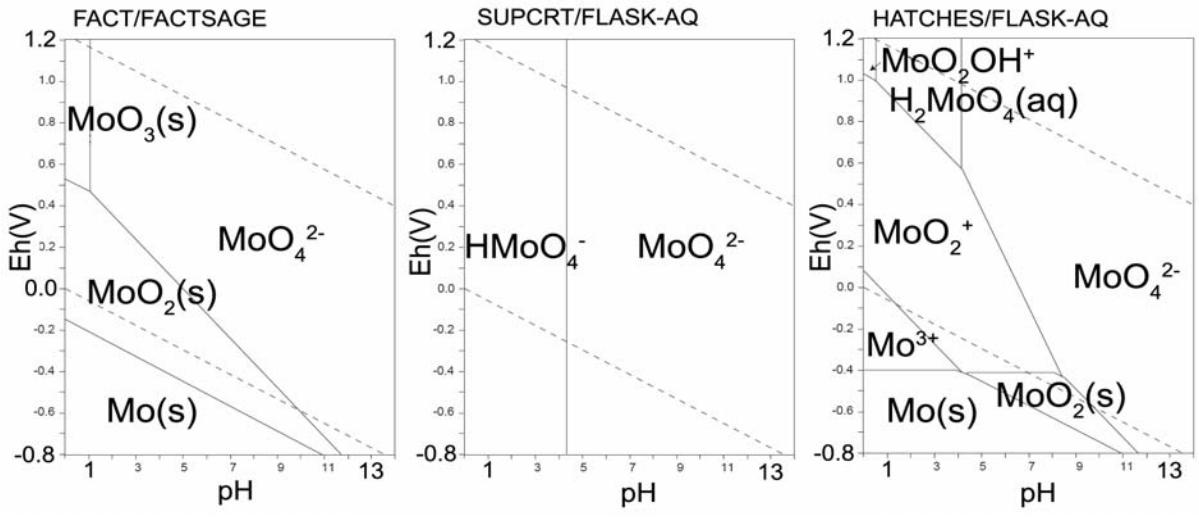

Figure 1.4 – Mo stability diagrams using different thermodynamic databases (modified from Takeno, 2005)

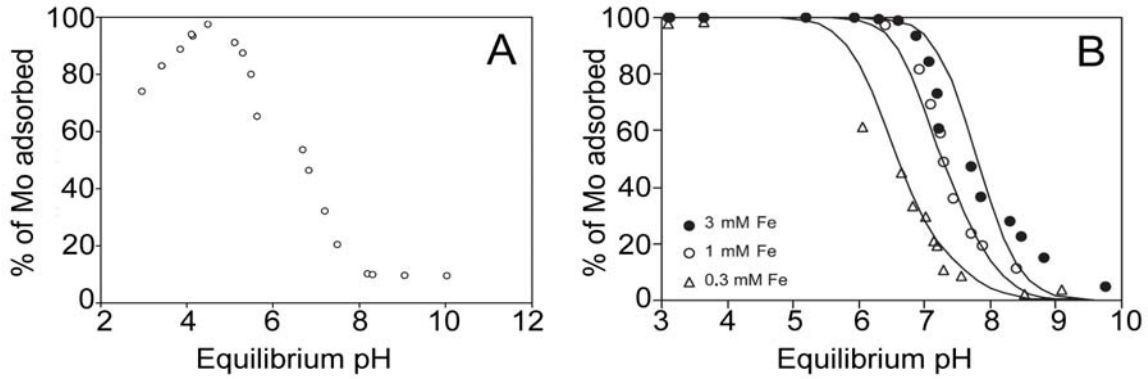

Figure 1.5 – a) MoO_4^{2-} adsorption onto pyrite. Initial Mo = 0.05 mM, Fe(II) = 2 g L^{-1}, Fe(III)=0.3 g L^{-1}, electrolye = 0.1 M NaCl (modified from Xu et al., 2006). **b)** Adsorption of 0.05 mM of molybdate to ferrihydrite. Lines are model fits of the Diffuse Layer Model (DLM) (modified from Gustafsson, 2003)

Table 1.1 – Mo concentrations within rocks (ppm) and water (μg L^{-1}) (Drever, 1997)

Granite	Basalt	Shale	Sandstone	Limestone	Streams	Ocean
1	1.5	2.6	0.2	0.4	0.5	10

Table 1.2 – Field cell results from Golder (2007). All concentrations in mg L^{-1}, except pH

	Hornfels, marble, Limestone	Intrusive, Endoskarn, Exoskarn	Low and Medium Grade ore
Zn	0.002 - 0.2	0.06-3	0.06-8.2
Cu	<0.01	0.01-0.03	0.01-0.04
Mo	<0.01-0.3	0.01-41	0.03-45
As	<0.06-3	0.006-0.4	0.001-0.02
SO_4	<500	<1000	<500-1000
pH	8-8.5	7.1-8.9	7.5-8.5

1.6 References

Amirbahman, A., Schönenberger, R., Johnson, C.A., Sigg, L., 1998. Aqueous- and solid-phase biogeochemistry of a calcareous aquifer system downgradient from a municipal solid waste landfill (Winterthur, Switzerland). Environmental Science and Technology 32, 1933-1940.

Antamina Mine Geology Logging Manual, 2000. Draft Version 1.53: Antamina Mine Geology Logging Manual and Coding Instructions. Antamina, Peru.

Aoun, M., Plasari, E., David, R., Villermaux, J., 1999. A simultaneous determination of nucleation and growth rates from batch spontaneous precipitation. Chemical Engineering Science 54, 1161-1180.

Aubé, B., 2004. The Science of Treating Acid Mine Drainage and Smelter Effluents. EnvirAubé Technical Report, Ste-Anne-de-Bellevue, QC.

Bertine, K.K., 1972. The Deposition of Molybdenum in Anoxic Waters. Marine Chemistry 1, 43-53.

Bideaux, R.A., 1990. The desert mineral: Wuifenite. Rocks and Minerals 65, 11-30.

Bostick, B.C., Fendorf, S., Helz, G.R., 2003. Differential Adsorption of Molybdate and Tetrathiomolybdate on Pyrite (FeS_2). Environmental Science and Technology 37(2), 285-291.

Branam, T.D., Smith, R.T., Ennis, M.V., Rybarczyk, J.P., Comer, J.B., 1999. Trace Element Partitioning in Ground Water at an Abandoned Mine-Land Site Reclaimed with Coal Combustion Products. 1999 International Ash Utilization Symposium, University of Kentucky, Paper 68.

Burclová, J., Prášilová, J., Beneš, P., 1973. The State and Adsorption Behaviour of Traces of Molybdenum(VI) in Aqueous Solutions. Journal of Inorganic and Nuclear Chemistry 35, 909-919.

Canadian Environmental Quality Guidelines, 2002. Summary Table of Existing Canadian Environmental Quality Guidelines. Environment Canada.

Carroll, K.C., Artiola, J.F., Brusseau, M.L., 2006. Transport of Molybdenum in a Biosolid-Amended Alkaline Soil. Chemosphere Article In Press.

Cubillas, P., Köhler, S., Prieto, M., Causserand, C., Oelkers, E.H., 2005. How do mineral coatings affect dissolution rates? An experimental study of coupled CaCO3 dissolution—CdCO3 precipitation. Geochimica et Cosmochimica Act 69(23), 5459-5476.

Dalton, J.B., King, T.V.V., Bove, D.J., Kokaly, R.F., Clark, R.N., Vance, J.S., Swayze, G.A., 2000. Distribution of Acid-Generating and Acid-Buffering Minerals in the Animas River Watershed as Determined by AVIRIS Spectroscopy. U.S. Geological Survey, Denver, CO.

Drever, J.I., 1997. The Geochemistry of Natural Waters: Surface and Groundwater Environments. 3rd Edition. Prentice Hall, Upper Saddle River, NJ.

Essington, M.E., 1990. Calcium Molybdate Solubility in Spent Oil Shale and a Preliminary Evaluation of the Association Constants for the Formation of $CaMoO4^0$(aq), $KMoO_4^-$(aq), and $NaMoO_4^-$(aq). Environmental Science and Technology 24(2), 214-220.

Evans, D., Letient, H., Aley, T., 2005. Aquifer Vulnerability Mapping in Karstic Terrain at Antamina Mine, Peru. Robertson GeoConsultants Inc. Technical Report, Vancouver, BC.

Felmy, A.R., Rai, D., Mason, M.J., 1992. The Solubility of $CaMoO_4$(c) and an Aqueous Thermodynamic Model for Ca^{2+}-MoO_4^{2-} Ion-Interactions. Journal of Solution Chemistry 21, 525-532.

Fox, P.M., Doner, H.E., 2002. Trace Element Retention and Release on Minerals and Soil in a Constructed Wetland. Journal of Environmental Quality 31, 331-338.

Goldberg, S., Forster, H.S., Godfrey, C.L., 1996. Molybdenum Adsorption on Oxides, Clay Minerals, and Soils. Soil Science Society of America Journal 60(2), 425-432.

Goldberg S., Lesch, S.M., Suarez, D.L., 2002. Predicting Molybdenum Adsorption by Soils Using Soils Using Soil Chemical Parameters in the Constant Capacitance Model. Soil Science Society of America Journal 66, 1836-1842.

Golder Associates Ltd, 2004. Final Version 4.0, Waste Rock Geochemistry – Phase 2, Antamina Mine Peru. Mississauga, ON.

Golder Associates Ltd, 2007. Final Version 4.0, Waste rock and tailings geochemistry – field cell monitoring 2002 to 2006, Antamina Mine Peru. Mississauga, ON.

Gustafsson, J.P., 2003. Modelling Molybdate and Tungstate Adsorption to Ferrihydrite. Chemical Geology 200, 105-115.

Hyacinthe, C., Van Cappellen, P., 2004. An authigenic iron phosphate phase in estuarine sediments: composition, formation and chemical reactivity. Marine Chemistry 91, 227-251.

Hyacinthe, C., Bonneville, S., Van Cappellen, P., 2005. Reactive iron(III) in sediments: Chemical versus microbial extractions. Geochimica et Cosmochimica Acta 70, 4166-4180.

Langedal, M., 1997. Dispersion of Tailings in the Knabeåa–Kvina Drainage Basin, Norway, 2: Mobility of Cu and Mo in Tailings-Derived Fluvial Sediments. Journal of Geochemical Exploration 58, 173-183.

Lipten, E.J., 2003. The Geology and Metal Zonation of the Antamina Deposit. Compania Minera Antamina Presentation. Antamina, Peru.

Meima, J.A., van der Weijden, R.D., Eighmy, T.T., Comans, R.N.J., 2002. Carbonation Processes in Municipal Solid Waste Incinerator Bottom Ash and their Effect on the Leaching of Copper and Molybdenum. Applied Geochemistry 17, 1503-1513.

Mineral Data Publishing, 2005. Ferrimolybdite, Version 1. AZ, U.S.A.

Peinemann N., Helmy, A.K., 1994. Molybdate Sorption by Hydroxyl-Aluminium Treated Montmorillonite. Applied Clay Science 8, 389-396.

Petrunic, B.M., Al., T.A., Weaver, L., 2006. A transmission electron microscopy analysis of secondary minerals formed in tungsten-mine tailings with an emphasis on arsenopyrite oxidation. Applied Geochemistry 21(8), 1259-1273.

Reddy, K.J., Gloss, S.P., 1993. Geochemical speciation as related to the mobility of F, Mo and Se in soil leachates. Applied Geochemistry 2 Suppl. Issue, 159-163

Rodriguez, J.A., Hanson, J.C., Chaturvedi, S., Maiti, A., Brito, J.L., 2000. Studies on the Behavior of Mixed-Metal Oxides: Structural, Electronic, and Chemical Properties of β-$FeMoO_4$. Journal of Physical Chemistry B 104, 8145-8152.

Rosemeyer, T., 1990. Wulfenite occurrences in Colorado. Rocks and Minerals 65, 58-61.

Roychoudhury, A.N., 2006. Time dependent calibration of a sediment extraction scheme. Marine Pollution Bulletin 52, 397-403.

Salminen, R., 2005. Geochemical Atlas of Europe, Part 1 - Background Information, Methodology and Maps. Geological Survey of Finland.

Saripalli, K.P., McGrail, B.P., Girvin, D.C., 2002. Adsorption of Molybdenum on to Anatase from Dilute Aqueous Solutions. Applied Geochemistry 17, 649-656.

Schöll, J., Vicum, L., Müller, M., Mazzotti, M., 2006. Precipitation of L-Glutamic Acid: determination of nucleation kinetics. Chem. Eng. Technol. 29(2), 257-264.

Smith, L., Beckie, R., 2003. Environmental Aspects of Mine Wastes, Chapter 3: Hydrologic and Geochemical Transport Processes in Mine Waste Rock. Mineralogical Association of Canada, 51-72.

Stanley, S.J., Mann, R., Primrose, K., 2005. Interrogation of a precipitation reaction by electrical resistance tomography (ERT). AIChE Journal 51(2), 607-614.

Stollenwerk, K.G., 1995. Modeling the Effects of Variable Groundwater Chemistry on Adsorption of Molybdate. Water Resources Research 31(2), 347-357.

Takeno, N., 2005. Atlas of Eh-pH diagrams: Intercomparison of thermodynamic databases. Geological Survey of Japan Open File Report No.419.

Usataya, E.S., 1952. Oxidation of Molybdenite by Water Solutions. Zapiski Vserossiiskogo Mineralogicheskogo Obshchestva 81, 298-303.

Vlek, P.L.G., Lindsay, W.L., 1977. Thermodynamic stability and solubility of molybdenum minerals in soils. Soil Science Society of America Journal 41, 42-46.

Wang, L., Reddy, K.J., Munn, L.C., 1994. Geochemical Modeling for Predicting Potential Solid Phases Controlling the Dissolved Molybdenum in Coal Overburden, Powder River Basin, WY, U.S.A. Applied Geochemistry 9, 37-43.

Wong, D.C.Y., Jaworski, Z., Nienow, A.W., 2001. Effect of ion excess on particle size and morphology during barium sulphate precipitation: an experimental study. Chemical Engineering Science 56(3), 727-734.

Xie, R.J., MacKenzie, A.F., 1991. Molybdate Sorption-Desorption in Soils Treated with Phosphate. Geoderma 48, 321-333.

Xu, N., Christodoulatos, C., Braida, W., 2006. Adsorption of Molybdate and Tetrathiomolybdate onto Pyrite and Goethite: Effect of pH and Competitive Anions. Chemosphere 62, 1726-1735.

Yang, L., Steefel, C.I., 2007. Kaolinite dissolution and precipitation kinetics at 22^{o}C and pH 4. Geochimica et Cosmochimica 72, 99-116.

Zhang, P.C., Sparks, D.L., 1989. Kinetics and mechanisms of molybdate adsorption/desorption at the goethite/water interface using pressure-jump relaxation. Soil Science Society of America Journal 53, 1028-1034.

Chapter 2 – Solubility Controls for Molybdenum in Neutral Rock Drainage[1]

2.1 Introduction

Molybdenum is a trace element present at low concentrations in the natural environment, but is also found at high concentrations in ore deposits around the world (*1*). Molybdenum is typically recovered from the sulfide mineral molybdenite (MoS_2). Residual or non-economic accumulations of MoS_2 often remain in mining waste rock or tailings and provide a long-term source for Mo release from weathering (*2*). In its oxidized form, Mo is present as the oxyanion molybdate (MoO_4^{2-}). Subsequently, Mo is effectively attenuated under acidic conditions through adsorption reactions (*3-5*) making it less of a concern at acid rock drainage (ARD) mine sites. However, Mo adsorption is ineffective at sites with neutral rock drainage (NRD) (*3, 6*) and under these conditions Mo release may pose a more significant risk to the environment. Although Mo toxicity is limited for human consumption, Mo released to groundwater and surface water can have negative effects on surrounding communities by impacting livestock and wildlife. Grazing animals are most significantly affected by Mo due to bioaccumulation (*3, 7*). Such animals may suffer from molybdenosis, a secondary Cu deficiency, which is more severe when sulfur is present (*8*). Forage Mo concentrations above 2 ppm and surface water concentrations greater than 10 μg L^{-1} have been found to cause molybdenosis in cattle around mining regions (*9, 10*).

Mo often occurs in association with other metals such as Cu, Pb, and Zn (*2*). Such conditions exist at the Antamina mine site in Peru where Cu, Zn, Pb, and Mo are extracted simultaneously (*11*). Similar to many other sites, the mineralization at Antamina occurs due to an intrusion of igneous rock into a pre-existing limestone formation, where calcite ($CaCO_3$) is present as one of the main rock-forming minerals. Under these conditions, metal molybdates ($MeMoO_4$), where Me is a divalent metal, may act as an effective sink for Mo, limiting its mobility and release. Possible secondary

[1] A version of this chapter will be submitted for publication.
Conlan, M.J.W; Mayer, K.U; Beckie, R.D.; Blaskovich, R.J. Solubility controls for molybdenum in neutral rock drainage.

molybdate phases include powellite ($CaMoO_4$), wulfenite ($PbMoO_4$), $CuMoO_4$ and $ZnMoO_4$.

Powellite solubility has been investigated (*12-15*) and is expected to be an important mineral phase controlling Mo leaching in alkaline waste materials (*16-17*). Wulfenite is one of the most stable Mo minerals (*12*), potentially limiting dissolved Mo concentrations in alkaline soils (*12, 18*); as a result wulfenite is also thought to provide a control on Mo release at existing mining sites (*19-21*). However, the Pb-bearing minerals anglesite ($PbSO_4$) and cerrusite ($PbCO_3$) often control Pb solubility (*22*) and both sulfate and carbonate are readily available at neutral drainage mine sites due to the oxidation of sulfide minerals and dissolution of carbonate minerals. Information whether $CuMoO_4$ or $ZnMoO_4$ formation provides an effective mechanism for molybdate attenuation is not available.

The objective of this study is to determine the potential for molybdate attenuation due to mineral precipitation under neutral rock drainage conditions. Specifically, this research investigates 1) which molybdate phases provide a control for Mo mobility, 2) the effectiveness of molybdate precipitation in limiting dissolved Mo concentrations, 3) the rate of molybdate removal and mineral formation, and 4) whether molybdate formation is occurring under field conditions. Batch and column experiments simulating the conditions at typical NRD mine sites such as the Antamina mine were conducted to address these objectives. Batch experiments with varying metal concentrations and calcium sources were performed to study the precipitation of powellite and other molybdates. A column experiment was conducted with differing metal inputs to simulate Mo attenuation in a NRD waste rock pile under active flow conditions. In addition, the mineralogy of samples from weathering experiments at a field site was determined using mineral liberation analysis (MLA).

2.2 Materials and Methods

2.2.1 Batch Experiments

Batch experiments were conducted to determine the potential for molybdate precipitation from solutions containing Ca (Table 1). Initial batch systems to analyze the

potential for powellite precipitation were created to simulate conditions expected within the waste rock piles, including Mo, SO_4, and calcite. 200 mg L^{-1} Mo solutions were created using $Na_2MoO_4 \cdot 2H_2O$ (Sigma Aldrich) and placed in 200 mL, 250 mL, 500 mL, or 1 L glass beakers at room temperature and covered with Parafilm to inhibit evaporation. To simulate the effect of sulfide mineral oxidation, SO_4 was added to the solution using 5 M sulfuric acid (Riedel-de Haën). Excess powdered $CaCO_3$ (Fisher Scientific) with a surface area of 0.1 m^2 g^{-1} (nitrogen BET) was subsequently added to the beaker and most batches were stirred for the extent of the experiment using a magnetic stirrer.

Additional batch experiments were conducted to determine the potential for wulfenite and other metal molybdate precipitation under neutral pH conditions. These experiments included Cu, Pb, or Zn, which were added at specified concentrations using $CuSO_4 \cdot 5H_2O$, $Pb(NO_3)_2$, and $ZnSO_4 \cdot 7H_2O$ (Sigma Aldrich).

As the experiments progressed, 2 mL samples were extracted from the beakers using a syringe and filtered through a 0.45 μm Millipore filter, acidified with nitric acid to a pH below 2, and stored at 4°C until analysis using an ICP-OES (Varian 725-ES). pH measurements were obtained for each sample (Thermo Orion 250A+) and alkalinity was determined at the end of experiments when possible. Final precipitates within the batches were analyzed using XRD (Siemens D5000) and SEM (Philips XL-30).

2.2.2 Column Experiment

A column experiment was performed to investigate Mo attenuation with aqueous Pb, Cu, and Zn present under conditions similar to the field. An acrylic column with eleven uniformly spaced sampling ports was filled with marble originating from Texada Island, B.C., Canada (Lafarge Ltd., Coquitlam, B.C., Canada) that was crushed to a medium sand, sieved between 280 and 800 μm (Figure 2.1). Leaching tests on the marble indicate that Mo, Pb, Cu, and Zn concentrations were below the detection limit of approximately 0.5 mg L^{-1}. The marble was packed in the column as a slurry prepared with deionized water in order to prevent air from being trapped within the pores. The sand had a porosity of 0.4, dry bulk density of 1.39 g cm^{-3}, and surface area of 0.06 m^2 g^{-1}

using nitrogen BET. The experiment was conducted at room temperature and completely covered with aluminum foil to inhibit bacterial growth.

Three solutions containing Mo, Zn and Pb (Table 2) were simultaneously passed into the column using low-flow peristaltic pumps, resulting in a total flow of 0.22 mL min^{-1} and a residence time of 4 days. The inflow solutions were created using deionized water and the same reagents as the batch experiments and were mixed in the column just past the three distinct inlets located at the base. Conservative tracers (K, Na, and Li) were added to each solution and species concentrations were normalized to these conservative tracer concentrations to account for small mixing variability within the column. Prior to initiation of the experiment, one pore volume of deionized water was passed through the column.

To reduce disturbances by sample collection, 4 mL samples were collected from every second port for each pore volume during the extent of the experiment. On a few occasions, every port was sampled for higher resolution. Additional samples were not collected until a complete pore volume had passed through the column. pH was measured for every sample and alkalinity of the effluent was measured periodically. The initial solution concentrations and pumping rates were continuously monitored to ensure inflow concentrations remained constant. Samples were stored and analyzed in the same fashion as the batch experiments.

2.2.3 Modeling

The geochemical code PHREEQC (*23*) was used with the WATEQ4F database to determine saturation indices of measured samples. The reactive transport code MIN3P (*24*) was used to calibrate kinetic parameters for mineral precipitation within the batch experiments. Chemical reactions and thermodynamic constants involving Mo were added to the database of both models (Table 3).

2.3 Results and Discussion

2.3.1 Batch Experiments

2.3.1.1 Powellite Formation (Ca-System)

The first series of batch experiments investigated the potential for powellite formation in the presence of calcite. Under these conditions, the generalized reaction promoting Mo attenuation from calcite dissolution is as follows:

$$CaCO_{3\,(s)} + H^{+} \rightarrow Ca^{2+} + HCO_3^{-} \qquad (2.1)$$

$$Ca^{2+} + MoO_4^{2-} \rightarrow CaMoO_{4\,(s)} \qquad (2.2)$$

Results consistently show that powellite precipitation occurs, but is kinetically limited (Figure 2.2). For stirred experiments, crystallization was inhibited for approximately 24 hours, likely due to the initial lack of suitable nucleation sites. Mo then decreased exponentially until no further precipitation occurred after approximately 30 days. The processes controlling the kinetics of Mo removal were not analyzed but rate limited diffusion of ions to the nucleation sites may be a contributing factor (*25*).

Ca concentrations decreased concordantly with Mo until precipitation rates decreased. Mass balance calculations confirmed that all Ca removal was due to powellite precipitation until Mo removal fell below 2.5 mg L^{-1} per day (Figure 2.3). Near the end of the experiment, Ca increased modestly due to limited evaporation. Calcite was slightly supersaturated, with calculated saturation indices ranging from 0.3 to 0.7, suggesting that calcite dissolution did not cause the Ca increase. The pH of all experiments remained relatively constant at 7.78 ± 0.06, similar to that observed in NRD at the Antamina mine site.

Two unstirred batch experiments were conducted to evaluate the effect of physical mass transfer within the solution. Both unstirred batches displayed slower precipitation rates and longer lag times prior to onset of precipitation. However, the exponential decline of Mo concentrations was similar to that observed for the stirred experiments, suggesting that the geochemical processes are the same but that precipitation rates differ.

2.3.1.2 Wulfenite Formation (Ca-Pb-System)

Batch experiments (called Wulf 1, Wulf 2) conducted to determine the potential for wulfenite formation indicate that it has a high probability of being a sink for Mo at mine sites with Pb mineralization. Precipitation reduced aqueous Pb to concentrations below detection within seconds in batch Wulf 1, with a pH of 2. Aqueous Mo decreased simultaneously, and subsequent XRD analyses confirmed that wulfenite was the sole phase present. Wulfenite also formed immediately in batch Wulf 2, with Pb dropping to below detection limits within 15 minutes. With excess Ca and Mo remaining in solution after wulfenite formation, powellite formed in the same manner as in a solution without Pb present. Therefore, wulfenite precipitates more readily than powellite if the solution is supersaturated with respect to both phases.

2.3.1.3 – Me-Molybdate Formation (Ca-Cu-Pb-Zn-System)

An unstirred competition batch experiment (Comp 1) was conducted to investigate molybdate precipitation in the presence of multiple metals (Ca, Cu, Pb and Zn) for pH-conditions similar to the powellite batch systems. Results indicate that Pb and Mo concentrations decreased immediately with a stoichiometry consistent with wulfenite formation (Figure 2.4). Although both Cu and Zn molybdates are predicted to form based on thermodynamic modeling, these phases could not be detected by XRD. $CuMoO_4$ had saturation indices between 3 and 5 in the solutions whereas malachite saturation indices ranged from 0 to 2.5. XRD analysis confirmed that the Cu decrease to levels below detection within two days was due to malachite precipitation. Zn decreased substantially but remained in solution at concentrations of 1.5 mg L^{-1}. Zn was removed at a slower rate than both Pb and Cu, with constant concentrations being reached after approximately two weeks. Although calculated saturation indices for $ZnMoO_4$ ranged between 0 and 2, Zn-phases were not detected with XRD, motivating further examination with a column experiment. Powellite precipitation rates were comparable to other unstirred batch experiments indicating that the presence of other metals did not affect the formation of powellite.

2.3.2 Column Experiment

For the most complex system (Ca-Cu-Pb-Zn), a column experiment was conducted to assess Mo mobility under active flow conditions. The dynamic flow conditions within a column separates precipitates with differing formation rates, with minerals subject to rapid precipitation kinetics forming near the inlet and precipitates with slower kinetics forming throughout the column.

Mo and Pb concentrations dropped sharply near the column inlet and Pb remained below detection limit for the entire length of the column (Figure 2.5 and 2.6). A yellow precipitate was visible near the column inlet, which was confirmed as wulfenite by XRD. The remaining Mo decreased both with distance and with time (pore volumes) at each sampling point (Figure 2.5). During the first few pore volumes, Mo concentrations remained elevated throughout the column, suggesting kinetic limitations for powellite precipitation, similar to observations in the batch experiments. Over time, powellite precipitated more rapidly leading to a more significant Mo removal within the column, likely due to the development of suitable nucleation sites. Relatively low Mo concentrations in certain ports of the column were likely due to heterogeneities in hydraulic conductivity and flow paths allowing for locally prolonged residence times and more extensive powellite formation. XRD analyses conducted at the end of the experiment identified powellite throughout the length of the column, except directly adjacent to the inlet where only wulfenite was found.

Ca concentrations remained relatively stable throughout the column, with slight decreases observed with time (Figure 2.5). Concentrations were high near the inflow due to the dissolution of calcite caused by sulfuric acid present in the inflow solution. The subsequent Ca decrease occurred due to the precipitation of powellite and small amounts of gypsum.

Although Cu concentrations decreased substantially within the first quarter of the column, $CuMoO_4$ could not be identified by XRD as a sink for Mo. Green staining on the marble grains and XRD results indicate that the formation of malachite is responsible for Cu-removal. As time progressed and the column moved towards a quasi-steady state condition, Cu concentrations stabilized at approximately 2.5 mg L^{-1} throughout the length of the column (Figure 2.6).

Zn concentrations remained high throughout the column. $ZnMoO_4$ and $ZnCO_3$ were both supersaturated for the duration of the experiment, but neither of these phases could be identified with XRD analyses. Additional Zn batch experiments indicate that limited Zn removal at early time is likely due to adsorption onto calcite rather than Zn precipitation, with no solid phases detected but almost complete Zn removal. Zn sorption to calcite occurs more prominently at elevated pH levels via exchange with Ca^{2+} in an adsorption surface layer (*26*). Consistent with sorption, Zn breakthrough in the column was retarded with respect to a conservative tracer (see Figures 2.6 and 2.7). After breakthrough, Zn concentrations were typically slightly lower at the outflow than the inflow, likely due to Zn adsorption and mass transfer into calcite grains.

SEM images of the marble grains from the column indicate typical spherical malachite precipitation (*27*, *28*) along with powellite precipitation on rough surfaces (Figure 2.8). The lack of precipitation on cleavage faces suggest that they do not provide a surface rough enough for nucleation. Powellite precipitation coats the marble grains, possibly inhibiting calcite dissolution. The samples shown here were obtained from the first quarter of the column, and grains farther away from the inlet were coated with less precipitate.

2.3.3 Powellite Precipitation Kinetics

Batch and column experiments indicate that powellite and wulfenite provide sinks for molybdate; however, wulfenite precipitation is too rapid for a quantitative analysis of precipitation rates. The slower formation of powellite allows us to quantify precipitation kinetics. Powellite precipitation of each batch system was modeled using MIN3P (*24*) accounting for the solution composition. It was found that the rate of powellite precipitation under far-from-equilibrium conditions (R [mol L^{-1} per day]) is adequately described by a second order rate expression dependent on the concentrations of Ca^{2+} and MoO_4^{2-} with a precipitation rate coefficient k_p, [L mol^{-1} day^{-1}].

$$R = k_p \cdot \left[Ca^{2+}\right]\left[MoO_4^{2-}\right] = k_p \cdot IAP \qquad (2.3)$$

Observed MoO_4 concentration decreases are modeled well for the unstirred batch systems (Figure 2.9). A precipitation rate coefficient of 1.3 x 10^{-4} L mol^{-1} day^{-1} was determined for the unstirred powellite batch experiments (Pow 3 and Pow 4) and a

precipitation rate coefficient of 1.6 x 10^{-4} L mol^{-1} day^{-1} was found for the competition batch experiment (Comp 1), which was also unstirred. The precipitation rate coefficients of these experiments are in excellent agreement indicating that other metals in solution do not significantly affect the rate of powellite precipitation.

Stirred batch systems promote precipitation due to agitation and increased energy within the solution. In this case, the precipitation rate expression requires an affinity term to describe powellite precipitation correctly as equilibrium conditions are approached:

$$R = -k_p \cdot IAP\left(1 - \frac{K_{sp}}{IAP}\right) \qquad (2.4)$$

Simulated results for Pow 6, one of the stirred powellite batch experiments, used a precipitation rate coefficient of 9.6x10^{-4} L mol^{-1} day^{-1} based on calibration to early-time data (Figure 2.10). This value is an order of magnitude higher than for the unstirred systems. The literature log K_{sp} of -8.05 for powellite (*13*) was initially used to describe conditions as equilibrium is approached; however, Mo removal was overestimated significantly at late time. This finding suggests that powellite forming under stirred conditions is more amorphous and soluble or that the geochemical database used is missing aqueous complexes of MoO_4. A log K_{sp} of -6.40 was subsequently used for this simulation to fit Mo concentration under near-equilibrium conditions. Precipitation rates found in the field will likely be closer to the unstirred batch experiments due to the lack of agitation. In addition, the K_{sp} estimated here will likely provide an upper limit for powellite solubility under field conditions. Other parameters including aqueous Ca and pH were reproduced well with the simulation, providing further support that the reaction network was captured adequately (Figure 2.10).

2.3.4 Waste Rock Analysis

Waste rock samples from the Antamina mine in Peru were analyzed using MLA (*29*) with the goal to confirm that secondary Mo-bearing mineral phases form under field conditions. The samples were obtained from existing field cells that have been exposed to atmospheric conditions for over five years. Secondary mineral phases with transitional compositions close to powellite and wulfenite were detected in the samples, providing direct evidence that these minerals provide a sink for Mo in waste rock (Figure 2.11). The

minerals are described as transitional because the elemental proportions determined by the MLA did not exactly match the compositions of powellite and wulfenite, likely due to the low abundances of these mineral phases or impurities.

Powellite was detected more frequently and in higher abundances than wulfenite, as expected due to limited Pb availability. The images indicate that powellite forms readily as coatings on grain surfaces of carbonates and silicates or in association with molybdenite (Figure 2.11). Its presence directly beside both calcite and molybdenite indicates that powellite formation is relatively fast in relation to water flow. A wulfenite-powellite transitional phase was found beside a molybdenite crystal indicating that aqueous Pb was not previously attenuated before reaching the Mo source, similar to previous observations (*30*). Small amounts of wulfenite were also found as coatings on grains in a similar fashion as powellite.

2.3.5 Implications for Mo Release From Mine Waste

Mo removal under NRD conditions highly depends on the specific environmental conditions. In the presence of Pb, wulfenite precipitation will attenuate Mo almost immediately. Ca concentrations are expected to be elevated in NRD environments, allowing for the precipitation of powellite. Kinetic limitations and the residence time in waste rock will likely determine the extent of powellite formation. The kinetically limited formation of powellite can be described using a relatively simple rate expression independent of the solution composition. The discovery of powellite and wulfenite in a NRD waste rock pile is encouraging and confirms the importance of secondary minerals as sinks for Mo. Cu and Zn do not appear to affect Mo attenuation, even with predicted supersaturation of Cu and Zn molybdates. Malachite precipitation and Zn adsorption occur before Cu and Zn phases can sequester molybdate precipitation, indicating that they will not attenuate Mo.

Whether or not Mo will be an environmental concern in neutral rock drainage sites still must be assessed under field conditions on a larger scale, but the present experiments indicate that both powellite and wulfenite may lower aqueous Mo concentrations to levels much closer to environmental guidelines. Kinetic limitations could limit the extent of attenuation, depending on the rate of Mo-release from Mo-

sulfide oxidation and residence time of Mo in neutral groundwater, but with extended exposure powellite is hypothesized to act as a prominent sink for Mo under NRD conditions.

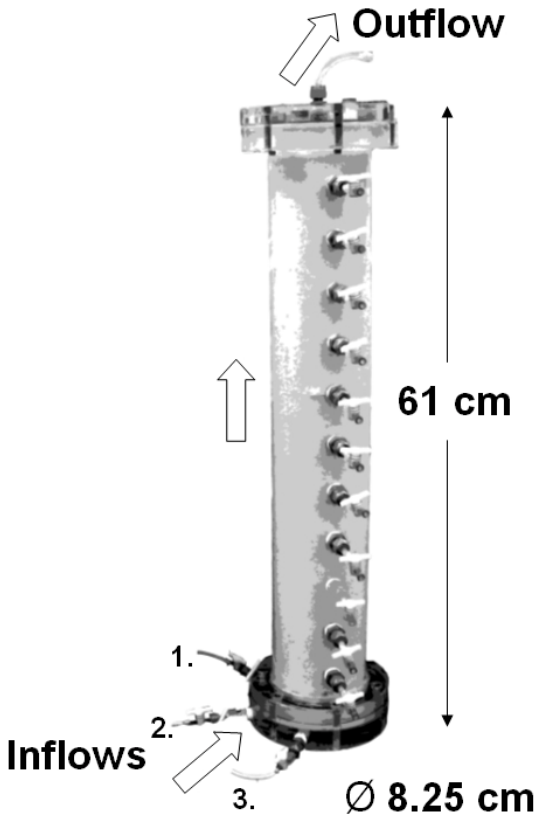

Figure 2.1 – Schematic of the column experiment showing its dimensions, the three inlets and single outlet, sampling ports, and direction of flow of within the column.

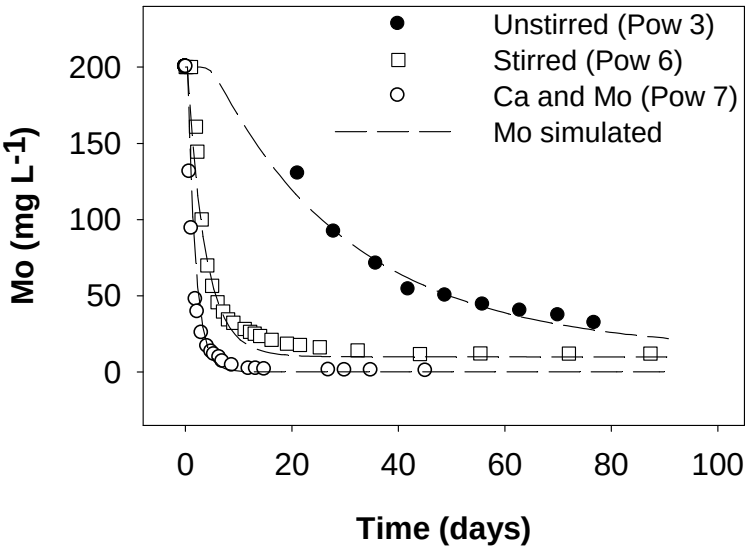

Figure 2.2 – Observed (symbols) and simulated (lines, using MIN3P) Mo removal due to powellite formation for different batch experiments initially containing 200 mg L^{-1} Mo. Stirred and unstirred batch experiments (Pow 3 and Pow 6) included 1000 mg L^{-1} SO_4 and excess powdered $CaCO_3$ in solution whereas Pow 7 contained 600 mg L^{-1} calcium.

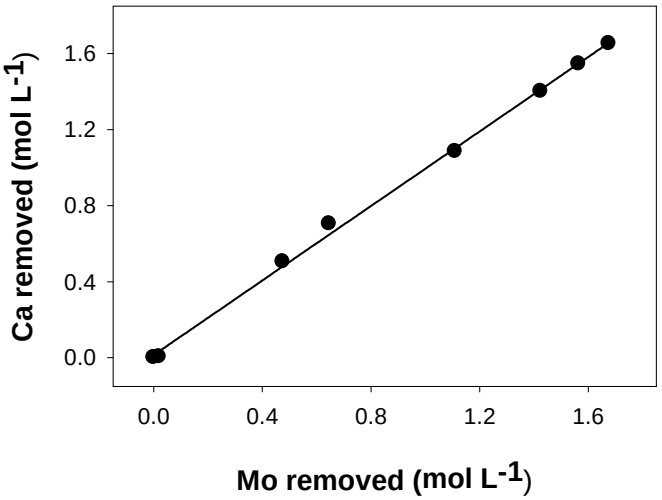

Figure 2.3 – Stoichiometric agreement for powellite formation with Mo and Ca removal from solution in batch Pow 6 for the first six days.

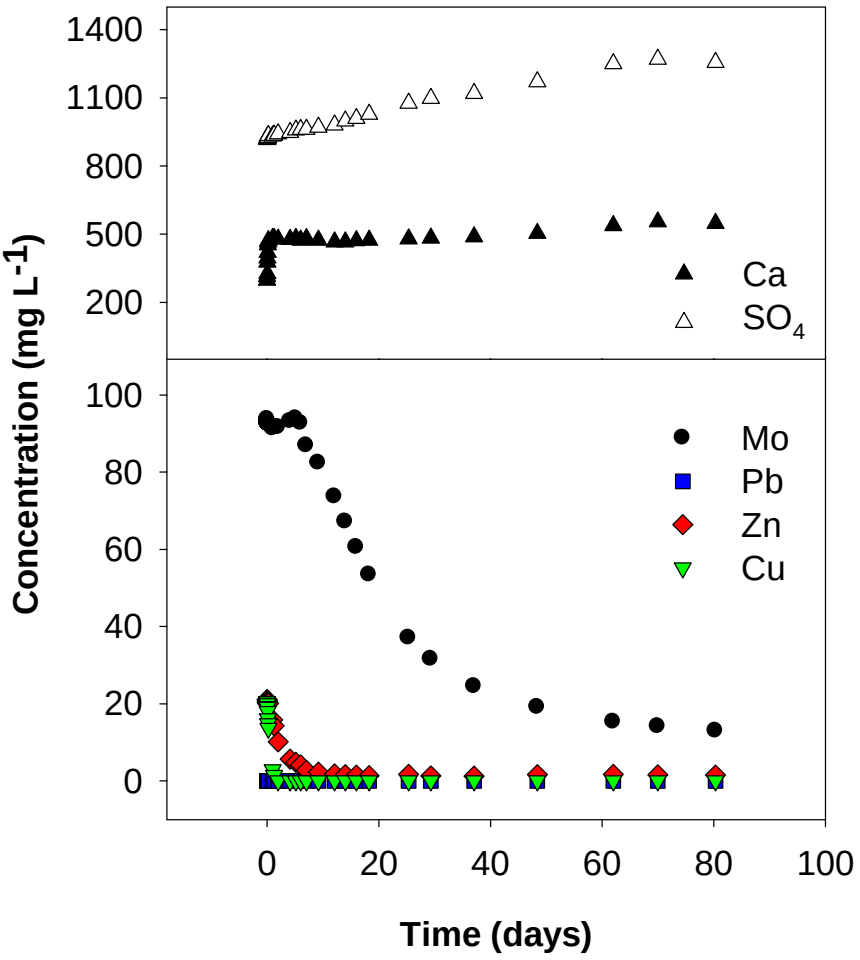

Figure 2.4 – Observed results for unstirred competition batch experiment (Comp 1). Pb removal due to wulfenite formation is nearly instantaneous; the removal of the remaining Mo by powellite is gradual and initially inhibited. Cu and Zn are also removed from solution, but not as molybdate phases.

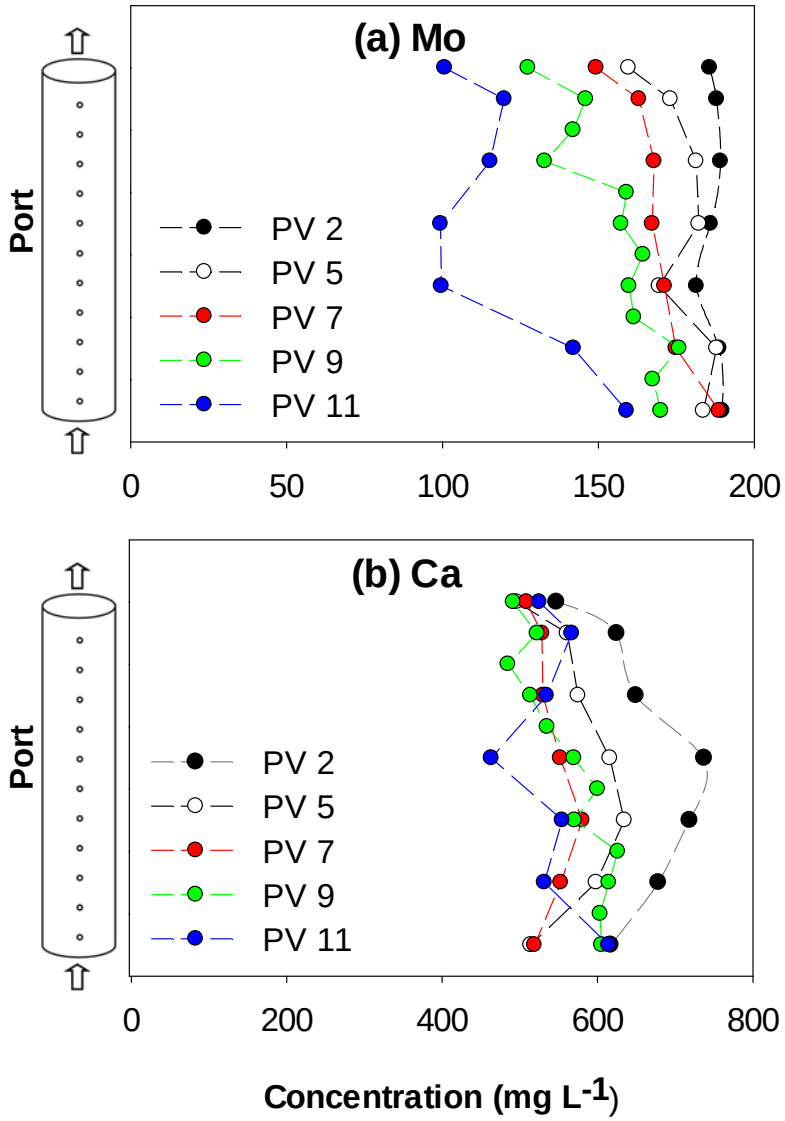

Figure 2.5 – Vertical profiles of a) Mo and b) Ca in the competition column for selected pore volumes (PV). Mo concentrations show an instantaneous drop from 200 mg L^{-1} due to wulfenite precipitation near the inlet. The increase of Mo and Ca removal along the flowpath and with time are due to powellite formation and suggesting an initial lack of nucleation sites.

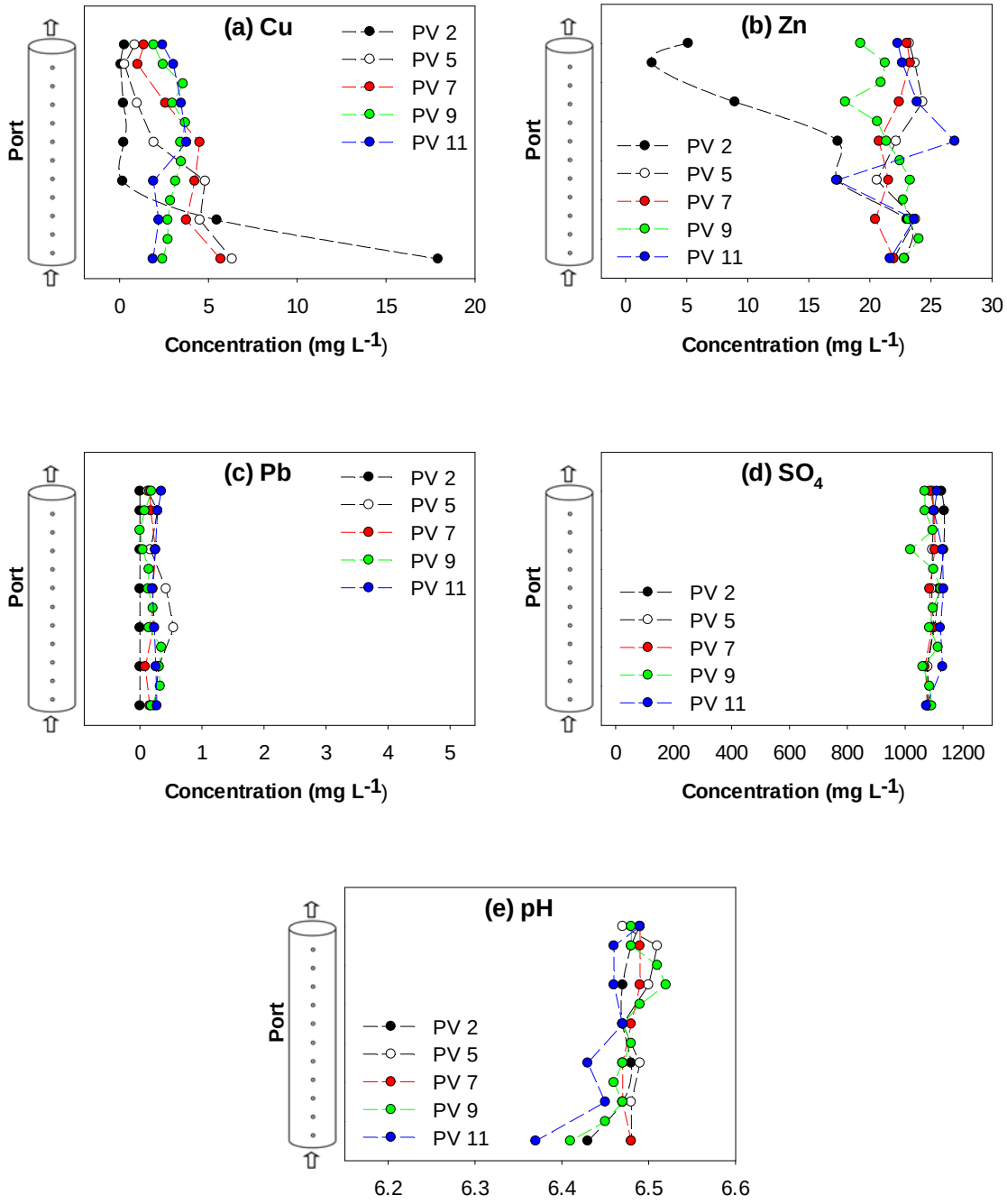

Figure 2.6 – Vertical profiles of a) Cu, b) Zn, c) Pb, d) SO_4, and e) pH in the competition column for selected pore volumes (PV).

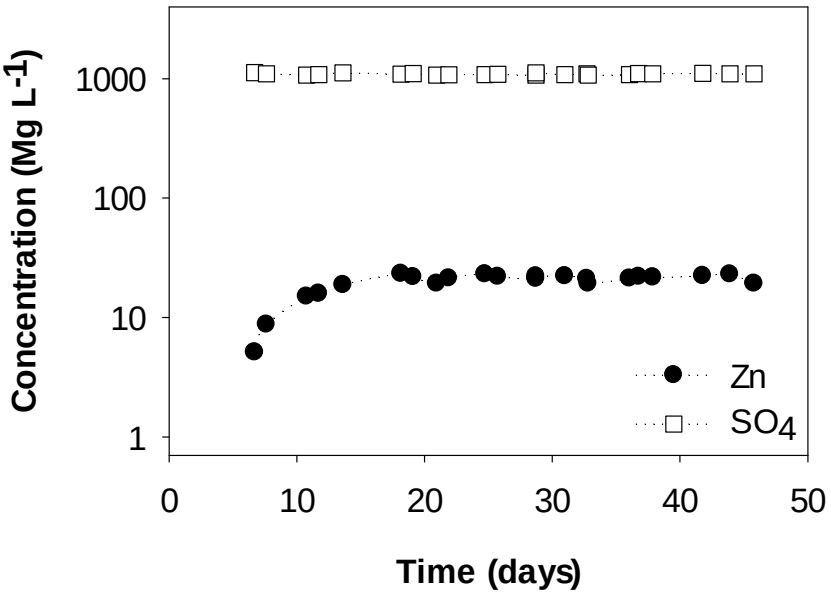

Figure 2.7 – Observed Zn retardation at the outflow of the column in comparison to SO_4, which acts as a relatively conservative species.

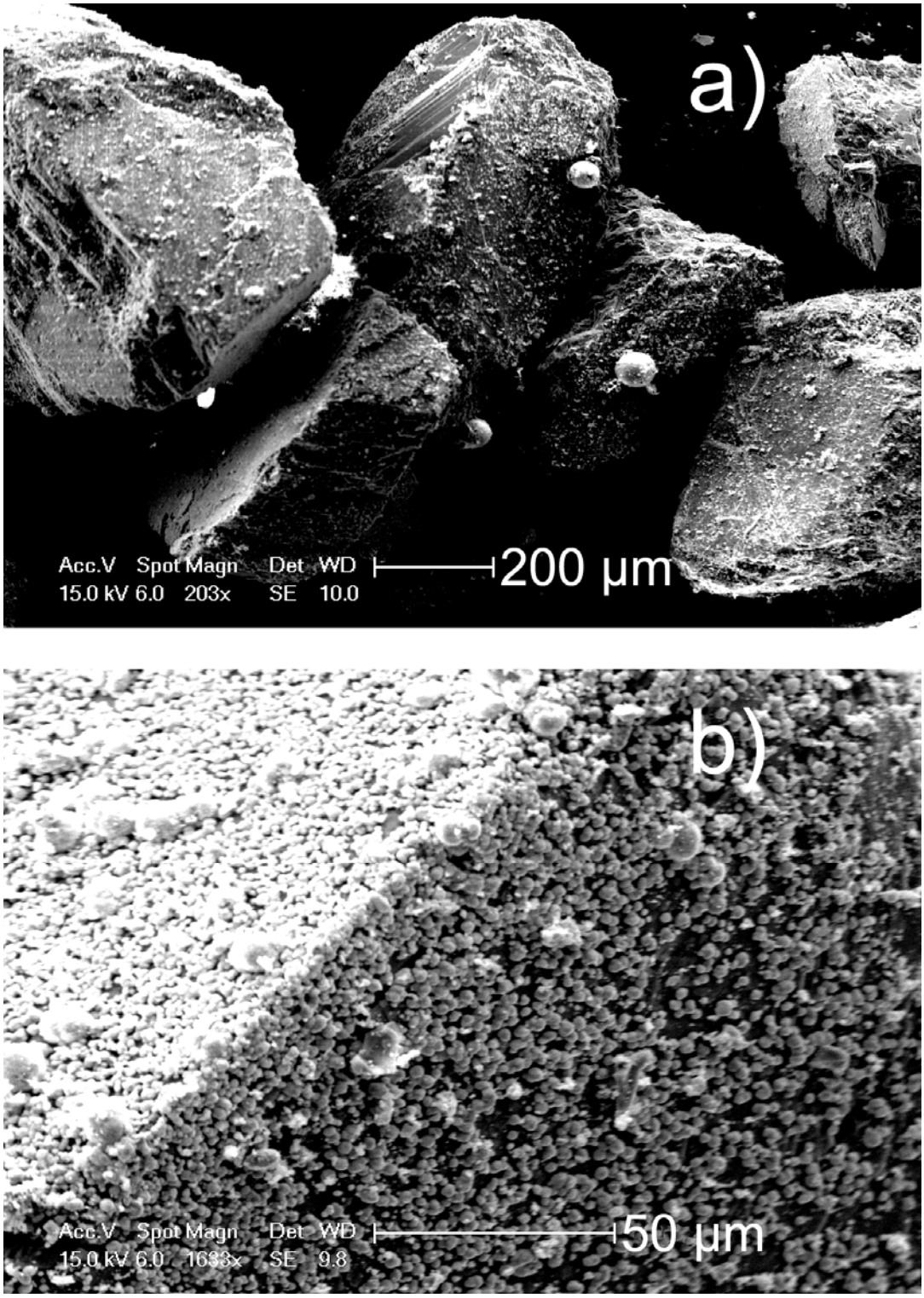

Figure 2.8 – SEM images showing **a)** spherical malachite precipitate and smaller powellite crystals on rough surfaces of calcite grains and **b)** powellite precipitate on a sand-sized marble grain.

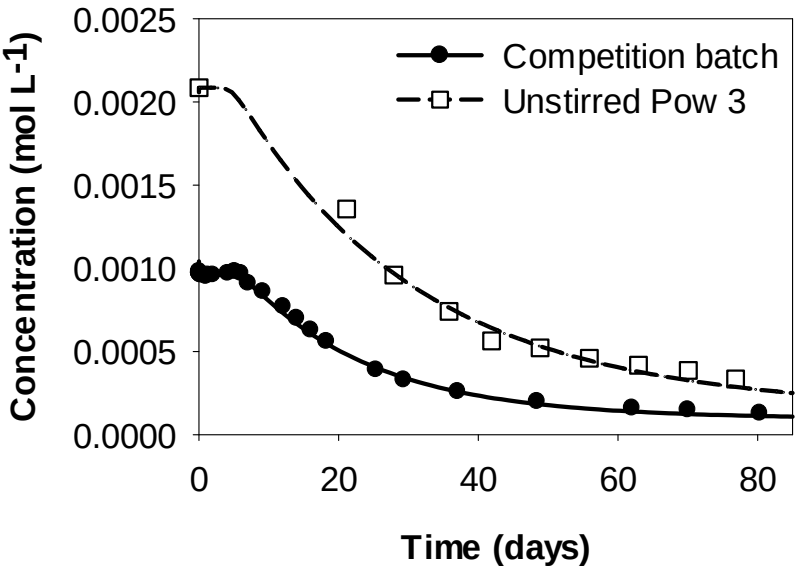

Figure 2.9 – Measured (symbols) and simulated (lines) data for unstirred batch experiments.

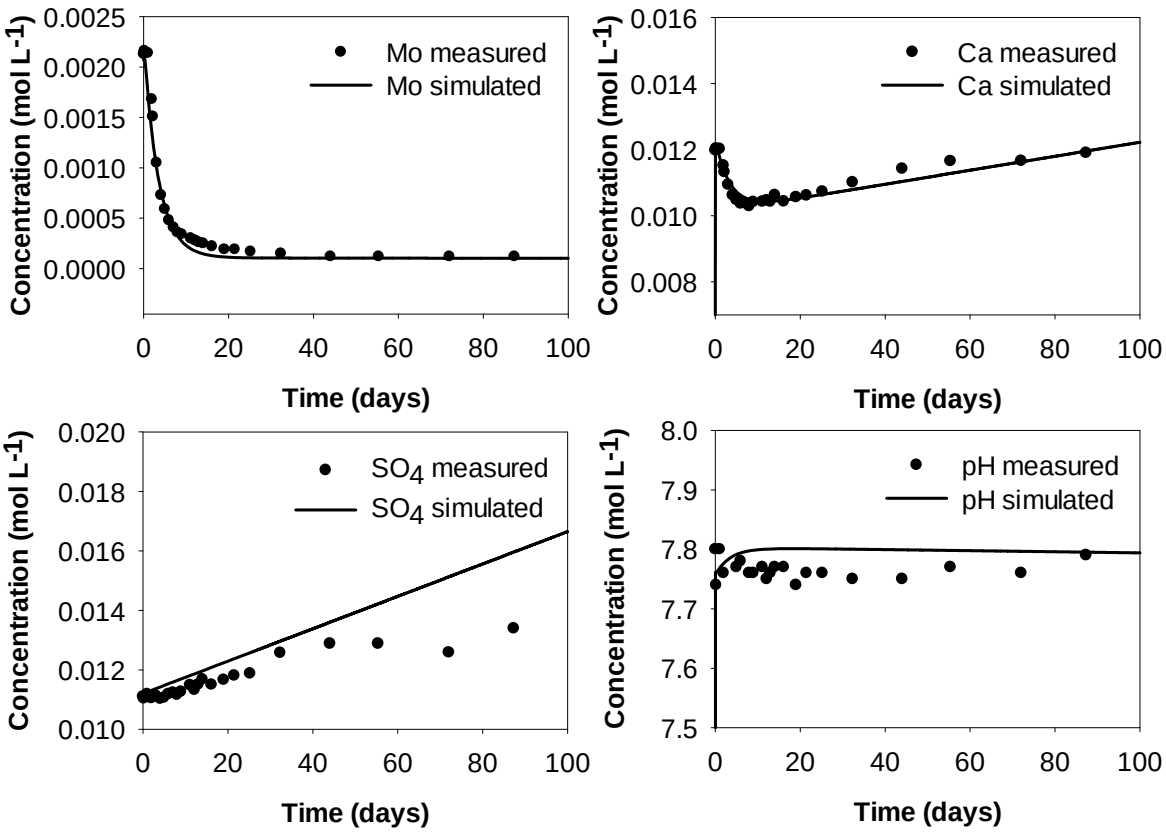

Figure 2.10 – Observed and simulated data for stirred powellite batch experiment Pow 6. The fact that other parameters such as Ca and pH could be reproduced well provides support that the reaction network was captured adequately. SO_4 was not modeled as well, which may be explained by gypsum formation, which was observed in XRD analyses of the solids. Simulations predicted gypsum saturations that remain marginally undersaturated towards the end of the experiment (results not shown). Figure 2.10 also shows that some evaporation occurred during the experiments, which explains the long-term concentration increases for Ca and SO_4. Evaporation was accounted for in the MIN3P simulation, but had little effect on the interpretation of powellite precipitation kinetics.

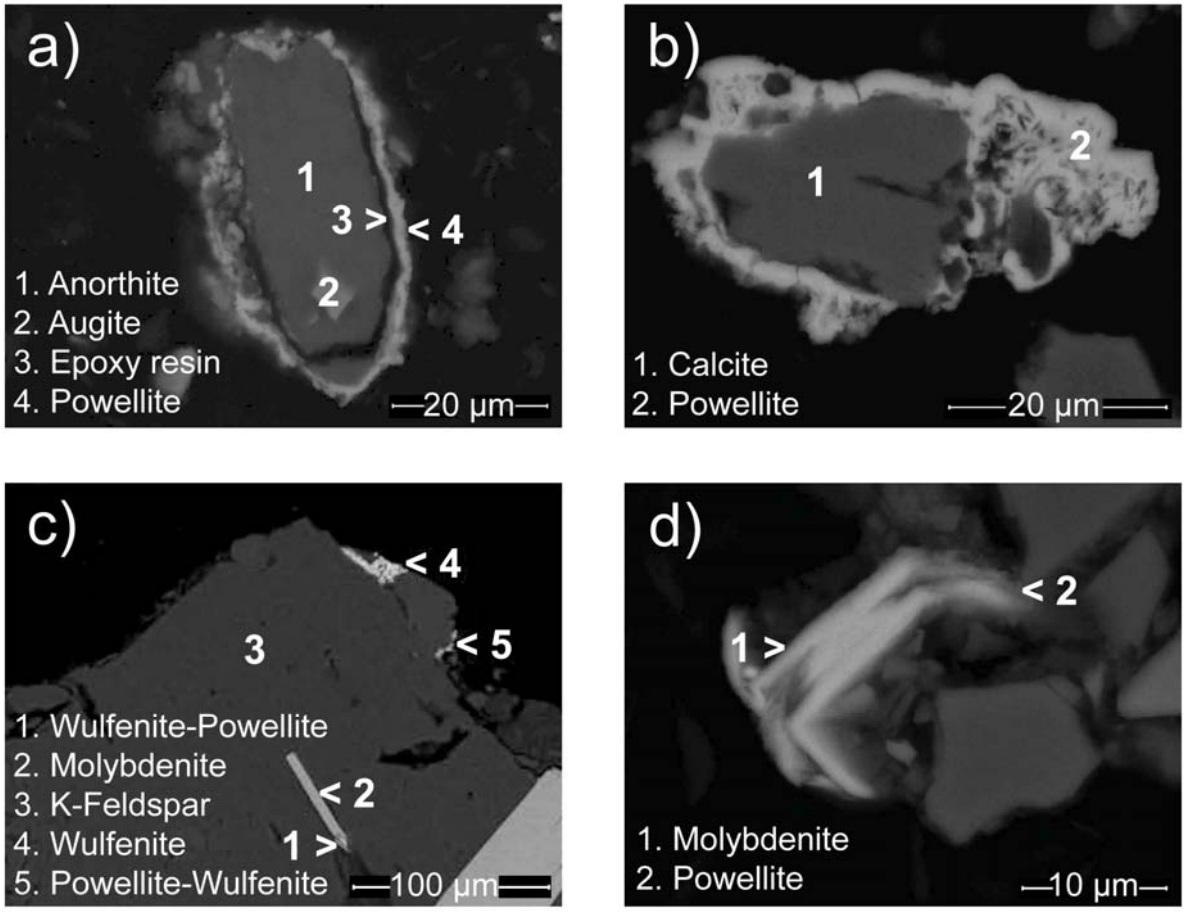

Figure 2.11 – MLA images of waste rock samples extracted from field cells at the Antamina mine site showing that secondary Mo mineral formation in the field is ubiquitous and takes place on silicate minerals (a and c), carbonates (b) and in association with Mo-bearing sulfide minerals (c and d).

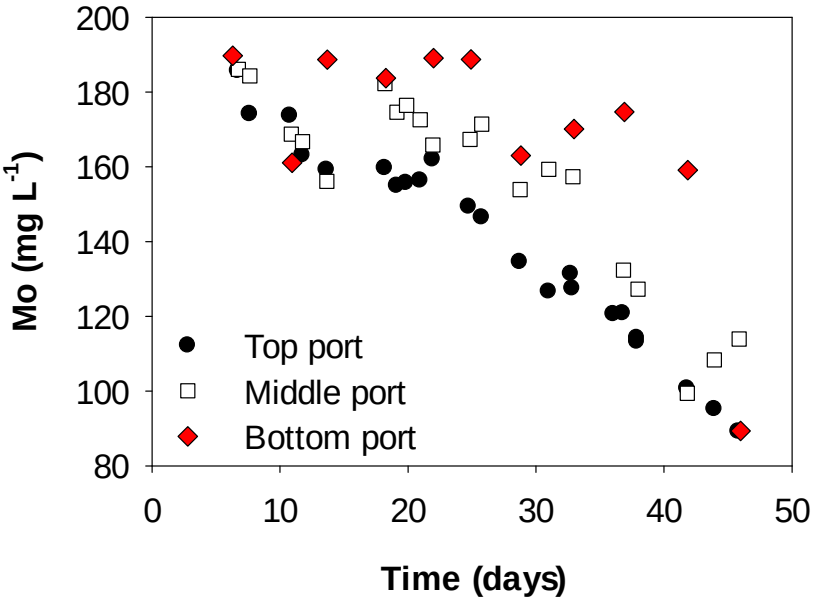

Figure 2.12 – Mo concentrations with time at top, middle, and bottom ports of the column.

Table 2.1 – Initial concentrations and conditions for batch experiments (all values mg L^{-1})

Batch	Mo	SO_4	Ca source	Pb	Cu	Zn	Stirred
Pow 1	200	1000	calcite powder				Yes
Pow 2	200	1000	calcite powder				Yes
Pow 3	200	2000	calcite powder				No
Pow 4	200	20000	calcite powder				No
Pow 5	200	1000	crushed marble sand				Yes
Pow 6	200	1000	calcite powder				Yes
Pow 7	200		600 mg L^{-1} from CaCl				Yes
Wulf 1	200		calcite powder	20			Yes
Wulf 2	200	1000		20			Yes
Comp 1	100	1000	crushed marble sand	20	20	20	No

Table 2.2 – Composition of inflow solutions for column experiment.

	Solution 1	**Solution 2**	**Solution 3**
Reactive species	60 ppm Pb	600 ppm Mo 1500 ppm SO_4	60 ppm Cu 60 ppm Zn 1500 ppm SO_4
Tracer	50 ppm K	335 ppm Na	20 ppm Li
pH	5.05	1.98	1.87

Table 2.3 – Molybdenum reactions added to the PHREEQC and MIN3P databases.

Aqueous Reactions	**log K**	**Source**
$MoO_4^{-2} + H_+ = HMoO_4^-$	4.24	*31*
$MoO_4^{-2} + 2H^+ = H_2MoO_4$	6.85	*32*
$3H^+ + MoO_4^{-2} = MoO_2OH^+ + H_2O$	7.89	*32*
$4H^+ + MoO_4^{-2} = MoO_2^{+2} + 2H_2O$	8.34	*32*
$MoO_4^{-2} + e^- + 4H^+ = MoO_2^+ + 2H_2O$	20.95	*32*
$MoO_4^{-2} + 3e^- + 8H^+ = Mo^{+3} + 4H_2O$	29.52	*32*
$Ca^{+2} + MoO_4^{-2} = CaMoO_4$	2.57	*33*
$Na^+ + MoO_4^{-2} = NaMoO_4^-$	1.66	*33*
Powellite Precipitation Reaction		
$Ca^{+2} + MoO_4^{-2} = CaMoO_4$	8.05	*33*

Table 2.4 – XRD results of powellite batch precipitates analyzed at the end of the experiments.

Sample	***SO_4 (mg L^{-1})***	***Powellite***	***Gypsum***
Pow 1	1000	Yes	No
Pow 2	1000	Yes	No
Pow 3	2000	Yes	Yes
Pow 4	20000	Yes	Yes
Pow 5	1000	Yes	Trace
Pow 6	1000	Yes	Trace
Pow 7	0	Yes	No

2.4 References

(1) Drever, J.I. *The Geochemistry of Natural Waters: Surface and Groundwater Environments, 3rd, ed.*; Prentice Hall: Upper Saddle River, NJ, 1997.

(2) Borden, R.K. Environmental geochemistry of the Bingham Canyon porphyry copper deposit, Utah. *Environ. Geol.* **2002**, *43*, 752-758.

(3) Goldberg, S.; Forster, H.S.; Godfrey, C.L. Molybdenum Adsorption on Oxides, Clay Minerals, and Soils. *Soil Sci. Soc. Am. J.* **1996**, *60*(2), 425-432.

(4) Gustafsson, J.P. Modelling Molybdate and Tungstate Adsorption to Ferrihydrite. *Chem. Geol.* **2003**, *200*, 105-115.

(5) Xu, N.; Christodoulatos, C.; Braida, W. Adsorption of Molybdate and Tetrathiomolybdate onto Pyrite and Goethite: Effect of pH and Competitive Anions. *Chemosphere* **2006**, *62*, 1726-1735.

(6) Fox, P.M.; Doner, H.E. Trace Element Retention and Release on Minerals and Soil in a Constructed Wetland. *J. Environ. Qual.* **2002**, *31*, 331-338.

(7) Gupta, U.C. *Molybdenum in Agriculture*; Cambridge University Press: Cambridge, 1997.

(8) O'Connor, G.A.; Brobst, R.B.; Chaney, R.L.; Kincaid, R.L.; McDowell, L.R.; Pierzynski, G.M.; Rubin, A.; Van Riper, G.G. A modified risk assessment to establish molybdenum standards for land application of biosolids. *J. Environ. Qual.* **2001**, *30*, 1490–1507.

(9) Alloway, B.J. Copper and molybdenum in swayback pastures. *J. Agr. Sci.* **1973**, *80*, 521-524.

(10) Stone, L.R.; Erdman, J.A.; Fedder, G.L.; Holland, H.D. Molybdenosis in areas underlain by uranium-bearing lignites in the Northern Great Plains. *J. Range Manage.* **1983**, *36*, 280-285.

(11) Evans, D.; Letient, H.; Aley, T. *Aquifer Vulnerability Mapping in Karstic Terrain at Antamina Mine, Peru*. Proceedings from the Society of Mining Engineers Conference, Salt Lake City, USA, 2005.

(12) Vlek, P.L.G.; Lindsay, W.L. Thermodynamic stability and solubility of molybdenum minerals in soils. *Soil Sci. Soc. Am. J.* **1977**, *41*, 42-46.

(13) Essington, M.E. Calcium Molybdate Solubility in Spent Oil Shale and a Preliminary Evaluation of the Association Constants for the Formation of CaMoO40(aq), KMoO4–(aq), and NaMoO4–(aq). *Environ. Sci. Technol.* **1990**, *24*(2), 214-220.

(14) Felmy, A.R.; Rai, D.; Mason, M.J. The Solubility of CaMoO4(c) and an Aqueous Thermodynamic Model for Ca2+-MoO42– Ion-Interactions. J. Solution Chem. **1992**, *21*, 525-532.

(15) Carroll, K.C.; Artiola, J.F.; Brusseau, M.L. Transport of Molybdenum in a Biosolid-Amended Alkaline Soil. Chemosphere **2006**, *65*(5), 778-785.

(16) Essington, M.E. Fluorine and molybdenum solubility relationships in combusted oil shale. *J. Environ. Sci. Heal. A* **1992**, *27*(2), 547–564.

(17) Meima, J.A.; van der Weijden, R.D.; Eighmy, T.T.; Comans, R.N.J. Carbonation Processes in Municipal Solid Waste Incinerator Bottom Ash and their Effect on the Leaching of Copper and Molybdenum. *Appl. Geochem.* **2002**, *17*, 1503-1513.

(18) Reddy, K.J.; Gloss, S.P. Geochemical speciation as related to the mobility of F, Mo and Se in soil leachates. *Appl. Geochem.* **1993**, *8*(SUP2), 159-163.

(19) Bideaux, R.A. The desert mineral: Wulfenite. *Rocks and Minerals* **1990**, *65*, 11-30.

(20) Rosemeyer, T. Wulfenite occurrences in Colorado. *Rocks and Minerals* **1990**, *65*, 58-61.

(21) Wang, L.; Reddy, K.J.; Munn, L.C. Geochemical Modeling for Predicting Potential Solid Phases Controlling the Dissolved Molybdenum in Coal Overburden, Powder River Basin, WY, U.S.A. *Appl. Geochem.* **1994**, *9*, 37-43.

(22) Martínez, C.E.; Motto, H.L. Solubility of lead, zinc, and copper added to mineral soils. *Environ. Pollut.* **2000**, *107*, 153-158.

(23) Parkhurst, D.L.; Appelo C.A.J. *User's guide to PHREEQC (Version 2) – a computer program for speciation, batch-reaction, one-dimensional transport, and inverse geochemical calculations.* U.S. Geological Survey Water-Resources Investigations Report 99-4259; 1999.

(24) Mayer, K.U.; Frind, E.O.; Blowes, D.W. Multicomponent reactive transport modeling in variably saturated porous media using a generalized formulation for kinetically controlled reactions. *Water Resour. Res.* **2002**, *38*(9), 1174-1194.

(25) Tweet, A.G. Precipitation of Cu in Ge. *Phys. Rev.* **1957**, *106*(2), 221-224.

(26) Zachara, J.M.; Kittrick, J.A.; Harsh, J.B. The mechanism of Zn^{+2} adsorption on calcite. *Geochim. Cosmochim. Ac.* **1988**, *52*, 2281-2291.

(27) Kratohvil, S.; Matijević, E. Preparation of copper compounds of different compositions and particle morphologies. *J. Mater. Res.* **1991**, *6*(4), 766-777.

(28) Candal, R.J.; Regazzoni, A.E.; Blesa, M.A. Precipitation of Copper(II) Hydrous Oxides and Copper(II) Basic Salts. *J. Mater. Chem.* **1992**, *2*(6), 657-661.

(29) Gu, Y. Automated scanning electron microscope based mineral liberation analysis. *J. Miner. Mater. Charact. Eng.* **2003**, 2(*1*), 33-41.

(30) Petrunic, B.M.; Al., T.A.; Weaver, L. A transmission electron microscopy analysis of secondary minerals formed in tungsten-mine tailings with an emphasis on arsenopyrite oxidation. *Appl. Geochem.* **2006**, *21*(8), 1259-1273.

(31) Gu, Smith, R.M., Martell, A.E. *Critical Stability Constants, Vol. 4. Inorganic Complexes*; Plenum Press: New York, 1976.

(32) Kaback, D.S.; Runnells, D.D. Geochemistry of molybdenum in some stream sediments and waters. *Geochim. Cosmochim. Ac.* **1980**, *44*, 447–456.

(33) Essington, M.E. Calcium Molybdate Solubility in Spent Oil Shale and a Preliminary Evaluation of the Association Constants for the Formation of CaMoO40(aq), KMoO4–(aq), and NaMoO4–(aq). *Environ. Sci. Technol.* **1990**, *24*(2), 214-220.

Chapter 3 – Mo Adsorption in Neutral Rock Drainage[2]

3.1 Introduction

Sorption is an attenuation mechanism that includes such processes as adsorption, surface precipitation, and diffusion of solutes into porous materials (Davis and Kent, 1990). Certain materials such as oxide minerals, clays, and organic matter have a high affinity to adsorb dissolved constituents, such as trace metals. Iron oxides such as ferrihydrite are of particular interest for this study, as they are weathering products of primary iron sulfide minerals. The formation of iron hydroxides occurs when iron sulfide minerals such as pyrite are exposed to atmospheric conditions or oxygenated groundwater:

$$4FeS_2 + 15O_2 + 14H_2O \rightarrow 4Fe(OH)_3(am) + 8SO_4^{2-} + 16H^+ \qquad (3.1)$$

The amorphous ferric hydroxide ferrihydrite ($Fe(OH)_3(am)$ or $Fe_2O_3 \cdot nH_2O$), also known as hydrous ferric oxide (HFO) and amorphous iron oxyhydroxide (Dzombak and Morel, 1990), readily forms after the oxidation of pyrite, which typically coats mineral grains (Jenne, 1977). It is these secondary minerals that dominate the adsorptive capacity in many systems, such as waste rock piles, even though they constitute only a minor fraction of the media (Davis and Kent, 1990).

Ferrihydrite acts as an excellent adsorption site for dissolved constituents in groundwater, including Mo, as it has proton-bearing surface functional groups (Davis and Kent, 1990; Dzombak and Morel, 1990). This also makes the extent of sorption pH dependent. That is, adsorption on hydrous oxides changes dramatically over a narrow pH range, which is often called the adsorption edge. The adsorption edge can shift depending on competing ions, amount of adsorptive material, and solute concentrations.

The objectives of this chapter include 1) the evaluation of the suitability of different extraction techniques to quantify the concentrations of Mo adsorbed on waste rock samples that were exposed to weathering, 2) a preliminary quantification of the mass of Mo presently adsorbed on weathered waste rock samples, and c) an assessment of the

[2] A version of this chapter will be submitted for publication.
Conlan, M.J.W; Mayer, K.U; Beckie, R.D. Mo adsorption in neutral rock drainage.

Mo-adsorption capacity of selected waste rock materials from Antamina. To achieve these goals, a series of desorption experiments were conducted using existing waste rock material from the Antamina mine. Three different methods were utilized including a weak distilled-deionized water (DI) leach and a reductive dissolution approach. In addition, a series of adsorption tests was carried out.

3.2 Sample Selection and Approach

To determine the probable extent of Mo adsorption onto HFO's within the waste rock piles, waste rock was obtained from the surface of the experimental waste rock piles at Antamina as well as from field cells. The cells had been exposed to atmospheric conditions for over a year, allowing the infiltration of natural rainwater. The effluent has been collected and analyzed for its chemical composition to assess the extent of metals leaching. Five field cells were selected for sorption analyses based on their outflow concentrations over the previous year. Samples were collected from the field cells with the highest Mo concentrations to assess the extent of Mo sorption. The five field cells selected were Field Cell 5, 6, 7, 8 and 14 (Golder, 2007). Their characteristics are summarized in Table 3.1.

3.3 Methodology

Desorption tests are difficult to conduct with rock types similar to those at Antamina; most selective leach methods use acidic solutions that attack specific mineral phases but leave others intact, but this is a problem when the host rock is carbonate-rich, as the entire sample will dissolve under acidic conditions (Amirbahman et al., 1998). This is not desired, as Mo is only adsorbed onto hydrous ferric oxides that coat the rock material. Determining a method that releases the molybdate but leaves the rest of the rock intact is therefore required.

3.3.1 Desorption Using pH-Modification

A simple method was initially employed to investigate desorption. The method relied on increasing the pH of a slurry composed of DI water and suspended waste rock.

It was hypothesized that this method would be effective, because Mo adsorption is low in the basic pH range. This method is also not aggressive towards the dissolution of mineral phases contained in the sample intact, which is required to target the adsorbed mass.

In order to determine if Mo is currently adsorbed onto waste rock material, desorption tests were conducted on 9 samples from differing waste rock types from Antamina. The samples consisted of endoskarn, intrusive, marble, and hornfels rock types, which are the main waste rock classifications at the mine. The desorption study was conducted by placing 1 g of waste rock consisting of the <2 mm fraction into 25 mL of deionized water for 76 hours while in a shaking bath at 125 RPM and 23^{o}C. The pH of sample solutions that were initially below 7 were increased to a pH above 8 by adding 1 M NaOH solution. The pH of the solution was monitored during the experiment to ensure that it remained basic. Samples were then filtered through a 0.45 μm syringe filter and analyzed for pH and Mo content using a Hach D2400 spectrophotometer.

3.3.2 Desorption Using Ascorbic Acid Leach

Aggressive leach procedures utilizing strong acids are not desirable, because these methods lead to the total or partial dissolution of carbonate minerals, making it impossible to distinguish between adsorbed Mo and Mo present within these mineral phases. A reduction-based ascorbate leach was therefore used to determine Mo adsorbed onto the samples. Although this technique is relatively new, it has been utilized on amorphous and poorly crystalline iron oxyhydroxides (Hyacinthe et al., 2006; Roychoudhury, 2006), in iron-phosphorus phases (Hyacinthe and Van Cappellen, 2004) and to analyze Fe(III) specifically in calcareous-rich environments (Amirbahman et al., 1998). The leach is based upon the reductive dissolution of iron oxides at high pH and thus minimizes carbonate dissolution. The leach therefore targets Mo adsorbed onto iron oxides.

The samples obtained were mainly fine-grained matrix material, as this is where the majority of adsorption occurs due to increased surface area. The samples were oven dried for approximately an hour at 80^{o}C and subsequently sieved to a less than 2 mm fraction and stored in bags at room temperature until experimentation.

The ascorbate leach was created as follows: 5 g of sodium citrate and 5 g of sodium bicarbonate were added to a volumetric flask and diluted to 100 mL. This solution was purged with nitrogen gas for an hour in order to make it anaerobic. At this point, 1 g of ascorbic acid was added to the solution and stirred, to create a 50 g L^{-1} sodium citrate, 50 g L^{-1} sodium bicarbonate, and 10 g L^{-1} ascorbic acid leach. The leach was continually bubbled with nitrogen gas to keep it anaerobic.

Approximately 25 mL, by mass, of the solution was added to Erlenmeyer flasks and stopped. A tube was passed through the solution via a valve in the flask, which continually passed nitrogen through the leach. 1 g of waste rock sample was then added to the solution, along with a magnetic stir bar, and placed on a magnetic stirrer to constantly mix the solution. The sample was left for 24 hours before being extracted using a syringe and passed through a 0.45 um syringe filter. 1.5 mL of concentrated nitric acid was then added to lower the pH to below 2. The samples were stored at 4^{o}C until analysis using an ICP-OES (Varian 725-ES). Images of the experimentation can be found in Appendix 4.

3.3.3 DI Leach

A deionized water leach was performed on the same field cell waste rock material in order to differentiate between strongly sorbed and loosely bonded Mo. This is the weakest leach that can be performed on a sample and has been studied both in partial extraction and continuous leach techniques (Kelley et al., 2003; MacFarlane et al., 2005; Bin-Shafique et al., 2006).

The deionized water leach was conducted by adding 1 g of waste rock sample into a vial containing 25 mL if DI water. The vials were placed in a shaking bath kept at 23^{o}C for 2 hours. The vials were subsequently centrifuged for 20 minutes at approximately 800 RPM. 10 mL of the solution was extracted using a syringe and filtered through a 0.45 μm Millipore syringe filter, acidified with 15 μL of nitric acid and stored at 4^{o}C. The remaining fraction of the solution was poured directly into a Nalgene vial, acidified with 15 μL of nitric acid and stored at 4^{o}C. Both the filtered and unfiltered fractions were analyzed by ICP-OES.

3.3.4 Adsorption

To determine potential Mo adsorption onto existing waste rock material, adsorption studies were conducted in the laboratory. 1 g of sample consisting of the <2 mm fraction was placed in 20 mL of a 200 mg L^{-1} Mo solution for 20 hours and then centrifuged at approximately 800 RPM for 20 minutes. Samples were then filtered through a 0.45 μm syringe filter and analyzed for pH and Mo content using a spectrophotometer.

3.4 Results and Discussion

3.4.1 Desorption Using pH Modification

All Mo concentrations measured were below the detection limit of 0.3 mg L^{-1}, indicating that little if any Mo is currently adsorbed onto these waste rock samples. However, this was expected for the majority of the samples, since the pH of the solution during the analyses were mainly above 7.7 (Table 3.2). Based on the fact that Mo only adsorbs strongly below a pH of about 6.5 with almost no adsorption above a pH of 8, it is expected that minimal sorption will occur with a solution pH of 7.5.

One sample had a pH value around 4.3, and was quite weathered with each grain being coated with iron oxides. This sample was analyzed with strictly DI water as well as by increasing the solution pH to above 8 using 1 M NaOH. Both analyses resulted in Mo concentrations below detection limit. It should be noted that a more advanced analytical method such as ICP-MS may provide a more detailed view with concentrations being so low.

It is expected that the samples obtained from the existing waste rock piles at Antamina have not been weathered long enough or had insufficient contact with Mo-rich groundwater to have a detectable amount of adsorbed molybdate. All of the samples obtained were taken from the top meter of the waste rock pile, as it was too difficult and dangerous to obtain deeper samples. Therefore, the only water to pass around the samples would be from clean rain or runoff from the top of the pile. These sources

should have low adsorbed Mo concentrations, as they would not have enough time to be in contact with Mo rich waste rock to allow leaching of Mo from molybdenite.

As well, the natural pH values of the groundwater for most of these samples quickly falls above a pH of 7.5 due to the extensive amount of carbonate material, meaning Mo will be mobile and will not preferentially adsorb onto iron oxides present. For the endoskarn sample that had a pH of around 4, it is probable that there was not enough time for Mo rich groundwater to reach that material, especially with it being located near-surface.

3.4.2 Ascorbic Acid and DI Leaches

The method of ascorbic extraction is worth discussing, since it is a novel technique applied in only a few cases in literature. Ideally, the entire experiment would be conducted within a glove box in order to ensure no oxygen presence, but the methodology applied in this case should be adequate. There was only one main stage in which nitrogen was not being bubbled through the leachate, which was during the mass measurement. This only lasted approximately half a minute though, at which point dedicated nitrogen hoses were passed into the flasks. To test the ability of the nitrogen to prevent oxygen ingress, a beaker was placed in a beaker of water. No water entered the flask due to the strength of the nitrogen bubbles, indicating that the system should be anaerobic.

Results of the ascorbic extraction and DI leach show that Mo is likely being adsorbed to HFO's (Table 3.3). Ascorbate extraction methods show relatively high Mo concentrations, especially for molybdenite-bearing waste rock. Low-grade Cu ore showed the largest amount of adsorbed Mo, followed by endoskarn and intrusive. These three rock types exhibit the highest Mo outflow concentrations in the field cells, which correlates directly to the highest Mo concentrations observed in the effluent of the fieldcells. This correlation indicates that the Mo may be loosely bonded Mo, but the DI extraction found negligible Mo, strengthening the argument of Mo adsorption onto Fe oxides. Other metals appear to be adsorbed onto HFO's, with complete data found in Table 3.4.

The ascorbic extraction results are somewhat misleading though, as there is more Mo detected than Fe for the Cu ore and endoskarn samples. This indicates that Mo must also be coming from another source or that not all of the iron hydroxides were reduced, as there cannot be more adsorbed Mo than available iron hydroxide sites.

There is no apparent correlation between Fe and Mo concentrations, indicating that adsorption sites are readily available within hornfels rocks, which have high Fe content but low molybdenite content. This is potentially a sink for Mo if rock types are mixed within the piles. However, as previously discussed it should be noted that Mo exceeded Fe concentrations for some samples.

There is some correlation observed between the grain size distribution and concentration of Mo (Table 3.5). It was hypothesized that the finer grained samples would show higher adsorbed Mo concentrations, and this is apparent for some samples. The highest Mo concentrations are found in the fine-grained material for the intrusive and marble, whereas the highest Mo was found in the mixed material for the remaining rock types. It should be noted that there was no scientific approach to determining fine versus coarse material; it was strictly done by visually selecting the desired grain size.

3.4.3 Adsorption

Mo adsorbed onto existing waste rock material as hypothesized; the endoskarn sample that had a solution pH near 4.3 adsorbed almost all Mo present in solution whereas the other samples with pH values of 7.5 and above only adsorbed a small amount of Mo. These results are consistent with previous studies determining adsorption edges onto different minerals and soils as seen in Chapter 1.

For the acidic endoskarn sample, a desorption study was conducted after the adsorption study to see if the entire Mo would desorb, returning the solution to 200 mg L^{-1}. This was, however, not the case, as the solution only returned to 44 mg L^{-1}, meaning that only about 25% of the Mo desorbed. When adding the NaOH to solution, the fine iron oxide suspension altered to a clumpy suspension, likely being the precipitation of an amorphous stage. It is therefore possible that some of the Mo was trapped (co-precipitated) in this structure.

3.5 Conclusions

Desorption studies based on increasing the solution pH did not show significant Mo-release, possibly because the material analyzed was only recently placed in the waste rock piles. No detectible molybdenum was found on the waste rock, which is expected for the hornfels and marbles as calcite dissolution increases the pH to levels where Mo adsorption is low.

The ascorbic acid extraction appeared to have successfully reduced HFO's, subsequently dissolving all adsorbed elements. However, the fact that Mo concentrations exceed Fe concentrations indicates that further research is required. Mo adsorption appears to be relatively strong, as minimal Mo was observed in a weak DI extraction. Mo adsorption is highest in rock types containing relatively high concentrations of molybdenite, due to Mo availability.

The large discrepancies between the ascorbic acid extractions and the DI-based desorption studies suggest that Mo-concentrations from the ascorbic acid extractions may not be limited to Mo sorbed on HFO. Future work should be designed to further evaluate these extraction techniques and to allow a reliable identification of the various Mo pools.

The potential for further adsorption is significant in the hornfels and marbles, because little Mo is currently being adsorbed onto HFO's that are present. This rock type does not visually have high HFO content though. With further pyrite oxidation, mixing of waste rock could appear to play a role in Mo attenuation. Precipitation is still expected to play a more dominant role, because there is only a relatively small amount of HFO's present in the waste rock, and sites will be used up quickly, as seen with high effluent concentrations in the field cells.

Table 3.1 – Field cell waste rock desorption sample descriptions

	Rock type	max Mo in fieldcell drainage (ppm)	Geological Description
Cell 5	Intrusive	30	intruvisive (pure monzonite). Contains some felspars, with minor biotites and silicates. Quartz veins present
Cell 6	Marginal Cu Ore	45	Pink endoskarn, with some intrusive. Fine calcite in the matrix.
Cell 7	Endoskarn	60	Pink endoskarn, trace instrustive. Calcite matrix
Cell 8	Hornfels	0.3	Typical grey hornfels. Scattered pyrite and pyrrhotite present, Oxidized fractures in the stratification.
Cell 14	Marble	0.7	Combinations of marble, marble diopside, grey marble and white marble. Scattered pyrite and pyrrhotite. Calcite veins. Rarely magnesium oxides

Table 3.2 – Waste rock desorption results

	Rock Type	*Description*	*Final pH*	*Desorbed Mo*
WR1	Intrusive	only very small amount of orange iron oxides visible on grains	8.82	0
WR2	Endoskarn	some small amounts of iron staining, dark grey material and wet	7.78	0
WR3	Endoskarn	very weathered. orangy-red ferric oxides, green oxidation of Cu	4.37	0
WR4	endoskarn	small amounts of Cu weathering	7.97	0
WR5	endoskarn	some distinct Cu weathering and iron oxides on larger pebbles	8.23	0
WR6	Endoskarn	red soil-like	7.82	0
WR7	marble	very clean	9.04	0
WR8	marble/ hornfels	marble/hornfels with practically no iron oxides - pyrite grains intact and clean	9.29	0
WR9	marble/ hornfels	marble/hornfels with practically no iron oxides - pyrite grains intact and clean	8.77	0

Table 3.3 – Prominent ascorbic and DI extract results

Rock type	***Mo (mg/g rock)***		***Fe (mg/g rock)***		***Mo Field cell outflow (mg L^{-1})***
	ascorbic	*DI*	*ascorbic*	*DI*	
Intrusive	0.083	0.02	0.57	0	20
Cu ore	0.431	0.03	0.12	0	40
Endoskarn	0.364	0.04	0.19	0	40
Hornfels	0.002	0.00	1.505	0	0.1
Marble	0.017	0.00	0.105	0	0.08

Table 3.4 – Ascorbic extraction results

	Sample	*rock type*	*initial pH*	*final pH*	*Ca (mg/g rock)*	*Cu (mg/g rock)*	*Fe (mg/g rock)*	*Mo (mg/g rock)*	*Pb (mg/g rock)*	*Zn (mg/g rock)*
	Cell 5-1	mix	8.28	9.28	1.200	0.001	0.537	0.081	0.024	0.135
Intrusive	Cell 5-2	coarse	8.34	9.34	1.028	0.000	0.610	0.065	0.033	0.130
	Cell 5-3	fines	8.45	9.37	1.446	0.001	0.567	0.103	0.028	0.125
	Cell 6-1	fines	8.26	9.38	1.145	0.001	0.125	0.410	0.001	0.002
Cu Ore	Cell 6-2	coarse	8.09	9.36	1.056	0.001	0.110	0.413	0.001	0.001
	Cell 6-3	mix	7.98	9.41	1.117	0.001	0.134	0.470	0.002	0.001
	Cell 7-1	fines	8.24	9.41	1.584	0.001	0.207	0.360	0.002	0.011
Endoskarn	Cell 7-2	coarse	8.24	9.28	1.075	0.001	0.184	0.319	0.004	0.001
	Cell 7-3	mix	8.28	9.39	1.093	0.001	0.189	0.413	0.002	0.002
	Cell 8-1	fines	7.92	9.30	2.528	0.001	1.557	0.002	0.023	0.013
Hornfels	Cell 8-2	mix	7.99	9.32	2.755	0.001	1.450	0.003	0.017	0.008
	Cell 8-3	mix	7.84	9.22	2.610	0.001	1.510	0.002	0.020	0.010
	Cell 14-1	fines	8.29	9.40	0.532	0.001	0.081	0.024	0.029	0.003
Marble	Cell 14-2	mix	8.16	9.08	0.791	0.002	0.134	0.013	0.018	0.003
	Cell 14-3	mix	8.18	9.47	0.514	0.001	0.098	0.012	0.013	0.002

Table 3.5 – Correlation between grain size and Mo concentration

	rock type	*Mo (mg/g rock)*
	fines	0.103
Intrusive	coarse	0.065
	mix	0.081
	fines	0.410
Cu Ore	coarse	0.413
	mix	0.470
	fines	0.360
Endoskarn	coarse	0.319
	mix	0.413
	fines	0.002
Hornfels	mix	0.003
	mix	0.002
	fines	0.024
Marble	mix	0.013
	mix	0.012

3.6 References

Amirbahman, A., Schönenberger, R., Johnson, C.A., Sigg, L., 1998. Aqueous- and solid-phase biogeochemistry of a calcareous aquifer system downgradient from a municipal solid waste landfill (Winterthur, Switzerland). Environmental Science and Technology 32, 1933-1940.

Bin-Shafique, S., Benson, C.H., Edil, T.B., Hwan, K., 2006. Concentrations from water leach and column leach tests on fly ash-stabilized soils. Environmental Engineering Science 23(1), 53-67.

Davis, J.A., Kent, D.B., 1990. Surface complexation modeling in aqueous geochemistry. Reviews in Mineralogy and Geochemistry 23(1), 177-260.

Dzombak, D.A., Morel, F.M.M., 1990. Surface Complexation Modeling: Hydrous Ferric Oxide. Wiley-Interscience, New York.

Hyacinthe, C., Van Cappellen, P., 2004. An authigenic iron phosphate phase in estuarine sediments: composition, formation and chemical reactivity. Marine Chemistry 91, 227-251.

Hyacinthe, C., Bonneville, S., Van Cappellen, P., 2005. Reactive iron(III) in sediments: Chemical versus microbial extractions. Geochimica et Cosmochimica Acta 70, 4166-4180.

Jenne, E.A., 1977. Trace element sorption by sediments and soils: sites and processes. In: W.R. Chappell and K.K. Peterson, Editors, Molybdenum in the environment, Marcel Dekker, New York, 425-553.

Kelley, D.L., Hall, G.E.M., Closs, L.G., Hamilton, I.C., McEwen, R.M., 2003. The Use of Partial Extraction Geochemistry for Copper Exploration in Northern Chile. Geochemistry: Exploration, Environment, Analysis 3, 85-104.

MacFarlane, W.R., Kyser, T.K., Chipley, D., Beauchemin, D., Oates, C., 2005. Continuous leach inductively coupled plasma mass spectrometry: applications for exploration and environmental geochemistry. Geochemistry: Exploration, Environment, Analysis 5(2), 123-134.

Roychoudhury, A.N., 2006. Time dependent calibration of a sediment extraction scheme. Marine Pollution Bulletin 52, 397-403.

Chapter 4 – Summary and Conclusions

Chapters 2 and 3 present and analyze the results for the most important the experiments conducted. However, several supporting analyses and experiments were not included, but further aid in the understanding of Mo attenuation. This chapter provides a general discussion that integrates all aspects of the research conducted with an emphasis on current knowledge and future implications. Also included is a discussion of the strengths and weaknesses along with the significance of this research.

4.1 Integration of Results

As thoroughly described in Chapters 2 and 3, the experiments conducted indicate that there are multiple processes and phases that will act as Mo sinks within neutral rock drainage. Both mineral precipitation and adsorption have shown great potential in controlling dissolved Mo concentrations, as further discussed below.

4.1.1 Precipitation

The analysis of metal molybdate precipitates was discussed in Chapter 2 and complete methodologies and analyses of the batch and column experiments can be found in Appendices 1 and 2. Results of the batch and column experiments conducted with different metals and other elements in solution confirm that the two most important precipitates that will attenuate Mo are powellite and wulfenite. Powellite is the likeliest of precipitates due to the abundance of calcium present in the waste rock piles from the dissolution of calcareous minerals. However, its formation is kinetically limited which may allow Mo to be released from the waste rock piles, if the rate of Mo-release exceeds the rate of attenuation. Experimental results indicate that there is an initial inhibition of powellite formation due to a lack of nucleation sites, but once powellite crystals start to form, Mo decreases exponentially in a batch system. Residence time is therefore an important factor in determining whether powellite formation will be controlling Mo attenuation.

The powellite column experiment (described in Appendix 2) showed that powellite would not initially precipitate in a slow advective system with a residence time of 3 days. The competition column showed that powellite initially did not precipitate, but that its rate of formation increased with time. It is therefore quite possible that the powellite column experiment would have in fact started to show Mo attenuation. Similar to the batch experiments, it is hypothesized that this initial inhibition is due to a lack of nucleation sites, and that formation occurs more quickly once initial powellite crystals are present. The powellite column was not analyzed long enough to see if this was the case.

Wulfenite formation occurred immediately, but it may not act as a major sink for Mo due to limited Pb availability in natural systems. Pb is highly insoluble under neutral pH conditions and will therefore precipitate readily, keeping aqueous Pb concentrations low (Pierrard et al., 2001). The fact that wulfenite has been found in waste rock collected from existing field cells confirms that some Pb will be sequestered in this phase; the extent will depend on Pb-release rates from the oxidation of Pb-rich minerals in the waste rock piles.

Other potential metal molybdates such as ferrous, copper, and zinc molybdates did not form within batch or column experiments. The concentrations of these metals are controlled by other processes, even though thermodynamic modeling suggests that the solution is supersaturated with respect to such metal molybdates. Malachite controlled Cu concentrations and Zn adsorption on calcite may be responsible for Zn retardation. Calculations quantifying Zn adsorption observed in the competition column experiment are found in Appendix 3. No Zn precipitates were found with XRD, indicating that further tests are required to analyze its release potential.

With powellite formation being kinetically limited, the residence time of groundwater within the waste rock piles will likely significantly affect the extent of Mo removal. It was determined from the column experiment designed to investigate powellite formation under dynamic flow conditions that the powellite precipitation rate is similar to the rate in unstirred batch experiments. Although equilibrium was never reached in the unstirred batch experiments, extrapolation of the unstirred powellite experiments indicates that Mo should decrease from 200 mg L^{-1} to an equilibrium concentration of ~10 mg L^{-1} within approximately one year; 170 mg L^{-1} of Mo was

removed after only 4 months, but the Mo removal rate prior to terminating the experiments was only 3 mg L^{-1} per month. The competition batch which initially included 100 mg L^{-1} Mo show similar precipitation rates with ~80 mg L^{-1} removal over a 2.5 month span. The good correspondence between the experiments is expected, considering that powellite precipitation rate coefficients determined in Chapter 2 are similar for these experiments.

The column for investigating Mo removal in the presence of multiple metals, however, provided near the end of its operation Mo removal rates more similar to stirred batch experiments, with approximately 100 mg L^{-1} of Mo being removed after 4 days. It is hypothesized that the fast precipitation rates are due to an abundance of available nucleation sites, likely on previously precipitated powellite crystals. Further batch experiments that contain existing powellite crystals in solution are required to test this hypothesis.

The removal rates can be related to flow path lengths, knowing average groundwater velocity. With flow expected to be dominantly in the fine-grained material in the waste rock piles, relatively slow velocities are expected. Assuming that initial Mo concentrations are ~200 mg L^{-1} and that the waste rock pile is 300 m tall, groundwater velocities of under approximately 1 m day^{-1} should allow for Mo to reach concentrations around ~10 mg L^{-1} by the end of the flow path. This calculation assumes that Mo-release only occurs near the top of the waste rock piles, which is somewhat unrealistic. Molybenite oxidation rates at Antamina need to be evaluated in order to determine the likely extent of release along the flow path.

As stated, this estimation is highly dependent on many factors such as initial Mo concentration, flow path length and the existence of preferential flow paths, availability of Ca or other competing cations such as Pb, location of the Mo source, temperature, etc. Further analyses within field-scale experiments are required to understand the potential for Mo removal.

4.1.2 Desorption

Extensive research has been conducted on Mo sorption to different materials, as summarized in the literature review of Chapter 1. However, some additional analyses

were conducted using waste rock samples from the Antamina site in order to determine whether Mo is currently being attenuated through this process and to determine the future potential for attenuation by adsorption, as discussed in Chapter 3.

A novel technique was applied to analyze the waste rock material from Antamina in order to determine whether Mo is being adsorbed to hydrous ferric oxides (HFO's), which is expected to provide dominant adsorption sites. The technique used is an ascorbic acid leach, which is a reductive dissolution approach. This approach is ideal for Antamina waste rock, as it will target the reductive dissolution of iron oxides and hydroxides, but will minimize dissolution of carbonate minerals (Roychoudhury, 2006), which comprise the bulk of the waste rock. The final solution concentrations target Mo liberated from the HFO's, but do not include Mo present within other solid phases. A deionized water leach was also conducted on these samples in order to differentiate between strongly and loosely bonded Mo.

Selective leaches are dependent on temperature, time, reagent used, and the chemical stability of the minerals within the leachate. The kinetics of such reactions will therefore determine which species reach the aqueous phase, which can typically be altered with temperature (Kelley et al., 2003). With the ascorbic acid leach being relatively new, results should be analyzed with the knowledge that such techniques are difficult and variable.

Results show that Mo is likely being adsorbed to HFO's. The amount of adsorbed Mo correlates well with the field cell outflow concentrations, with Cu ore and endoskarn waste rock showing the highest amount of adsorbed Mo as well as the highest field cell outflow concentrations. The high Fe content of the hornfels indicates that it could prove to be a potential sink for Mo, if waste rock types are mixed. Further tests are required to determine whether this is the case.

Additional sorption tests were conducted, including adsorption of Mo onto existing waste rock. Results confirm previous research, showing Mo adsorption on waste rock in solutions with pH values below 6 and no significant adsorption for pH-values above 8.

4.1.3 Rates of Precipitation and Adsorption

The precipitation of wulfenite and powellite and the adsorption of molybdate onto HFO's have been identified to act as Mo-sinks at Antamina. Many geochemical parameters including waste rock characteristics control which processes attenuate Mo. With a solution containing elevated Mo, Ca, and Pb within a medium of available HFO's, all three of the mechanisms could control Mo concentrations. Although tests in such conditions were not conducted, it is expected that wulfenite would be the first process to occur due to its fast rate of formation. If there was not enough aqueous Pb to completely remove Mo, adsorption to HFO's would also likely occur. Residual dissolved Mo would decline further due to powellite precipitation. Further tests are required to analyze this hypothesis.

4.2 Strengths and Weaknesses of Data

Although the experiments were typically based on proven methodologies that were previously employed by other investigators, there are weaknesses associated with some of the data due to unavailability of certain equipment and experimental parameters chosen.

4.2.1 Batch Experiments

The batch experiments provided a large amount of consistent data and showed trends that were previously unknown and unexpected. Their preparation was meticulous and the data was analyzed thoroughly in order to characterize the trends. There were, however, some areas that could have been improved in order to allow for additional data interpretation.

The majority of the powellite batch experiments were analyzed for pH and Mo using a spectrophotometer, as an ICP-OES was not available for a full geochemical analysis. Having the concentrations of all elements would have helped greatly so that other trends such as Ca could be analyzed within all of the experiments. Water samples from the final series of batch experiments were analyzed with a new ICP-OES, which provided the trends of the other elements in solution.

As previously discussed, measures were taken to inhibit evaporation of the solutions, but observed concentration trends show that it did play a role. A more detailed analysis of the effect of evaporation can be found in Appendix 5. Although the extent of evaporation could be estimated using conservative species, this is a weakness of the data, as the trends of some elements such as Ca could not be analyzed as it was uncertain whether the concentration changes were entirely due to evaporation or were also affected by other reactions. To further strengthen these experiments, a fully enclosed container should be used that will still allow for equilibration with atmosphere.

Finally, there is some thought that flow through cells provide more representative results than the beaker experiments conducted. This is due to the fact that concentrations always remain at maximum with the process of flow being involved. This technique is, however, also more complex. The column experiments were used to provide a representative simulation of Mo migration and attenuation in waste rock piles, so the batch experiments were strictly used to develop an initial understanding of the underlying geochemical processes. It is therefore unfair to say that the batch systems are a weakness of the research, even though a flow through batch system may be more representative.

4.2.2 Column Experiments

A main weakness of both column experiments is the fact that they were not analyzed long enough. Some components seemed to have reached equilibrium within the competition column, but others were still varying so the true equilibrium of the column is not entirely known. This provides supporting evidence that the powellite column also required further time, as Mo may have decreased once initial nucleation sites were present.

The data also indicates that there were regions of preferential flow within the column. Variability in the tracer concentrations indicates that there was not proper mixing at the inflow. Both of these processes are difficult to control, but future tests should keep this in mind.

4.2.3 Desorption Experiments

The potential strength of the methodology of the desorption experiments with ascorbic acid is still uncertain. It is theoretically the best option in determining Mo sorption onto iron hydroxides within calcareous rocks, but it is almost impossible to determine whether all iron hydroxides are reduced or if all Mo is even in solution. This has been shown to be an issue with the data obtained, as previously discussed. To strengthen the methodology further, it should be conducted within a glove box to ensure complete anoxic conditions. Further research should be conducted on this methodology in order to determine how well it works. The adsorption experiments were conducted by following the methodology of previous researchers, but a calibration of the methodology is required before trusting the results.

4.2.4 Sources of Error

Unlike a field investigation where extensive and unknown variability can affect the data, laboratory tests using mainly pure-phase material provide a relatively small amount of error with the data. The random and systematic errors involved with the batch and column experiments were decreased as much as possible.

Duplicates of samples were consistently obtained in order to reduce random error and ensure that the data was of the highest quality. Procedural blanks and standards were also analyzed. The error associated with the data from the sample procedural aspect is therefore very small, being much less than the size of the data points on the plots, which is why error bars are not present.

Systematic error was consciously thought of during the experiments. Instrumental error was minimized by using high precision equipment such as a continuously calibrated mass balance and powerful analytical instruments such as an ICP-OES. Since mass is a more precise measurement than volume with available laboratory equipment, the mass balance was used to create standard solutions and to create dilutions of samples. The batch experiments could be reproduced well, indicating the effectiveness of the techniques used.

When erroneous results were observed, the samples were either reanalyzed or the tests were conducted again. Although there is ultimately some error with the data obtained, the error associated with it is relatively small.

4.3 Significance and Contribution

The results of the experiments conducted have proved to be quite important for understanding Mo attenuation under neutral pH conditions. The data analyzed within this research provides evidence that Mo will be attenuated by powellite and wulfenite precipitation along with adsorption to iron hydroxides under neutral pH conditions. This is very important at Mo mines hosted in calcareous rocks, as it indicates that attenuation by precipitation and adsorption may limit Mo-release under these conditions. This information is useful in assessing whether there is a potential environmental concern with Mo-release and can also be utilized in the design of water treatment systems, should they be required.

This research has also brought forth more questions on the potential fate of other metals such as Zn and Cu. With the competition batch systems including both of these metals, data shows that Cu concentrations should remain low but the fate of Zn is currently unknown, indicating that further studies should be performed under similar geochemical conditions, possibly with higher Zn-concentrations.

The methodologies applied also aid the research community, as there is limited research on the ascorbic acid extraction. The data obtained in this thesis provides a different use of this method and confirms that it is an adequate method for targeting iron hydroxides. However, further work is required to determine if the method is selective for HFO only, or if other mineral phases are also dissolved. Among the experiments conducted as part of this work, the column experiments are most representative for conditions within the waste rock piles at Antamina, while still being pure-phase so as to be able to easily understand what was occurring in the column. This ultimately provided novel results, which will benefit the evaluation for the potential of Mo release at sites with similar conditions. Column experiments are also not used as often as batch

experiments due to the added complexity, so these results could potentially aid in helping future researchers perform similar experiments.

4.3.1 Applications of Research

This research has provided important insight into the potential fate of Mo within the waste rock piles at Antamina. Both powellite and wulfenite are sinks for Mo but the kinetic limitation of powellite formation and likely small amount of Pb availability will determine the extent of Mo attenuation from these phases. Further research at the field scale is needed to answer this question, but knowing that both powellite and wulfenite will form is very important. The extent of Mo removal is highly dependent on many scale- and site-dependent parameters. Although not directly applicable to predict Mo attenuation at the field scale, the results obtained through this research can be applied to delineate the likely extent of Mo removal at Antamina or similar NRD sites.

This knowledge could also be extended to a remedial approach for Mo. If outflow concentrations are found to exceed environmental guidelines, systems could be implemented that allow for an increased residence time in calcareous-rich soils to allow for powellite formation.

The results of this research are not limited to the Antamina mine, but are also applicable to other calcareous-rich environments that have a high Mo availability. Although the geochemistry of sites and mineralogy of waste rock varies greatly, this research provides further detail in understanding the fate of Mo in such regions.

4.3.2 Future Research

Not all aspects of Mo attenuation at NRD sites have been targeted with this work. Selected field cells at the Antamina mine show elevated Mo outflow concentrations, indicating that the attenuation mechanisms are not fully demobilizing Mo within the residence time in the field cells. Data obtained here indicates that the most prominent Mo sink, powellite, is kinetically limited in its formation, so further studies on powellite formation under dynamic flow conditions with an internal source of Mo (e.g. due to molybdenite oxidation) would be helpful in determining the fate of Mo in neutral drainage waste rock piles.

As discussed throughout this thesis, there are areas that require further research in order to have a comprehensive understanding of the fate of Mo under neutral drainage conditions. The replication and extended operation of some of the experiments conducted could aid in understanding Mo attenuation, including the powellite column experiment and the sorption experiments. It is likely that the powellite column was prematurely terminated, since Mo migration through the column appeared to be conservative. However, the competition column showed that this may initially be the case but once nucleation sites develop, powellite forms much more readily. It is not imperative that this experiment is analyzed again since the competition column provided similar results, but the powellite column is much simpler and could provide additional information about the formation of this phase.

Future analyses of the existing waste rock from Antamina are recommended. The extent of Mo adsorption to HFO's is unknown, but is expected to be relatively important. Further desorption and adsorption tests will aid in understanding this potential sink. Analyzing the waste rock for secondary mineral phases will also aid in bridging the gap between the laboratory experiments conducted and what occurs at the field-scale.

There currently is not any known research being conducted on Mo under neutral pH conditions, although other studies on Mo at the Antamina mine will likely occur within the University of British Columbia's Hydrogeology Group.

4.4 Concluding Remarks

Wulfenite and powellite formation along with adsorption to iron hydroxides are the likely attenuation mechanisms for Mo under neutral rock drainage conditions. Although thermodynamic models show that other metal molybdates should form (Cu and Zn molybdates), batch and column experiments simulating neutral drainage conditions did not produce such phases. These results will aid the Antamina mine when determining their closure plan. Further studies are required to strengthen the likely fate of Mo at Antamina, but knowing that there geochemical sinks for Mo exist is an important first step.

4.5 References

Kelley, D.L., Hall, G.E.M., Closs, L.G., Hamilton, I.C., McEwen, R.M., 2003. The Use of Partial Extraction Geochemistry for Copper Exploration in Northern Chile. Geochemistry: Exploration, Environment, Analysis 3, 85-104.

Pierrard, J-C., Rimbault, J., Aplincourt, M., 2001. Experimental study and modelling of lead solubility as a function of pH in mixtures of ground water and cement waters. Water Research 36, 879-890.

Roychoudhury, A.N., 2006. Time dependent calibration of a sediment extraction scheme. Marine Pollution Bulletin 52, 397-403.

Appendix 1 – Batch Experiments

A1.1 Powellite Batch Experiments

A1.1.1 Introduction

Powellite precipitation could prove to be an important sink for Mo within the waste rock piles. Essington (1990) concluded that powellite did not control Mo concentrations in spent oil shales but studies have also shown that powellite probably controls Mo in alkaline waste materials (Essington, 1992; Meima et al., 2002). The potential of powellite forming under neutral drainage conditions was still analyzed though, due to differing geochemical conditions from previous studies. Powellite requires relatively high oxidizing conditions to form, which are likely present in the waste rock piles (Hsu and Galli, 1973).

PHREEQC modelling was initially performed in order to determine the likely outcomes of systems containing elevated levels of Mo. A titration experiment was then conducted in order to determine whether powellite will precipitate under the most general conditions at Antamina, which includes elevated concentrations of sulfate from iron sulfide oxidation, molybdenum from molybdenite oxidation, and calcium due to the extensive amount of carbonate rocks. In order to do this, sulphuric acid was titrated into a molybdenum standard solution with excess calcium carbonate present.

Multiple batch experiments were subsequently conducted to analyze powellite precipitation, as discussed in Chapter 2. Each batch system was slightly altered in order to understand how different geochemical conditions affected the formation of powellite. Further batch experiments were conducted to analyze Mo attenuation in more complex systems and will later be discussed.

A1.1.2 Methodology

A1.1.2.1 PHREEQC Modelling

Multiple PHREEQC analyses were conducted to determined expected precipitates with the addition of Mo, Ca, and sulfate to a DI water solution. Multiple simulations with differing concentrations and constituents present were analyzed to look at the variability. The Reactions keyword was used to add sulphuric acid to solution in multiple

steps. The solution contained the same amount of calcite and sodium molybdate dihydrate added during the laboratory titration experiment. Powellite and gypsum were both allowed to precipitate, and atmospheric CO_2 and O_2 conditions were simulated. Further information about this modelling can be found in Appendix 6.

A1.1.2.2 Titration Experiment

A 200 mg L^{-1} Mo standard solution was created by diluting 0.2522 g of sodium molybdate dihydrate ($Na_2MoO_4 \cdot 2H_2O$, Sigma Aldrich) into 500 mL of deionized water. The solution was transferred to a beaker where 15 g of calcium carbonate ($CaCO_3$, Sigma Aldrich) was added. The beaker was placed on a magnetic stir plate to ensure thorough mixing during the titration. A pH probe was also added to the solution for measurements. The test was run in atmospheric conditions to simulate probable conditions within the waste rock piles at Antamina.

In order to represent sulfate from sulfide oxidation, 20.84 mL of 5 M sulfuric acid was titrated into the beaker to produce a final sulfate concentration of approximately 20000 mg L^{-1}. This was done over a 2 hour time period to allow the sulfate to dissolve the calcium carbonate and subsequently precipitate powellite. pH measurements were recorded every 15 to 30 seconds and the temperature of the solution was also recorded.

2 mL samples were extracted from the solution for chemical analyses after approximately 0, 0.275, 0.5, 1, 2, 3.5, 6, 10, 14, 18, and 20.84 mL of sulphuric acid was added. The samples were extracted using a 5 mL syringe and placed into vials through a 0.45 μL syringe filter. A sample of the 200 mg L^{-1} Mo solution was also taken before and after the calcium carbonate had been added. The sample obtained prior to the addition of calcium carbonate was not filtered. Duplicates were taken after 1 and 14 mL of acid was added. Duplicates were extracted using the same syringe but filtered through different filters. This was done due to the fact that it takes time to extract the solution using the syringe, and kinetics may play a role in this experiment. Another sample taken 4 minutes prior to the duplicates at the 1 mL mark was also extracted, so that it could be determined whether kinetic limitations over the minute scale played a role.

All samples were analyzed using a Hach DR-2400 Spectrophotometer using the high resolution setting (0.3-40 mg L^{-1} detection). 9.5 mL of deionized water along with

0.5 mL of sample were added to acid washed vials and mixed to provide a 20 times dilution. Sample duplicates, blanks, and standards were analyzed for quality assurance purposes.

A1.1.2.3 Batch Experiments

0.2522 g of sodium molybdate dihydrate was added to a 500 mL volumetric flask containing deionized water to create a 200 mg L^{-1} Mo solution. The standard solution was added to beakers ranging from 250 mL to 1 L, followed by the addition of 5 M sulphuric acid to create differing SO_4 concentrations, depending on the batch. $CaCO_3$ was then added; enough $CaCO_3$ was added using either calcite powder (Sigma Aldrich) or marble sand (Lafarge Ltd) to ensure a constant saturation of calcite.

The beakers were covered with Parafilm with only a small opening to allow gas exchange in order to promote open system conditions. All batches remained at room temperature for the extent of the experiment. Samples were obtained throughout the experiment, ranging from 1 to 3 mL. A syringe was used to extract the samples, which were then passed through a 0.45 μm Millipore syringe filter, acidified with nitric acid to ensure a pH below 2 and stored at 4^{o}C. Most samples were analyzed for Mo using a Hach D2400 spectrophotometer. Pow 6 and Pow 7 were analyzed using a Varian ICP-OES. pH of the solution was monitored for each sample and alkalinity was determined at the end of select experiments.

A1.1.3 Results and Discussion

A1.1.3.1 PHREEQC Modelling

Results from the analyses conducted using PHREEQC all show that powellite should precipitate readily and drastically reduce aqueous Mo concentrations. The main analysis conducted was a copy of the titration experiment, in which 20000 mg L^{-1} of sulfate was added in steps to a solution containing 200 mg L^{-1} Mo and excess calcite. The results show that Mo concentrations are reduced to concentrations of 0.73 mg L^{-1} with a SO_4 concentration greater than 2000 mg L^{-1} (Figure A1.1). Another analysis was conducted in order to resolve the first portion of the curve (Figure A1.2).

These results clearly show that powellite should form under the generalized conditions present at Antamina. They also show that powellite should form prior to gypsum ($CaSO_4 \cdot 2H_2O$), as gypsum's saturation index remains below 0 until 1650 mg L^{-1} of sulfate are added (Figure A1.3). However, this does not seem to be the case within the laboratory, as discussed later. The pH of the system remains basic for the duration of the experiment, which is expected due to the excess calcite in the system. Prior to sulfate addition, the pH is neutral, and then jumps to 8.7 with the addition of 40 mg L^{-1} sulfate. The pH drops until it reaches 7.75 after 1650 mg L^{-1} of sulfate has been added. These values correspond to the pH values measured in the kinetic cells and field cells at Antamina (Golder, 2004).

A1.1.3.2 Titration Experiment

Results from the titration experiment did not correspond to the PHREEQC analyses; the concentration of every sample obtained was still 200 mg L^{-1} Mo, indicating that kinetic limitations are likely occurring. During the experiment, it was apparent that calcite was being dissolved due to the large amount of bubbling from CO_2 formation. Subsequent addition of acid did not occur until the pH of the solution stabilized, but gas formation was still occurring even once the pH was constant. It is therefore probable that more time is required to reach equilibrium. Due to these results, the kinetic limitation batch experiments were conducted and analyzed over a much longer timeframe.

The pH of the system was also quite different from those produced in PHREEQC. With only a small amount of sulfate addition (just under 100 mg L^{-1}), pH values measured around 7.74 were somewhat comparable with the PHREEQC results, but with further sulfate addition the pH reached a low of 5.48. Figure A1.4 shows how pH varied with sulphuric acid addition during the experiment. Similarly to Mo concentrations, it is expected that pH values would eventually reach basic conditions with enough time. There was likely just not enough time for the calcite to dissolve and buffer the system.

The final precipitate was analyzed a few days after the completion of the experiment using X-Ray Diffraction. The precipitate was composed mainly of gypsum and calcite with only a small portion of powellite present. These results contradict with

those in PHREEQC, as it was found that powellite should precipitate before gypsum. However, this is probably due to kinetics, as there may not have been enough time for powellite to form when it preferentially would (i.e. below 1650 mg L^{-1} of SO_4^{2-}). Due to this observation, a kinetic limitation experiment with only 1000 mg L^{-1} sulfate was first completed.

A1.1.3.3 Batch Experiments

These results have been discussed in Chapter 2, but will be expanded upon here. The powellite batch experiments all followed a similar trend (Figure A1.5). Initial inhibition prevented Mo from decreasing for the first day and then an exponential decrease is observed until equilibrium is reached. Altering the parameters within the solution, such as sulfate concentration, slightly alters the rate of powellite precipitation, but the primary factor influencing precipitation is whether the system is stirred or not. The stirred systems all begin precipitation much earlier and reach equilibrium within weeks, whereas the unstirred systems took much longer for Mo to reach equilibrium.

The pH of all calcite-bearing systems equilibrated at 7.78 ± 0.05, directly relating to pH values observed in the waste rock piles at Antamina. Initial equilibration time of pH varied between the stirred and unstirred batch experiments, as expected. The stirred experiments equilibrated within approximately 24 hours whereas an unstirred system took at least twice as long.

Saturation indices calculated using PHREEQC indicate that powellite is consistently supersaturated for all batch experiments containing calcite (Figure A1.6). Powellite saturation decreases with time due to the Mo decrease. Even with Ca increase during the second half of the batch experiment, powellite saturation remained constant, signifying that there was always a large enough calcium source.

A system of purely dissolved Mo and Ca produce quicker powellite precipitation and a lower Mo equilibrium concentration than the more complex solutions including SO_4 and calcite, indicating that aqueous complexes may prevent Mo from reaching concentrations below 1 ppm. PHREEQC indicates that concentrations of all batch systems should reach approximately 0.7 ppm, but the fact that the complex batches do not is likely due to complexes not accounted for in the database.

Powellite saturation indices for the system containing purely dissolved Mo and Ca show similar trends to those observed in the other batch systems, except that saturation falls below 0 in this experiment, equilibrating around -0.3 with calculated Mo concentrations of 0.3 ppm (Figure A1.7). This experiment indicates that powellite is an exceptional sink for Mo under the simplest of conditions, assuming residence time is long enough. Mine drainage is typically complex with hundreds of dissolved species, which will likely alter these results. Even by adding SO_4 and calcite, Mo concentrations do not reach such low concentrations within the same amount of time.

The above factors are important when relating the experimental results to the waste rock piles at Antamina, as the flow within the piles will likely act more like an unstirred environment with relatively low flow rates. As well, the water composition is quite complex with high dissolved content, possibly inhibiting Mo precipitation and keeping concentrations above guidelines.

For batch experiments containing 1000 ppm SO_4, gypsum or any other sulfate phase is not expected to precipitate. Small amounts of gypsum have been found in XRD for these systems (Table A1.1), but not enough to significantly reduce SO_4 concentrations. Gypsum is found in relatively high amounts for systems with 2000 ppm and higher, as predicted by PHREEQC.

Ca concentrations were measured for one of the batch experiments (Figure A1.8). Initial concentrations are high at ~480 ppm due to the dissolution of calcite from the sulphuric acid. Ca concentrations decrease at a similar rate to Mo until powellite precipitation rates diminish, at which point Ca concentrations flatten out and slowly increase again. The majority of this increase is likely due to evaporation rather than calcite dissolution.

A1.1.3.4 Evaporation

PHREEQC simulations indicate that calcite saturation remained above zero, being calculated both by assuming a charge balance of C(4) and by utilizing the obtained alkalinity value (Figure A1.9). This provides evidence towards the fact that the Ca increase during the batch experiment was likely due to evaporation and not further calcite dissolution. As well, this indicates that calcium concentrations exceeded expected values

since saturation indices are above 0. This is potentially due to excess calcite dissolution from the quick addition of sulphuric acid at the start of the experiment.

Na concentrations provide further evidence towards evaporation affects. Na is a non-reactive species in these systems, although minor complexes may be present. An increase of Na is observed with time to concentrations well above the initial amount (Figure A1.10). This trend is also observed with the batch experiments containing 1000 ppm SO_4.

Mo and Ca results are therefore also affected by evaporation, but results have not been corrected for this since a single evaporation correction factor could not be determined to normalize both the Na and SO_4 concentrations, as further discussed in Appendix 5. The plots should therefore be analyzed knowing that evaporation is affecting the trends. It will hardly affect the Mo trend, as Mo decreased to low concentrations within a relatively short amount of time; correcting for evaporation will just make the exponential decrease slightly more prominent. Final Mo concentrations will be slightly lower as well. The Ca trend is more significantly affected by the evaporation trend as previously discussed, since concentrations are quite high.

A1.1.3.5 Kinetic limitations

The initial inhibition of powellite formation is likely explained by availability of nucleation sites. Tweet (1958) analyzed the affect of nucleation sites and determined that precipitation of Cu could be occurring on oxygen or some other unknown species, nucleation could be homogenous where Cu fits into the lattice without any help from localized regions of decreased free energy due to defects in the crystal lattice, or nucleation could occur on point defects in the lattice. It is unknown whether powellite initially crystallizes on calcite grains, the side of the beaker, or strictly within the aqueous phase so it is therefore unknown as to why this inhibition is occurring.

The reasoning behind the kinetic limitations of powellite formation was also not thoroughly evaluated. Tweet (1957) describes the kinetic limitations of Cu precipitates from a supersaturated solid solution in crystals of Ge. Cu decreased in a similar exponential decay fashion, indicating that similar processes may be occurring within the powellite batch systems. Tweet found that the expected rate limiting step is the process

of dissociation of a substitutional Cu into a vacancy and an interstitial Cu atom. This process may also be occurring for Ca in the powellite crystal lattice, but is unknown without further analyses.

A1.1.4 Conclusion

Powellite could act as a prominent sink for Mo. More complex solutions affect the effectiveness of Mo removal by powellite, with excess calcite and SO_4 resulting in higher aqueous Mo equilibrium concentrations. Residence time of Mo-rich water in the waste rock pile will also determine how dominant of a sink powellite is, as its precipitation is kinetically limited. Initial nucleation sites are required before relatively quick precipitation occurs, but it follows an exponential decrease, with slower Mo removal as it reaches lower concentrations. The reasoning behind this is not fully understood, but initial inhibition is likely due to a lack of nucleation sites.

The difference between stirred and unstirred batch systems is fairly large. An unstirred batch system takes a vast amount more time to reach equilibrium than a stirred system, which only takes approximately a month. Flow through a waste rock pile is expected to more closely resemble an unstirred batch system, indicating that powellite may not form before groundwater flows out of the piles, depending on residence times.

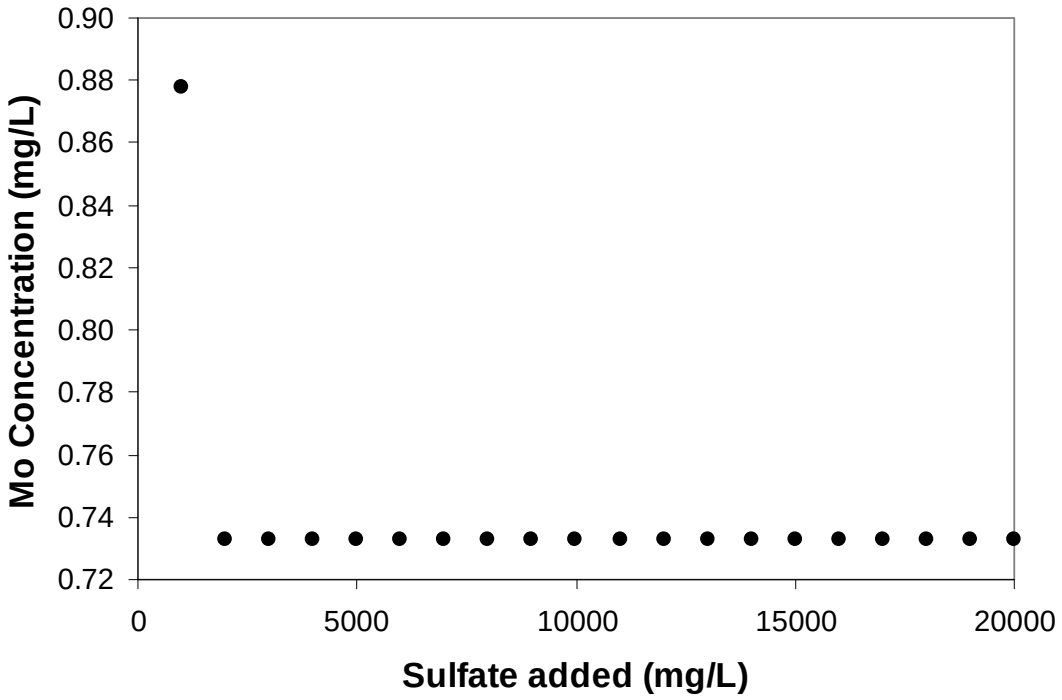

Figure A1.1 – PHREEQC titration experiment to analyze powellite precipitation (initial Mo concentration of 200 mg L^{-1})

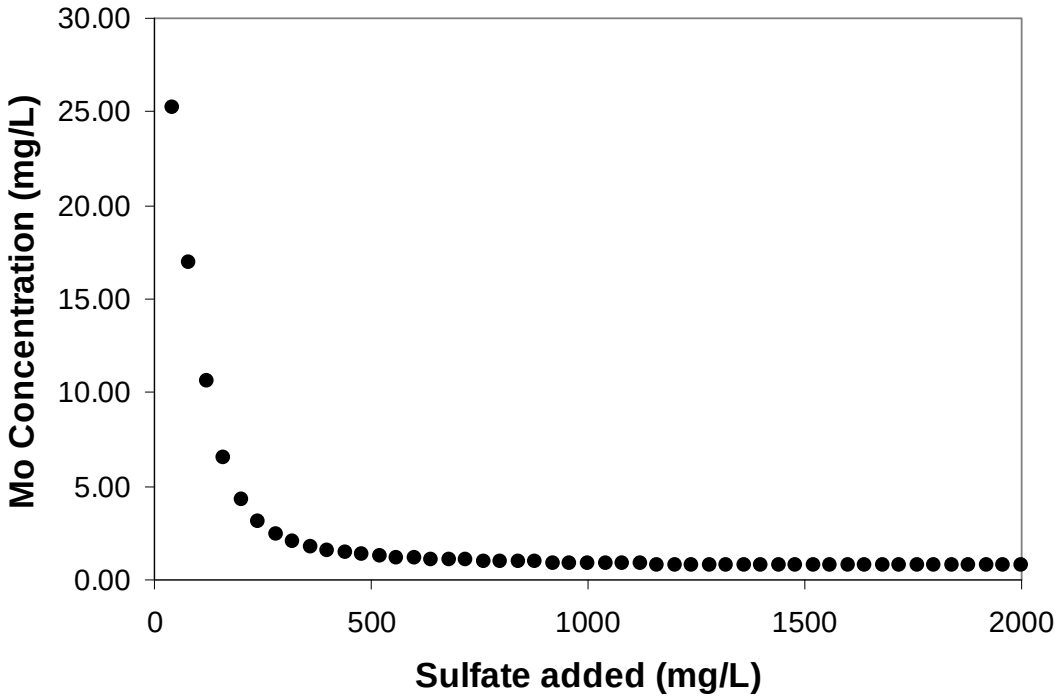

Figure A1.2 – PHREEQC powellite titration experiment up to 2000 mg L^{-1} SO_4

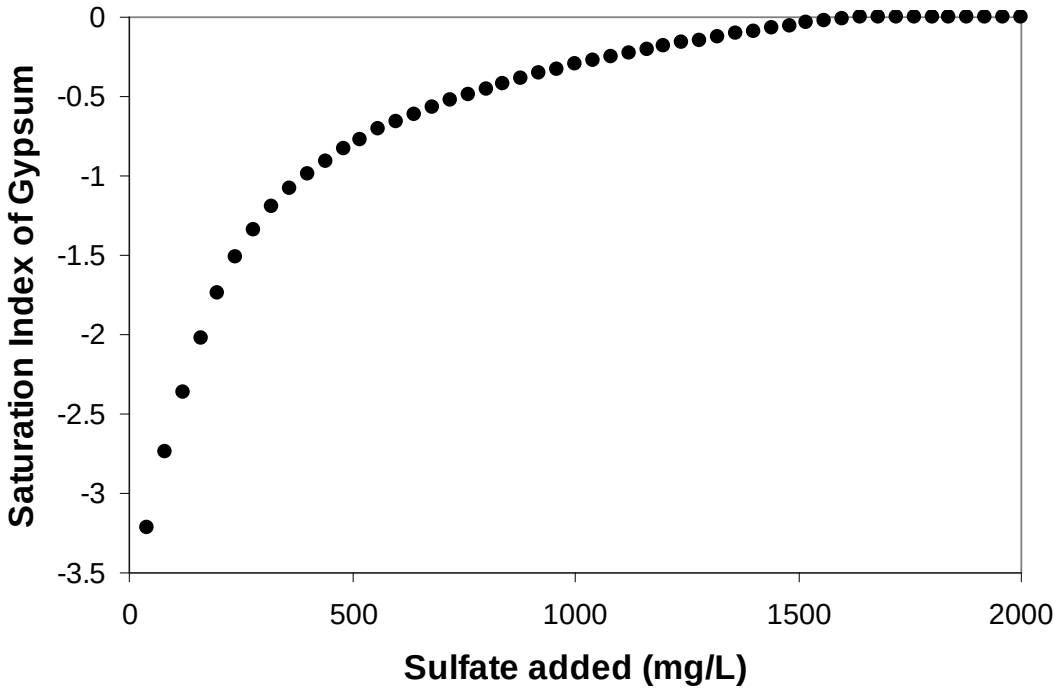

Figure A1.3 – Saturation indices of gypsum during titration simulation of 2000 mg L^{-1} SO_4

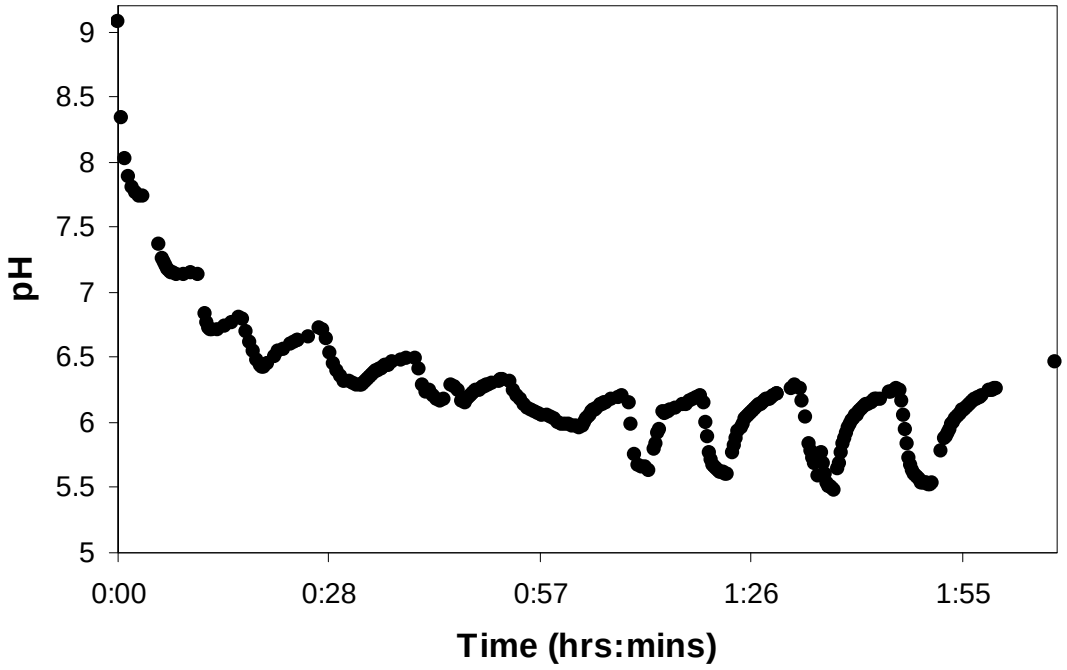

Figure A1.4 – pH variation with sulphuric acid addition during titration experiment

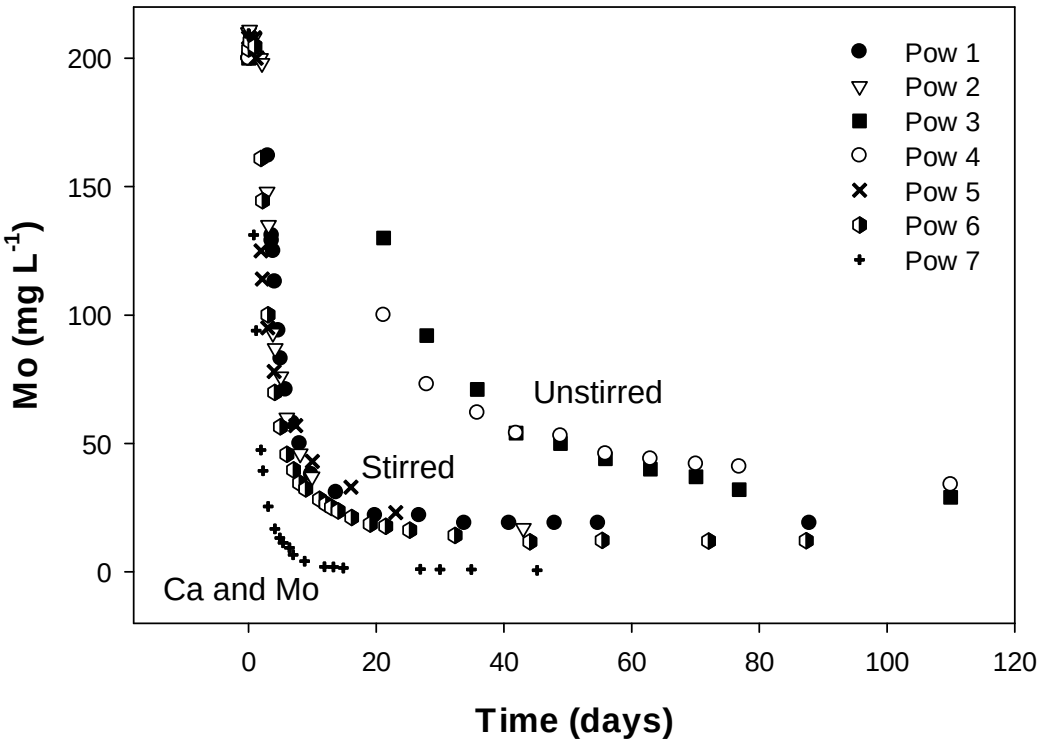

Figure A1.5 – Powellite precipitation batch experiments

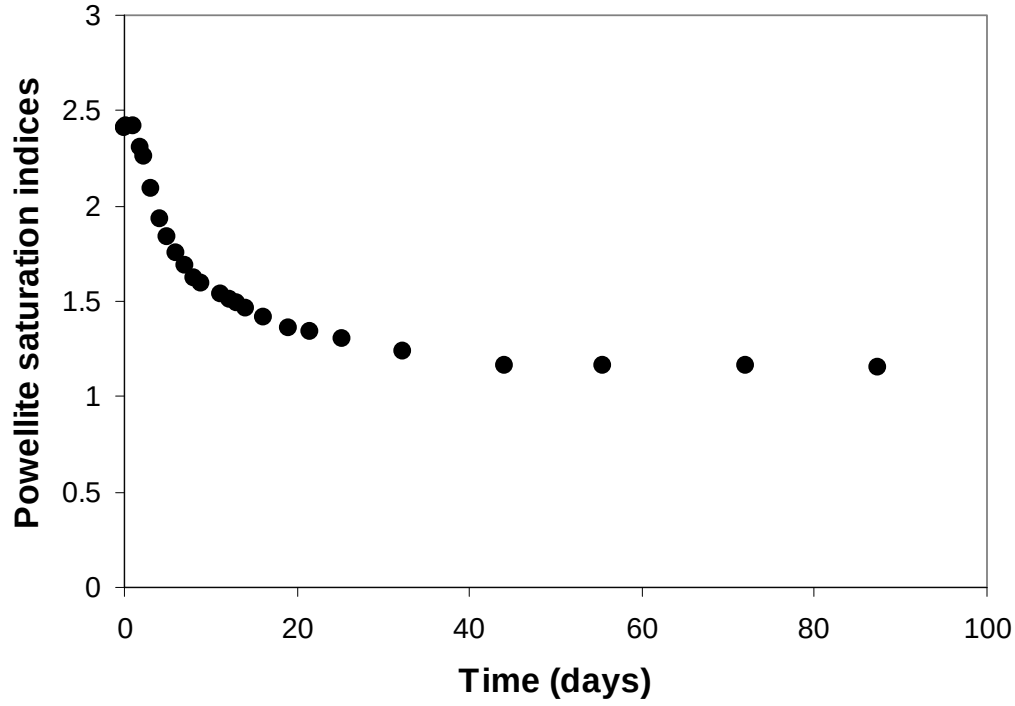

Figure A1.6 – Powellite saturation indices for Pow 6

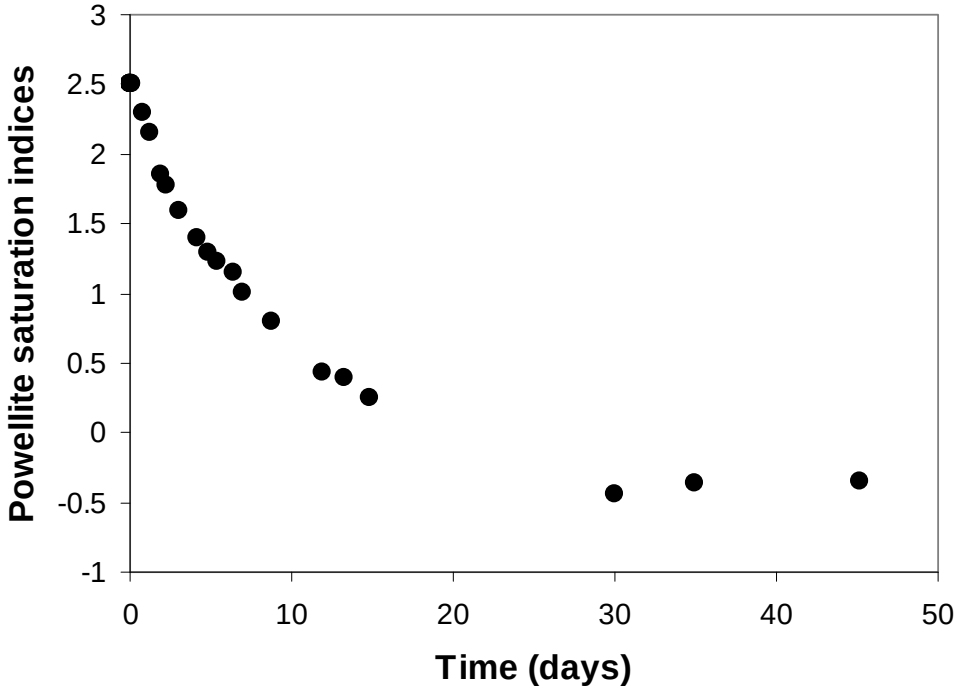

Figure A1.7 – Powellite saturation indices for Pow 7

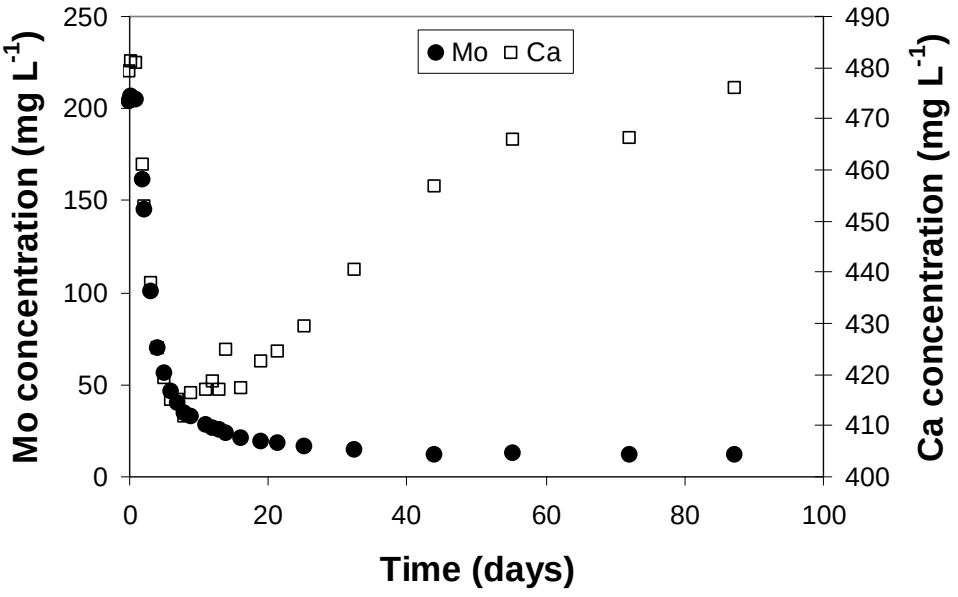

Figure A1.8 – Pow 6 results

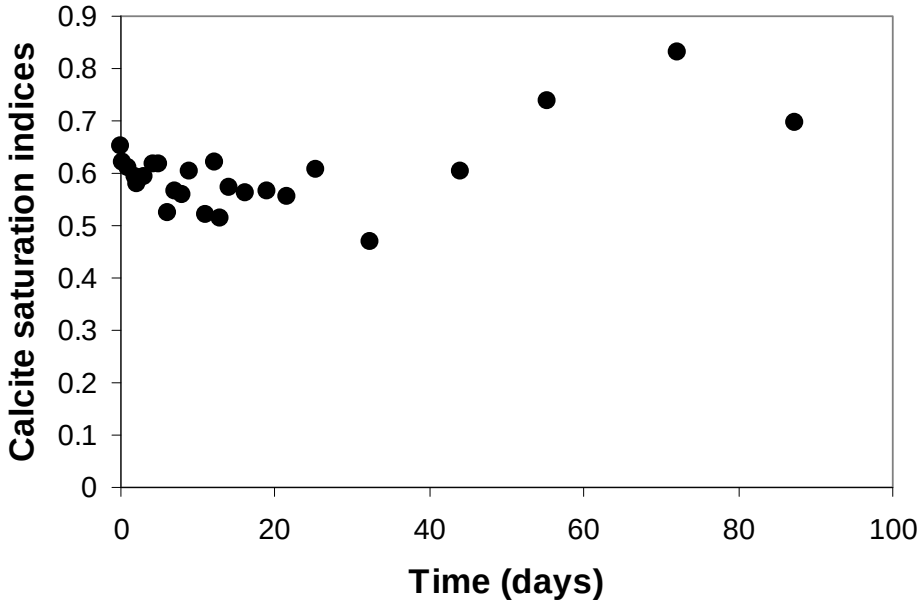

Figure A1.9 – Calcite saturation indices for Pow 6, assuming a charge balance of C(4)

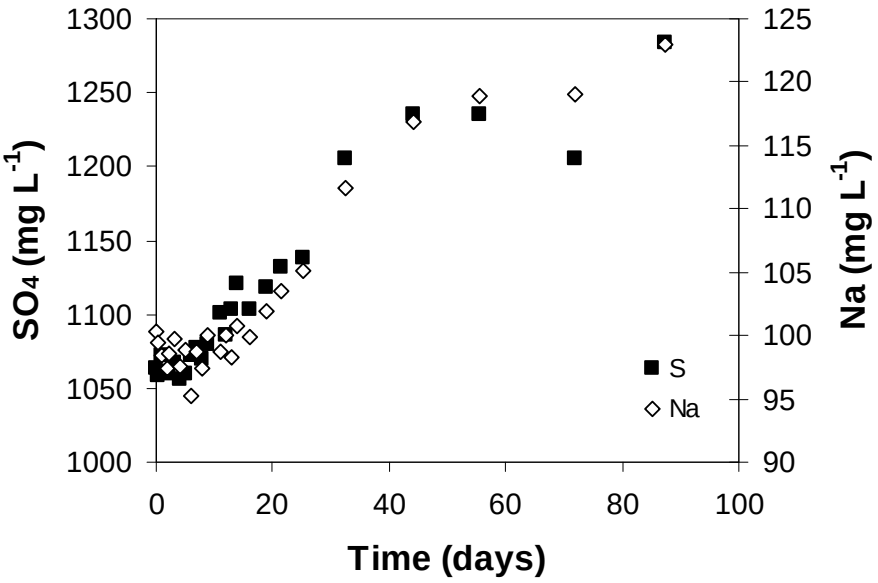

Figure A1.10 – Conservative species concentrations for Pow 6 batch experiment

Table A1.1 – XRD results for powellite batch experiments (all values in %)

	Powellite	***Gypsum***	***Calcite***
Pow 1	2.6	0	97.4
Pow 2	2.8	0	97.2
Pow 3	1.6	4.6	93.8
Pow 4	79.4	0.6	20
Pow 5	Relatively large	Small	Yes
Pow 6	Relatively large	Small	Yes
Pow 7	Yes	No	No

A1.1.5 References

Essington, M.E., 1990. Calcium Molybdate Solubility in Spent Oil Shale and a Preliminary Evaluation of the Association Constants for the Formation of $CaMoO_4^0$(aq), $KMoO_4^-$(aq), and $NaMoO_4^-$(aq). Environmental Science and Technology 24(2), 214-220.

Essington, M.E., 1992. Fluorine and molybdenum solubility relationships in combusted oil shale. Journal of Environmental Science and Health A27, 547–564.

Golder Associates Ltd, 2004. Final Version 4.0, Waste Rock Geochemistry – Phase 2, Antamina Mine Peru. Mississauga, ON.

Hsu, L.C., Galli, P.E., 1973. Origin of the Scheelite-Powellite Series of Minerals. Economic Geology 68, 681-696.

Meima, J.A., van der Weijden, R.D., Eighmy, T.T., Comans, R.N.J., 2002. Carbonation Processes in Municipal Solid Waste Incinerator Bottom Ash and their Effect on the Leaching of Copper and Molybdenum. Applied Geochemistry 17, 1503-1513.

Tweet, A.G., 1957. Precipitation of Cu in Ge. Physical Review 106(2), 221-224.

Tweet, A.G., 1958. Precipitation of Cu in Ge. II. Supersaturation Effects. Physical Review 111(1), 57-66.

A1.2 Wulfenite Batch Experiments

A1.2.1 Introduction

Wulfenite ($PbMoO_4$) could prove to be a prominent sink for Mo depending on Pb availability, as it is one of the most stable Mo minerals (Vlek and Lindsay, 1977). It has been studied extensively and is thought to control Mo concentrations at existing mining sites (Rosemeyer, 1990; Bideaux, 1990; Wang et al., 1994) and is expected to control Mo concentrations in alkaline soils (Vlek and Lindsay, 1977; Reddy and Gloss, 1993). Batch tests analyzing the likelihood of wulfenite precipitation were therefore conducted to determine if it is a potential Mo sink at Antamina.

A1.2.2 Methodology

Five stirred batch systems were analyzed (Table A1.2). Pb and Mo was added as $Pb(NO_3)_2$ and $Na_2MoO_4 \cdot 2H_2O$ (Sigma Aldrich). Standard solutions were created in separate volumetric flasks and added together at time t=0. SO_4 was added with 5 M sulphuric acid to the Mo standard solution for the Pb, Mo, SO_4 batches. NaOH was added to the third batch of this kind in order to increase the pH to near-neutral conditions. Samples were obtained periodically and pH was constantly measured. Samples were filtered, acidified, and stored at 4^oC until analysis using ICP-OES. Alkalinity was obtained at the end of the batch containing calcite. Calcite was subsequently added to the Pb and Mo batch system after wulfenite did not precipitate.

A1.2.3 Results and Discussion

A1.2.3.1 Pb and Mo

Wulfenite batch tests provided both expected and unexpected results. A system including solely dissolved Pb and Mo surprisingly did not precipitate wulfenite. pH of the system remained constant around 6.25, Mo remained at 200 ppm, and Pb jumped around from 9 to 18 ppm (Figure A1.11). Visually, the solution remained clear with only faint particles observed, while being stirred. PHREEQC predicts wulfenite to form completely, reducing Pb concentrations to 0 ppm, but the lack of available nucleation

sites is the probable explanation why this is not the case. To test this hypothesis, $CaCO_3$ in the form of crushed marble was added to the solution. Pb concentrations decreased immediately, along with an equivalent amount of Mo to produce wulfenite. pH increased accordingly and small amounts of Ca were added to solution. Wulfenite precipitation could therefore be attributed to nucleation site availability or pH change, which will be discussed later.

A1.2.3.2 Mo, Pb, $CaCO_3$

A system similar to the end of the previous test was conducted, which included Mo, Pb, and excess calcite. Wulfenite precipitated immediately, removing all 20 ppm of Pb within the first 15 minutes of the experiment (Figure A1.12). The batch was continued to determine the potential of further Mo removal. Powellite precipitation continued with a fairly linear Mo precipitation rate. The rate of removal was much slower than the previous powellite batch systems, as Ca concentrations were quite low due to the lack of sulphuric acid present. The lack of sulphuric acid also allowed for a higher alkalinity than other batch systems, being 4 meq L^{-1}. Ca concentrations decreased in the same fashion as Mo, with similar evaporation trends to that of the powellite batches observed with time. Some of the increasing trend can be attributed to calcite dissolution though, as saturation indices of calcite remained below 0 (Figure A1.13). Ca did not increase drastically though since calcite dissolution is relatively slow.

The calculated pCO_2 of the system is -3.4 using a charge balance of C(4) and -3.05 using a measured alkalinity value, which is relatively close to the expected value of -3.5 for an open system in equilibrium with atmosphere. A discussion of the approach used for calculating the saturation indices using a charge balance of C(4) and alkalinity values is found in Appendix 6. This batch can attain atmospheric equilibrium more easily than the systems with sulphuric acid, as there is much less calcite dissolution, allowing for less carbonate dissolution that requires degassing to reach equilibrium.

A1.2.3.3 Ca, Mo, SO_4

Calcite was removed for one of the experiments to determine if it played a role in wulfenite precipitation. Pb was completely removed from the aqueous phase within 30

minutes, with it decreasing from 20 ppm to ~0.5 ppm within the first minute (Figure A1.14). Mo concentrations were also decreased, indicating the likelihood for wulfenite precipitation. The yellowish precipitate was determined to be wulfenite using XRD. The pH of the solution remained around 2 due to the lack of a buffer such as calcite.

Another test where the pH was increased using NaOH was therefore conducted. Aqueous Pb was completely removed within seconds, but the precipitate was whiter, and determined to be approximately 50% wulfenite and 50% anglesite using XRD. This is likely due to the fact that Pb and Mo were added as salts rather than aqueous solutions. Due to this, Pb preferentially forms anglesite with SO_4 as it is readily available, whereas Mo first has to dissolve before wulfenite can be formed. The fact that some wulfenite does form at pH 7 is positive in determining whether Pb is a potential sink for Mo.

The methodology of the batch experiments has determined to be quite important. Whether the Pb and Mo are added as solid phases and mixed quickly together, or whether the species are added as concentrated solutions determined whether wulfenite or a wulfenite-anglesite mix formed. Two identical systems were created, with approximately 200 ppm Mo, 20 ppm Pb, and 1000 ppm SO_4. The Mo and Pb were added as solid-phase crystals for one of the batches and as a dissolved phase for the other batch. The first batch produced a yellowish precipitate, which was mainly wulfenite, whereas the second batch produced a whiter precipitate, which included some anglesite. The test was conducted both at regular pH of ~2 as well as 7.3, after increasing it using 1 M NaOH.

These results are important when analyzing the data of the more complex batch experiments. Although this was the case in a simpler system, it isn't necessarily the only outcome. Wulfenite was the sole Pb precipitate determined by XRD in the competition batch and competition column experiments, where Pb and Mo were added as solutions. It is possible that the addition of $CaCO_3$ affects the outcome, as both of the competition experiments included crushed marble. As well, the batch experiment containing Pb, Mo, and $CaCO_3$ also precipitated wulfenite. It is therefore expected that wulfenite is the likely precipitate with the conditions at Antamina.

A1.2.3.4 pH and Nucleation Affects

As discussed, the batch tests conducted all vary in equilibrium pH (Table A1.3). Wulfenite precipitated almost immediately in the Pb, Mo, $CaCO_3$ system as well as the Pb, Mo, SO_4 system, even with pH's varying from 8.35 to 2.02, respectively. The Pb and Mo system did not precipitate wulfenite until $CaCO_3$ was added. Due to the fact that this system's pH was between that of the other two batches, the reason that wulfenite did not precipitate is unlikely due to pH. A lack of nucleation sites available for wulfenite to precipitate in the Pb and Mo system is more of a likely answer, but one can then pose the argument that this was not an issue for the Pb, Mo, and SO_4 system which are all dissolved species as well. Further studies were not conducted to determine the reasoning of this, but it is likely that the required nucleation energy was not exceeded for this experiment.

A1.2.4 Conclusion

Wulfenite precipitation is a potential sink for Mo, depending on Pb availability. Precipitation occurred almost immediately, meaning it could play a more important role than powellite due to its kinetic limitations. Pb availability is the ultimate problem, as there are not many lead-rich minerals present in the waste rock piles. As discussed in Chapter 2, the determination of wulfenite in waste rock samples using the MLA provides evidence towards this being the case, but wulfenite is still expected to be a secondary sink for Mo, after powellite.

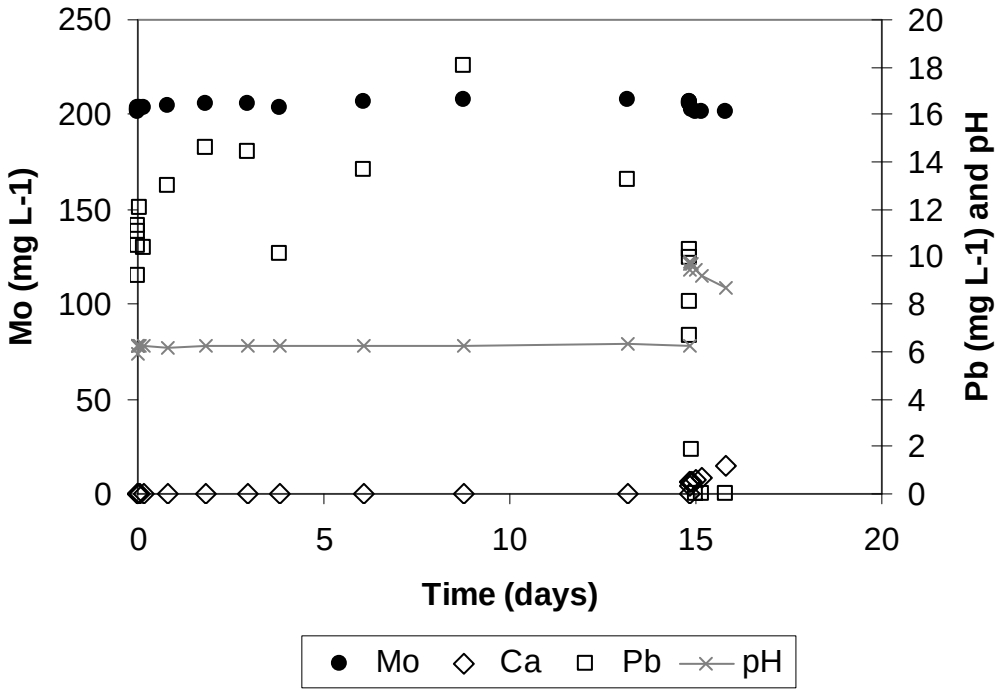

Figure A1.11 – Pb and Mo batch experiment results

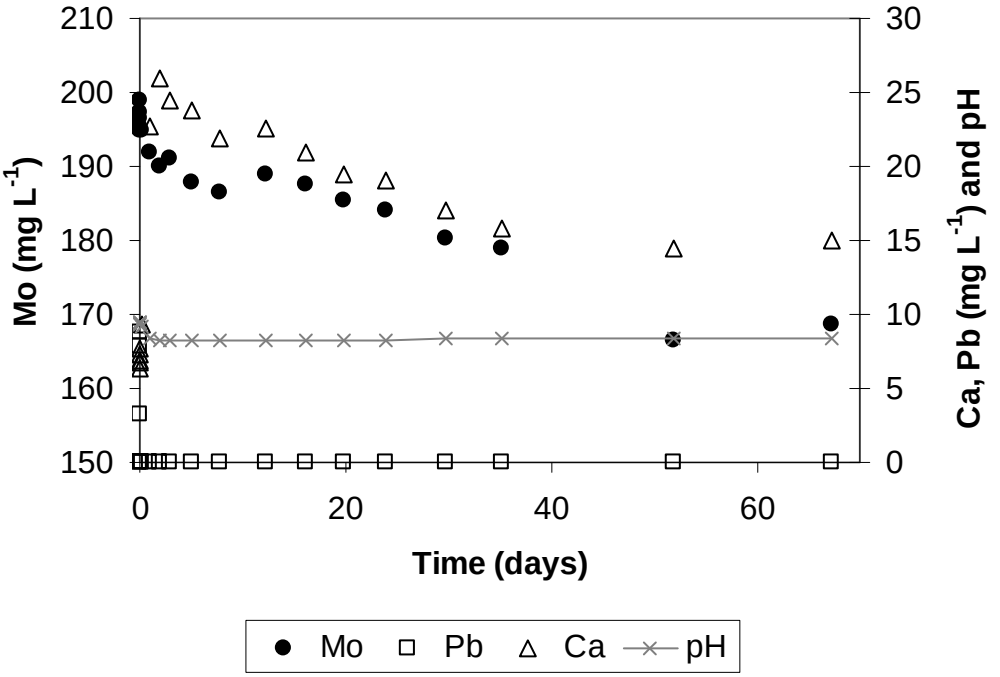

Figure A1.12 – Pb, Mo, $CaCO_3$ results

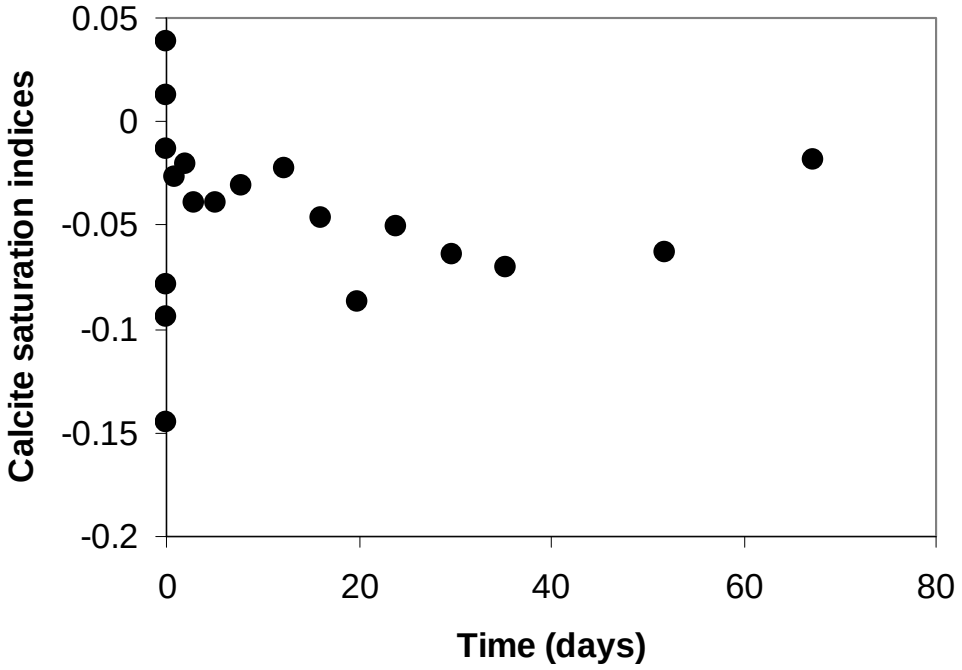

Figure A1.13 – Calcite saturation indices for Pb, Mo, $CaCO_3$ batch

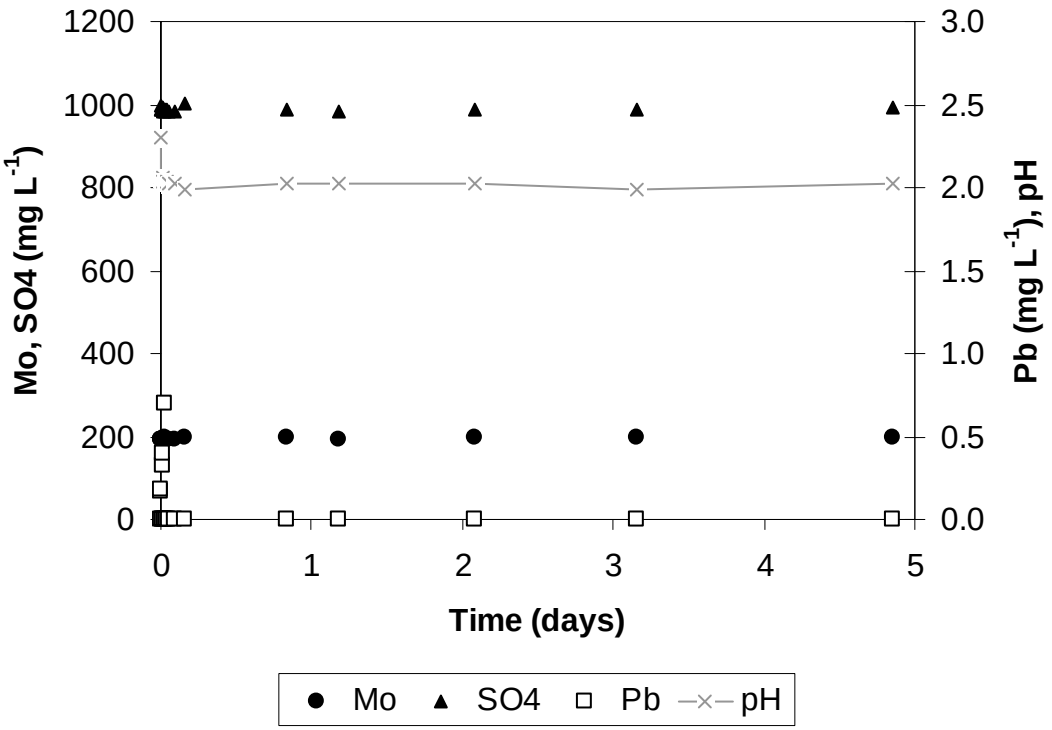

Figure A1.14 – Pb, Mo, SO_4 batch results

Table A1.2 – Wulfenite batch experiments

Batch	*Pb (mg/L)*	*Mo (mg/L)*	*$CaCO_3$*	*SO_4 (mg/L)*
Pb and Mo	20	200	crushed marble, added later	
Pb, Mo, CaCO3	20	200	Excess calcite powder	
Pb, Mo, SO4 1	20	200		1000
Pb, Mo, SO4 2	100	200		1000
Pb, Mo, SO4 3	100	200	0, but pH increased to 7 using NaOH	1000

Table A1.3 – Equilibrium pH of batch systems

Batch	*pH*
Pb and Mo	6.26
Pb, Mo, CaCO3	8.35
Pb, Mo, SO4 1	2.02
Pb, Mo, SO4 2	1.98
Pb, Mo, SO4 3	7.03

A1.2.5 References

Bideaux, R.A., 1990. The desert mineral: Wuifenite. Rocks and Minerals 65, 11-30.

Reddy, K.J., Gloss, S.P., 1993. Geochemical speciation as related to the mobility of F, Mo and Se in soil leachates. Applied Geochemistry 2 Suppl. Issue, 159-163

Rosemeyer, T., 1990. Wulfenite occurrences in Colorado. Rocks and Minerals 65, 58-61.

Vlek, P.L.G., Lindsay, W.L., 1977. Thermodynamic stability and solubility of molybdenum minerals in soils. Soil Science Society of America Journal 41, 42-46.

Wang, L., Reddy, K.J., Munn, L.C., 1994. Geochemical Modeling for Predicting Potential Solid Phases Controlling the Dissolved Molybdenum in Coal Overburden, Powder River Basin, WY, U.S.A. Applied Geochemistry 9, 37-43.

A1.3 Iron Molybdate Batch Experiments

A1.3.1 Introduction

Relatively insoluble ferrous molybdate ($FeMoO_4$) can form under the right conditions when Fe and Mo are in solution (Branam, 1999; Salminen, 2005). Under acidic conditions, $FeMoO_4$ forms readily after the oxidation of molybdenite (MoS_2). Iron scavenges Mo in solution and therefore acts as a control of Mo solution concentration (Branam, 1999). Another possibility is the formation of ferrimolybdite ($Fe_2^{3+}(MoO_4)_3 \cdot 8H_2O$), which is a secondary mineral associated with hydrothermal veins and molybdenum porphyry deposits (Mineral Data Publishing, 2005). It has previously been found as a possible Mo sink downstream of mine tailings (Langedal, 1997).

It is unexpected that ferrous molybdate can precipitate under the near-neutral conditions at Antamina. Iron concentrations are very low within the field cells due to a solubility control by ferrihydrite. Additionally, aerobic conditions are expected within the pile, which will oxidize any ferrous iron to ferric iron which subsequently precipitates out of solution. It is therefore unlikely that ferrous molybdate will be a sink for Mo, but PHREEQC analyses were performed along with a simple pure phase experiment to determine its potential.

A1.3.2 Methodology

A1.3.2.1 PHREEQC Models

Geochemical modelling was initially completed in order to determine whether iron molybdate should precipitate with the conditions present at Antamina. Different scenarios were conducted to more thoroughly examine the possibilities.

A1.3.2.2 Laboratory Experiment

A single pure phase experiment was conducted to simulate one of the models created in PHREEQC. A 200 mg L^{-1} Mo solution was created in a beaker by diluting 0.1261 g of $Na_2MoO_4 \cdot 2H_2O$ with 250 mL of deionized water. 0.0498 g of iron(II) sulfate heptahydrate ($FeSO_4 \cdot 7H_2O$, MW 278.01456 g mol^{-1}, Fluka) was added to the beaker, which is equivalent to 40 mg L^{-1} Fe and 68.8 mg L^{-1} of sulfate. The beaker was stirred

for the first 30 minutes and then left under atmospheric conditions at room temperature. Mo concentration was measured 10 minutes and 60 minutes after the solution was created, followed by measurements every few days. The samples were passed through a 0.22 μm filter and diluted 10 times before analyses on the Hach DR-2400 Spectrophotometer using the high range program.

A1.3.3 Results and Discussion

A1.3.3.1 PHREEQC Models

The models created all did not precipitate a significant amount of iron molybdate, indicating that even if Fe was present in solution, this would not be a sink for Mo at Antamina. The only experiments that significantly reduced Mo concentrations were those where calcite was present, as powellite precipitated out due to the presence of Ca in solution from the dissolution of calcite within the acidic solution.

The model that simulates the laboratory experiment conducted equilibrated with a final Mo concentration of 199.97 mg L^{-1} and a pH of 4.73. All of the initial 40 mg L^{-1} of ferrous iron oxidized to ferric iron and precipitated ferrihydrite. This is consistent with the conditions observed within the field cells at Antamina, as Fe concentrations are close to instrumental detection level (Golder, 2007).

A1.3.3.2 Laboratory Experiment

As expected, Mo concentrations remained near 200 mg L^{-1} for the extent of the experiment. The solution became slightly red after about half an hour, which is expected due to the oxidation of ferrous iron to ferric iron and the subsequent precipitation of iron oxides. After many hours, the solution became quite orange. After a day and a half, Mo concentrations did reduce by about 5 mg L^{-1}, but based on geochemical modelling it is expected that this is due to adsorption rather than iron molybdate precipitation. The small, insoluble particles of ferric oxides act as sorption sites for Mo, especially under the acidic conditions present in the solution. Mo will therefore adsorb onto the particles, ultimately lowering the aqueous concentration. With there only being 40 mg L^{-1} Fe present initially, there is not a great amount of ferric precipitate formation, but enough to lower the Mo concentration by about 5 mg L^{-1}.

The pH of the solution reduced as time went on. After 10 minutes, the pH of the solution was 5.52. 43 hours later, the pH had dropped to 5.24. It is expected that with enough time, the pH would lower to around 4.73, as PHREEQC indicates. These pH levels are much lower than those present at Antamina since there was a very low buffer capacity within the solution. It is expected that if the pH was increased to above 8, the Mo concentration would become much closer to 200 mg L^{-1} again as the molybdate would desorb from the ferrihydrite. This was further analyzed within the sorption chapter.

A1.3.4 Conclusion

Although Branam (1999) indicates that iron molybdate readily forms under certain conditions, it is expected that it does not at Antamina because the groundwater is not acidic enough. Performing the same experiment under anoxic conditions would probably provide different results, but this was not conducted as it is expected that Fe concentrations are not high enough and that conditions are mainly aerobic within the waste rock piles.

A1.3.5 References

Branam, T.D., Smith, R.T., Ennis, M.V., Rybarczyk, J.P., Comer, J.B., 1999. Trace Element Partitioning in Ground Water at an Abandoned Mine-Land Site Reclaimed with Coal Combustion Products. 1999 International Ash Utilization Symposium, University of Kentucky, Paper 68.

Golder Associates Ltd, 2007. Final Version 4.0, Waste rock and tailings geochemistry – field cell monitoring 2002 to 2006, Antamina Mine Peru. Mississauga, ON.

Langedal, M., 1997. Dispersion of Tailings in the Knabeåa–Kvina Drainage Basin, Norway, 2: Mobility of Cu and Mo in Tailings-Derived Fluvial Sediments. Journal of Geochemical Exploration 58, 173-183.

Mineral Data Publishing, 2005. Ferrimolybdite, Version 1. AZ, U.S.A.

Salminen, R., 2005. Geochemical Atlas of Europe, Part 1 - Background Information, Methodology and Maps. Geological Survey of Finland.

A1.4 Competition Batch Experiment

A1.4.1 Introduction

A batch experiment containing competing metals found at Antamina was conducted in order to determine the likelihood of other molybdate minerals forming other than powellite and wulfenite. Cu, Zn, and Pb were the metals included in the batch, along with Mo, SO_4 and marble sand. With Antamina being a Cu-Zn mine, concentrations of these metals are expected to be relatively high in drainage water. Lindsay (1979) found that Cu affected the precipitation of molybdenum. Initial PHREEQC simulations indicated that Cu and Zn molybdates are supersaturated in such solutions. Zn concentrations reach 10 ppm within the field cells, Cu reaches 2 ppm, and Pb is not detected. The results of the competition batch will therefore be important in determining the potential of further sinks for Mo.

A1.4.2 Methodology

A 20 ppm Cu and Zn solution was made in one 100 mL volumetric flask, while a 100 ppm Mo and 1000 ppm SO_4 solution was made in a separate 100 mL flask. The solutions were poured together into a 500 mL beaker containing approximately 50 g of sand-sized marble. 20 ppm Pb was added to the solution immediately. The solution remained unstirred for the duration of the experiment, and pH measurements and 1 mL samples were obtained throughout the experiment. All solution samples were analyzed on an ICP-OES and XRD was conducted on the fine-grained material at the end of the experiment.

A1.4.3 Results and Discussion

A1.4.3.1 Aqueous Species

The batch experiment provided important results in determining probable outcomes of a competition column, so as to determine the necessary characteristics of it. The pH of the system was originally ~3 due to the sulphuric acid, but was buffered to ~5.5 within an hour, and reached a constant value of ~7.8 within two days. The experiment was run for 80 days, and all species changed with time.

Pb decreased almost immediately, decreasing from 20 ppm to below detection limits within the first minute. Wulfenite is the expected precipitate, as Mo also decreased by at least 7 ppm; a 9.3 ppm Mo decrease is expected for complete wulfenite formation from 20 ppm Pb. XRD did not detect wulfenite, but this is due to the fact that calcite is in such abundance that most other precipitates are diluted below detection limit.

Cu removal began within the first 15 minutes and decreased to below detection limits after 48 hours. A distinct green-blue precipitate was visually observed during this time, but XRD did not identify any Cu phases due to the detection limit problem. Zn removal began approximately 24 hours into the experiment and reached an equilibrium value of 2.3 ppm after 13 days. It was unknown as to what phase Zn precipitated out as, with XRD showing no positive results. PHREEQC predicts a zinc molybdate or zinc carbonate phase, but further analyses were required in the competition column experiment to determine this.

Mo followed the typical powellite trend after the initial drop from wulfenite formation. The decrease was more gradual than the other powellite experiments due to the fact that it was an unstirred environment. It was decided that this test should be unstirred, as the column acts more similarly to an unstirred batch as found in the powellite column. The steady, gradual decrease of Mo provides evidence towards Zn not forming a Zn molybdate, as a quicker decrease of Mo would have been observed. This experiment therefore shows that the expected major sinks for Mo include powellite and wulfenite, depending on Pb availability.

Ca also followed similar trends as the powellite experiments. After a quick increase due to the presence of sulphuric acid, Ca decrease is observed within the first two weeks of the experiment after which it remains relatively constant and then increases, due to evaporation.

SO_4 data provides the most likely evidence towards evaporation trends, with a steady increase observed throughout the experiment. Gypsum was observed in very small amounts within the filtered precipitate, yet SO_4 concentrations increased with time. This upward evaporation trend would also affect the other species in solution. This indicates that all downward trends are likely more prominent than observed, although the

observed highest rate of evaporation occurred after most species are near-zero. Ca is the main species that is affected the most by this due to its high concentrations.

A1.4.3.2 Saturation Indices

Calculated saturation indices indicated that equilibrium was reached for most species. Mo and Zn remained above saturation, with powellite and $ZnMoO_4$ expected to precipitate until both species were near-zero (Figure A1.15). Other batch systems have shown that Mo concentrations may in fact reach equilibrium at much higher concentrations than PHREEQC predicts, indicating a potential absence of complexed species or incorrect solubility constants in the PHREEQC database. It is also possible that Mo concentrations will decrease further, but over a timescale much greater than that of the batch experiments.

Calculated pCO_2 values indicate open system conditions. Using the charge balance of C(4) approach, the SI of pCO_2 equilibrated at -2.6, however the calculated SI with the alkalinity value obtained at the end of the experiment indicated a pCO_2 of -3.32. With this being an unstirred system, it provides evidence towards both unstirred and stirred batch systems being in equilibrium with atmosphere.

A1.4.4 Conclusion

The batch experiment identified wulfenite and powellite as being the only potential sinks for Mo out of the species present in the competition batch. Wulfenite precipitated immediately once both Mo and Pb were in solution and powellite precipitation occurred with the same kinetic limitations as the previous powellite experiments. Cu preferentially precipitated malachite to a Cu molybdate and Zn also did not form a Zn molybdate. Further studies within the competition column were required to determine where Zn was going.

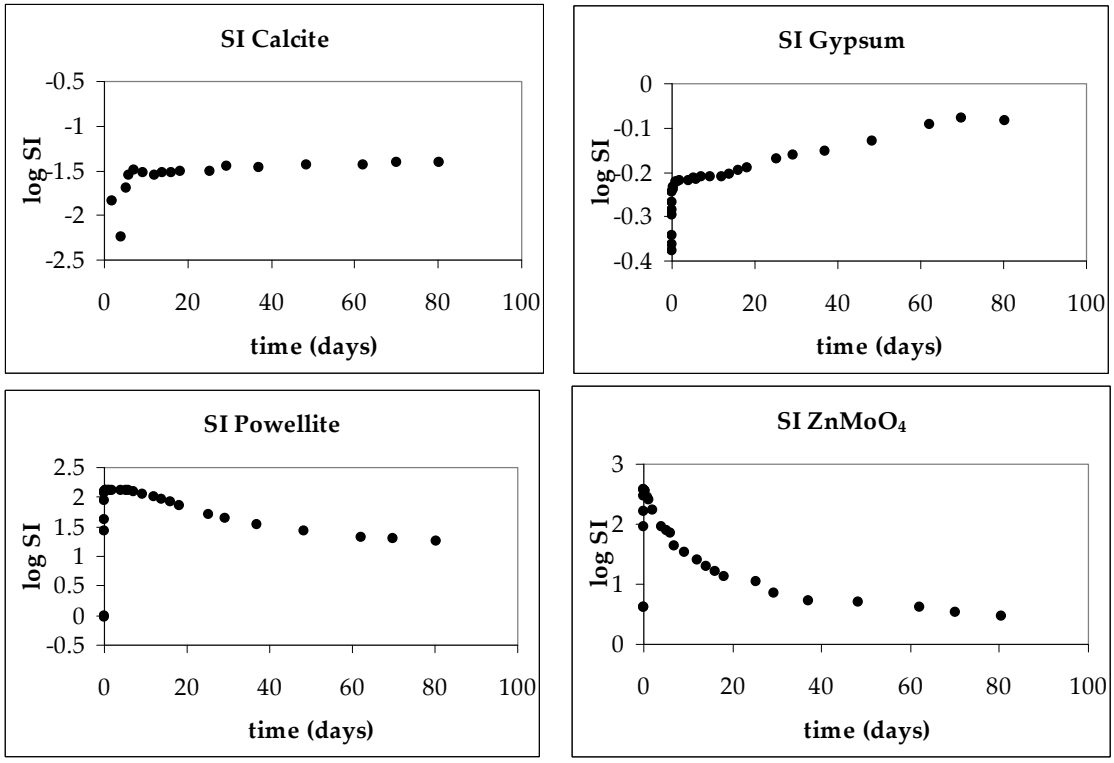

Figure A1.15 – Saturation indices of select phases

A1.4.5 References

Lindsay, W.L., 1979. Chemical equilibria in soils. Wiley-Interscience, New York.

A1.5 Batch Experiment Modelling

A1.5.1 Introduction

Modelling of the batch experiments was conducted in order to determine kinetic limitation rate reactions for powellite precipitation. The reactive transport code MIN3P (Mayer, 1999) was used to determine the rates, as discussed within Chapter 2.

A1.5.2 Methodology

Reaction rates of powellite formation were created using the generalized rate equation as follows:

$$R = -k_d \cdot IAP\left(1 - \frac{IAP}{K_{sp}}\right)\phi \qquad \text{(A1.1)}$$

where R is the reaction rate, k_d is a dissolution constant, IAP is the ion activity product, K_{sp} is the solubility product, and ϕ is a nucleation inhibition term. An evaporative term was also included for the competition batch and stirred powellite experiment. Powellite precipitation of each batch system was modelled and precipitation constants k_p were determined as follows:

$$k_p = \frac{k_d}{K_{sp}} \qquad \text{(A1.2)}$$

In order to match the equation to the data, both k_d and K_{sp} were altered to provide the best fit.

A1.5.3 Results and Discussion

There were four main batch systems modelled (Table A1.4). A complete data set of all species is present for all systems except for Pow 3, which only has data for Mo and pH. The precipitation constants were all found to be within an order of magnitude of one another. The two stirred experiments showed excellent agreement with one another, as did the unstirred systems.

A1.5.3.1 Pow 3

The model fit this unstirred batch experiment well (see Chapter 2), with a log K_{sp} of -8.05. Unfortunately the batch experiment was not run long enough with Mo still decreasing in it, so it is possible that this model may not fit the equilibrium conditions. The spectrophotometer was also used with this batch, so other species such as Ca and SO_4 could not be analyzed.

A1.5.3.2 Pow 6

The results of this experiment did not reach thermodynamic predictions, with Mo still remaining at approximately 10 ppm under equilibrium conditions. PHREEQC indicated that powellite precipitation should reduce concentrations to below 1 ppm using the literature log K_{sp} value of -8.05 from Essington (1990). A log K_{sp} of -6.35 was therefore used in this model in order to fit the data.

Modelled results fit measured data well (see Chapter 2). Simulated Ca and SO_4 increases due to the evaporative rate added to the model.

A1.5.3.3 Pow 7

The literature log K_{sp} was used for this experiment and fit the data well (Figure A1.16). Mo and Ca were modelled very well, but initial pH had to be adjusted to fit the data as best as possible. The initial solution was strictly DI water which ideally should have a pH of 7, but a starting pH of 6.4 was used in the model. This is probably satisfactory, since carbonic acid from atmospheric CO_2 reduces the pH of DI water with time as it equilibrates with atmosphere.

SO_4 was not modelled correctly in this system, as it did not account for gypsum precipitation. The model assumed that SO_4 should remain at initial concentrations whereas PHREEQC and experimental data show a quick initial SO_4 decrease due to the formation of gypsum.

A1.5.3.4 Competition

Experimental data was modelled very well (Figures A1.16 and A1.17). Evaporative trends of Ca and SO_4 are apparent in the measured data and were modelled

well with the added evaporative rates of each species. pH was modelled well except for some small variations. This is likely due to the fact that the system was not stirred, which made it more difficult for the batch to remain in equilibrium with atmospheric CO_2.

A1.5.4 Conclusion

Precipitation constants were determined and fell within one order of magnitude from one another. Each system was modelled remarkably well using MIN3P, with only minor variations between measured and modelled results.

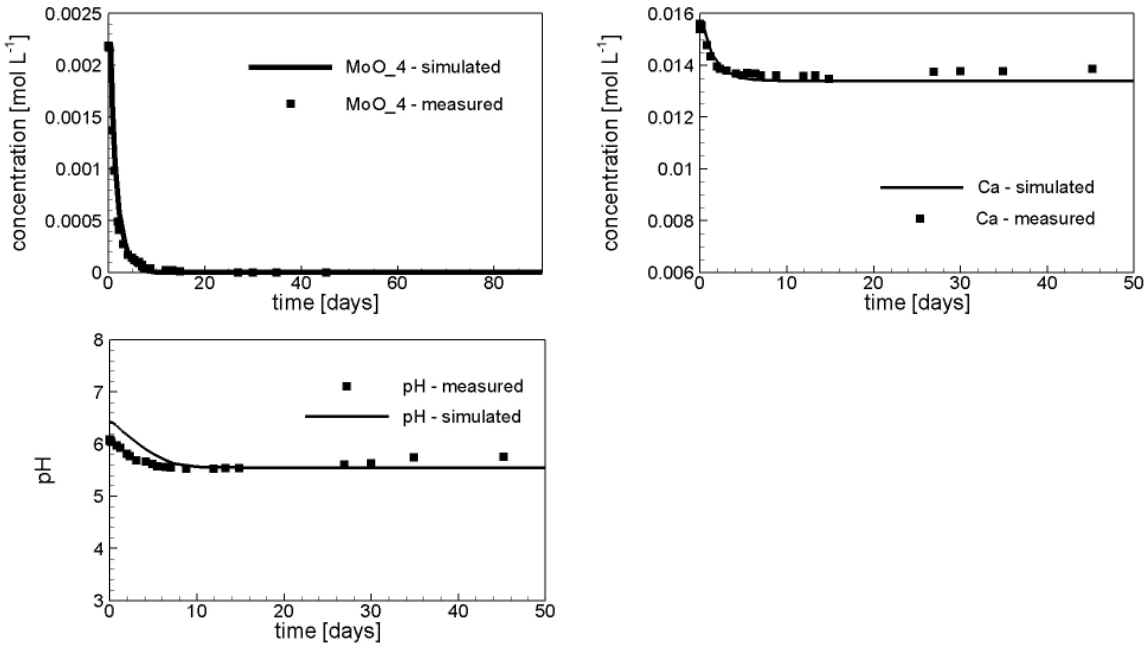

Figure A1.16 – Measured and modelled data for dissolved Ca and Mo batch

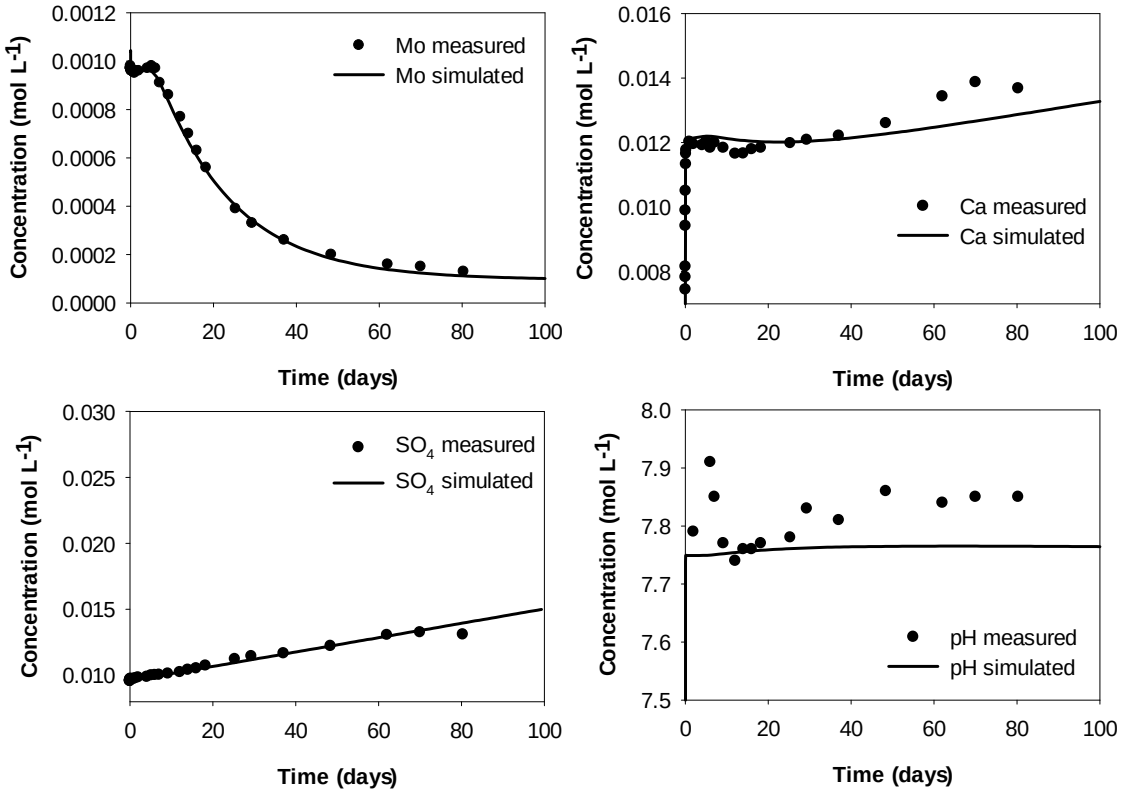

Figure A1.17 – Measured and modelled data for competition batch

Table A1.4 – Batch systems modelled

Batch	***Species present***	***Stirred or Unstirred***	k_p
Pow 3	Mo, SO_4, calcite	Unstirred	1.18×10^{-4}
Pow 6	Mo, SO_4, calcite	Stirred	9.57×10^{-4}
Pow 7	Mo, Ca	Stirred	1.39×10^{-3}
Competition	Mo, Pb, Zn, Cu, SO_4, calcite	Unstirred	1.55×10^{-4}

A1.5.5 References

Mayer, K.U., 1999. A numerical model for multicomponent reactive transport in variably saturated porous media. Ph.D. thesis, Department of Earth Sciences, University of Waterloo.

Appendix 2 – Column Experiments

A2.1 Powellite Column Study

A2.1.1 Introduction

After determining the potential for powellite precipitation with the batch experiments, a transport column was created so as to further understand the possibility of powellite as being a sink for Mo. A column study is more representative of the real-life waste rock piles, as it involves advective transport. Transport adds complexity compared to batch experiments, but it is a more realistic approach in quantifying the geochemistry occurring in environmental systems. Batch and column studies often produce differing results due to the added transport mechanism (Selim and Iskandar, 1999). Batch experiments have a much lower solid-solution ratio than column studies, which can affect precipitation and sorption reactions (Bajracharya et al., 1996).

Similar to the batch experiments, the conditions of the column study are created to represent the waste rock piles as much as possible. A system including calcite, molybdenum, sulfate, and bicarbonate was therefore created.

A2.1.2 Methodology

A 61 cm long acrylic column was used for this column experiment. To represent Antamina conditions as much as possible, a marble was obtained from Lafarge (Coquitlam, B.C.) that originated from Texada Island, B.C. and crushed to a medium sand (sieved between 280 and 800 um). Eleven screened ports to extract the inflow solution were located with a uniform distance along the column.

The column was packed as a saturated slurry in order to prevent oxygen from being trapped within the pores. The sand was first rinsed with deionized water and then dropped into the column until the first port was reached. Deionized water was added to the wet slurry until it overflowed out of the port, at which point the sand and water were stirred vigorously to let any trapped oxygen escape. The column was then dropped onto the floor 4-5 times from a distance of about a foot above the ground to allow for a more natural, gravitational packing rather than strictly physical force. More sand was added and the procedure was repeated until the compacted sand reached the port. The screened port was then screwed into the column and saturated sand was dropped around it. At this

point, the procedure started over again until the next port was reached. This was continued until the entire column was packed with the saturated sand.

The sand has a porosity of about 0.4 and dry bulk density of 1.39 g/cm^3. Deionized water was passed through the column for approximately one week in order to allow for trapped oxygen and contaminants to escape. The flow rate was consistently measured and it remained at 0.3 mL min^{-1} for the entire experiment. Based on this flow rate and the porosity of the sand, the residence time within the column was approximately 3 days. This was desired, as the stirred batch experiments showed Mo concentrations decreasing from 200 mg L^{-1} to around 100 mg L^{-1} after 3 days.

The inflow solution consisted of 200 mg L^{-1} Mo and 1000 mg L^{-1} SO_4 and was created in the same fashion as the batch experiments, using sodium molybdate dihydrate and sulphuric acid. The solution was constantly stirred magnetically in a 25 L Nalgene carboy.

A 1 RPM peristaltic pump (Masterflex) was used with Norprene tubing to create a flow rate of 0.3 mL min^{-1}. Approximately 6 mL samples were collected in either 4 or 15 mL Nalgene vials, split, and one was acidified with 5 uL of concentrated nitric acid directly whereas the other was filtered through a 0.45 um syringe filter prior to being acidified, to create a total and dissolved sample, respectively.

Samples were first collected from the top of the column after 70 hours and taken every 10 minutes to capture the breakthrough curve of Mo. Once concentrations reached their maximum, samples were taken from every second port for two days. It was then realized that Mo concentrations were not decreasing at all, so the column was turned off for approximately one month, with samples being collected every few days. This was achieved by turning the column back on for approximately 30 minutes to collect a sample, prior to turning it off again.

A2.1.3 Results and Discussion

A2.1.3.1 Breakthrough

Mo started to pass through the end of the column when expected, indicating that adsorption of Mo onto calcite is low as previously found by Fox and Doner (2002). The

initial and final portions of the curve were missed due to the fact that breakthrough lasted more than 13 hours, but the majority was analyzed (Figure A2.1). The curve is mainly due to diffusion since the advective rate is low. The outflow Mo concentration reached the inflow concentration, which was not expected.

Prior to adding the Mo and SO_4 solution, the pH of the system was 8.3 due to buffering of calcium carbonate. The inflow solution pH was 2 due to the sulphuric acid, but was immediately buffered once reaching the calcium carbonate sand. pH of the system decreased to 6.57 ± 0.02 once the solution was passed through, and is lower than the batch experiments since the column is a closed system. Carbon dioxide gas forms from the dissolution of calcium carbonate and cannot escape, increase carbonic acid concentrations and ultimately decreasing the pH.

A2.1.3.2 Post Breakthrough

Mo concentrations reached the maximum of 200 mg L^{-1} at the end of breakthrough. Originally it was hypothesized that concentrations should only reach around 100 mg L^{-1}, based on the results from the batch experiments. However, the batch experiments that precipitated powellite within days were all magnetically stirred, whereas the column experiment was strictly based on advection. The advective rate was extremely slow though, meaning that it acted much more similarly to the unstirred batch experiments. It was originally hypothesized that this wouldn't be the case, because all the calcium carbonate sat at the bottom of the batch experiment whereas there is plenty of solid-solution contact in the column experiment. This proved to not be the reason though, as no Mo was removed within the column with a residence time of 3 days.

The column experiment was subsequently turned off once outflow concentrations reached initial inflow concentrations so as to confirm that powellite would still precipitate. Powellite did begin to precipitate, with Mo decreasing from 200 mg L^{-1} to 66 mg L^{-1} over a period of just less than 4 months. This rate is much more comparable to the unstirred batch experiments. Calcium concentrations decreased as well and powellite was determined using XRD. SO_4 remained relatively constant, although a small amount of gypsum was found with XRD.

Based on these results, it is apparent that powellite is not as prominent of a Mo sink as first expected after the stirred batch experiments. With the column being much more representative of the real system within the waste rock piles, this result shows that Mo will in fact not be attenuated due to powellite precipitation, if residence time within the pile is short. Matrix-supported waste rock has low flow, however, indicating that residence times in the waste rock piles are likely fairly high (Smith and Beckie, 2003).

A2.1.4 Conclusion

Powellite precipitation does occur with transport through a column, but at rates much more comparable to an unstirred batch experiment than a stirred one. Although powellite did not precipitate with flow through this column, the breakthrough curve provides further evidence of little adsorption of Mo to calcite. Powellite precipitation would have occurred if the residence time in the column was longer but still at relatively slow rates compared to the stirred batch experiments.

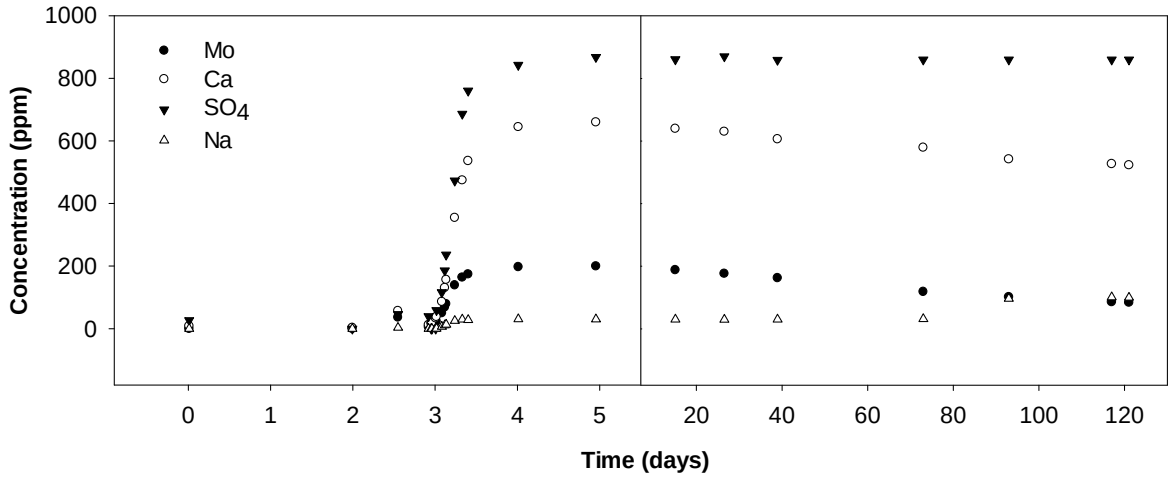

Figure A2.1 – Breakthrough and post-breakthrough of the powellite column

A2.1.5 Reference

Bajracharya, K., Tran, Y.T., Barry, D.A., 1996. Cadmium adsorption at different pore water velocities. Geoderma 73(3-4), 197-216.

Fox, P.M., Doner, H.E., 2002. Trace Element Retention and Release on Minerals and Soil in a Constructed Wetland. Journal of Environmental Quality 31, 331-338.

Selim, H.M., Iskandar, I.K., 1999. Fate and Transport of Heavy Metals in the Vadose Zone. Ann. Arbor Press, Chelsea, MI (320p.)

Smith, L., Beckie, R., 2003. Environmental Aspects of Mine Wastes, Chapter 3: Hydrologic and Geochemical Transport Processes in Mine Waste Rock. Mineralogical Association of Canada, 51-72.

A2.2 Competition Column Experiment

A2.2.1 Introduction

The competition column experiment was conducted to simulate conditions expected at Antamina and to further understand Mo attenuation. As previously discussed, columns provide conditions much more similar to real-life conditions than batch experiments. This was the most complicated and in-depth experiment performed so results were vigorously analyzed. The column contained the same general setup as the competition batch experiment which provided a good comparison between the two systems.

A2.2.2 Methodology

The column consisted of Mo, SO_4, Cu, Zn, and Pb passing through marble sand. The same column as the powellite column experiment was used, and was packed in the same fashion. Photos of the setup and sample procedure can be found in Appendix 10.

Influent was passed into the column using Masterflex low-flow peristaltic pumps. Three low-flow peristaltic pumps were required, as the different metals had to be separated to prevent premature precipitation. Each pump had a flow of 0.07 to 0.08 mL min^{-1} resulting in a total flow of approximately 0.22 mL min^{-1} and a subsequent residence time of 4 days. Conservative tracers were added to each carboy in order to account for mixing variability. The inlets within the column were placed close to each other in order to promote mixing near the bottom.

Samples were collected once every pore volume from every second port in order to reduce disturbances, however every port was sampled for a few pore volumes for a more detailed view. The outflow was also measured much more periodically as it did not affect the column. pH was measured prior to each sample and alkalinity was measured intermittently at the outflow. Samples were filtered with 0.45 μm Millipore syringe filters, acidified with nitric acid, and stored at 4^{o}C prior to analysis by ICP-OES (Varian Inc.). Precipitates from the batch and column experiments were analyzed using XRD (Siemens D5000) and SEM (Philips XL-30).

A2.2.2.1 Data Normalizing

Data normalization was required to account for the variability of mixing within the column. Normalization of Mo, Pb, Cu, Zn, and SO_4 was conducted using the measured tracer concentrations within each sample and comparing them to the average tracer concentration during the experiment. This was completed by dividing the measured tracer in the sample by the average tracer concentration, and subsequently multiplying the metal from the same inflow solution as the tracer by that ratio. The initial solutions were continuously measured to ensure that the concentrations did not vary during the extent of the experiment.

A2.2.2.2 Sample Procedure Verification

In order to ensure that samples were measured correctly, the tracers were used to determine the percentage of each carboy in the sample and summed up to see the total recovery. This was accomplished by dividing the measured tracer in the sample by the average tracer concentration from the carboys and multiplying by 100 to determine the percentage of that inflow solution in the sample. This was done for all three tracers and the results were summed. Retrieval was near 100% for all samples with the average being 98% (Figure A2.2).

A2.2.3 Results and Discussion

The competition column provided many important results in understanding Mo attenuation, as it was the most complex system analyzed, involving numerous elemental species as well as flow. Mo was most closely analyzed, but each species was studied to determine the potential environmental impacts from the waste rock piles.

A2.2.3.1 Molybdenum

Mo acted fairly similarly to the previous column experiment, but showed more prominent trends due to the extended time period of the experiment and slightly longer travel time through the column. Concentrations observed near the bottom of the column were lower than input concentrations, being at least 10 ppm less (Figure A2.3). This can

be directly related to wulfenite precipitation, as later discussed. Mo continued to decrease slightly as it passed up the column, as well as with time (Figure A2.4). Small amounts of powellite precipitation were expected to reduce Mo concentrations over the 4 day travel time, but only enough to decrease Mo by a few mg L^{-1}, which was observed for almost all pore volumes measured.

An apparent decrease of Mo at each port of the column with time was an unexpected result. This indicated that powellite precipitation may in fact have occurred more prominently than expected, as the system reached equilibrium. Mo initially remained near input values at the top of the column, but a linear decrease was observed with time, reaching below 90 ppm from an original 200 ppm after a month and a half (Figure A2.5). Powellite was the expected precipitate, with it being the only phase determined for all samples with XRD. It is possible that other Mo phases were present, but in such small amounts that they were below detection limit. It is unknown at what concentration Mo would equilibrate at within this column; in hindsight the column should have been analyzed further to determine this. This result is interesting though, as the rate of powellite precipitation initially acted similar to an unstirred batch experiment but moved towards that of a stirred batch experiment, with over half of the initial concentration precipitating out over the 4 day residence time. This is potentially due to the fact that minerals often precipitate more easily on existing mineral surfaces; once powellite started to form, rates increased with further precipitation onto those crystals. It is also likely that Mo concentrations would equilibrate not much lower than the values observed at the end of the column though, as removal should not exceed that of the stirred batch experiments.

Powellite saturation indices remained above 0 for every port of the column, throughout the experiment (Figure A2.6). It is therefore expected that Mo would decrease dramatically if the residence time was longer.

A2.2.3.2 Calcium

Calcium was present from the dissolution of calcite due to the sulphuric acid. Concentrations remained high throughout the column, though decreasing trends were observed with time as well as with residence time (Figure A2.7). Ca concentrations

decreased as it passed through the column, likely due to powellite precipitation, as it was the only Ca-rich secondary mineral determined by XRD.

For 100% powellite formation, 0.4 ppm of Ca is required for every 1 ppm of Mo. This would create a slope of 2.39 on a Mo vs. Ca plot (Figure A2.8). The trends observed in the bottom, middle, and top of the column show much more Ca removal than required for powellite formation though, meaning calcium must also be going somewhere else. The top and middle trends are almost identical with much more Ca removal, whereas the bottom of the column has less Ca removal, but still much more than required for powellite precipitation.

Calcite saturation indices remained above zero, likely due to the same calcite dissolution processes as the batch experiments. It is therefore possible that some Ca decrease was due to calcite precipitation, as carbonate concentrations were also high. Calcite's SI averaged around 0.13 which is relatively close to 0, meaning it is just as possible that calcite was only saturated. Re-precipitation of calcite would account for the high amount of Ca removal, however.

Gypsum remained undersaturated for the extent of the experiment, since SO_4 concentrations remained at 1000 ppm. A small amount of Ca removal was attributed to gypsum precipitation, although only one XRD sample found gypsum, in small quantities. It is expected that small amounts were present throughout the column, but of concentrations below detection limit and therefore of minor importance.

A2.2.3.3 Lead

Aqueous Pb was hardly present within the column, as expected with near-neutral pH conditions. The highest concentration measured was ~0.6 ppm, which is still relatively close to detection limits of the ICP-OES. The highest concentrations, hovering around 0.4-0.6 ppm, were observed near the end of the life of the column and within the first half of the column (i.e. first two days of residence time), indicating that equilibrium Pb concentrations may in fact be in this range (Figure A2.9). Concentrations decreased again in the second half of the residence time, to values around the instrument's detection limits. Equilibrium concentrations are therefore not fully known, since the values obtained could be noise or due to interferences with the instrumentation.

$PbMoO_4$ saturation indices remained well above zero when Pb was detected in solution. Pb was predicted to be near 0 so any detectible concentrations would produce supersaturation values for wulfenite. XRD determined that Pb was in fact removed from solution with the precipitation of wulfenite. This was expected based on PHREEQC simulations, the batch experiments, and the fact that a yellowish precipitate could be observed near the inflow valve. Mo concentrations were always below inflow values, corresponding to wulfenite formation. Saturation indices indicated that wulfenite should continue to form for any aqueous Pb, meaning the measured Pb was either experimental error or other processes such as complexation was preventing Pb precipitation.

A2.2.3.4 Copper

Cu trends varied for each location in the column. Concentrations at the bottom of the column originally remained near inflow concentrations, but decreased relatively linearly with time until an equilibrium value of ~2 ppm was reached (Figure A2.10). The majority of the Cu precipitated out of solution in the first quarter of the column (Figure A2.11). Concentrations increased until an equilibrium of around 2.4 ppm was consistently observed between ports 1 and 12.

The trends observed in the middle and top portions of the column look like typical breakthrough curves of a retarded species, indicating that either complete Cu removal occurred or that it was retarded due to other processes. Cu adsorption to calcite is the expected process and has previously been characterized (Kitano et al., 1976, Lee et al., 2004).

Cu removal was due to malachite precipitation, as found in XRD of a blue-green precipitate samples near the bottom of the column. $CuMoO_4$ had the highest saturation index, but malachite preferentially formed which was likely due to kinetic limitations of calcium molybdate. Antlerite, langite, tenorite, and brochantite also became supersaturated under conditions with high Cu concentrations, but were still much lower than saturation indices of the other species. Based on these results, Cu is not expected to affect Mo concentrations.

A2.2.3.5 Zinc

Zn concentrations remained high throughout the column (Figure A2.12). $ZnMoO_4$ and $ZnCO_3$ were both supersaturated for the extent of the experiment due to the high concentrations. Neither species were determined in XRD analyses though, and further Zn batch experiments indicated that any Zn removal was likely due to adsorption onto calcite rather than Zn precipitation. Retardation was observed at the top of the column during initial breakthrough and was likely due to this. Zn sorption to calcite occurs more prominently at elevated pH levels and high $CO2_{(g)}$ concentrations, via exchange with Ca^{2+} in an adsorption surface layer (Zachara et al, 1988). Zn adsorption is less prominent than Cu adsorption, resulting in the shorter breakthrough curve (Kitano et al., 1976). Few trends were present for Zn, but concentrations were typically slightly lower at the outflow than the inflow, and this was likely due to Zn adsorption (Figure A2.13).

The adsorption of zinc to calcite was quantified by determining a retardation factor of 4.3 and associated distribution coefficient of 0.95 mL g^{-1}. Complete calculations can be found in Appendix 3.

A2.2.3.6 Sulfate

The constant trends of SO_4 indicated consistency with the batch experiments (Figure A2.14). SO_4 concentrations remained constant at maximum values for the duration of the column experiment, as hypothesized. Small amounts of gypsum may have formed throughout the column, since XRD detected one sample containing low amounts. Saturation indices of gypsum were below 0, but small amounts have also been found in some of the batch experiments and powellite column experiment.

A2.2.3.7 pH, Alkalinity, pCO_2

pH remained relatively steady for the duration of the column experiment. An overall increasing trend was observed from the bottom to the top of the column but only by a maximum of 0.1 pH units, and typically much less (Figure A2.15). This trend is consistent with the hypothesis of high carbonic acid values near the bottom of the column from the dissolution of calcite. No prominent trends were seen as time progressed.

Alkalinity showed a slight but steady drop with time indicating a probable build up of carbonic acid (Figure A2.16). Samples were only obtained at the top of the column due to sample volume requirements, but it is expected to be relatively constant within the entire column.

pCO_2 values were much higher than atmospheric concentrations, averaging around $10^{-0.77}$. This was due to the calcium carbonate dissolution, where carbonate was dissolved and could not escape the system. Carbon dioxide concentrations therefore were elevated and producing such high pCO_2 concentrations.

A2.2.4 Conclusion

The competition column provided further evidence of powellite and wulfenite being potential sinks for Mo at Antamina. With immediate wulfenite formation and kinetically limited powellite formation, Mo concentrations could be decreased dramatically, depending on the residence time within the waste rock piles. Zn and Cu proved to not affect Mo attenuation, although both Zn and Cu attenuation were observed via adsorption and precipitation.

Initial inhibition of powellite formation was observed and was likely due to a lack of initial nucleation sites, similar to the batch experiments. Once sites are readily available, powellite readily forms with Mo removal acting more similarly to a stirred batch experiment. It is hypothesized that the column was close to reaching equilibrium, with over 50% Mo removal within the 4 day residence time, but the column required further analyses to prove this.

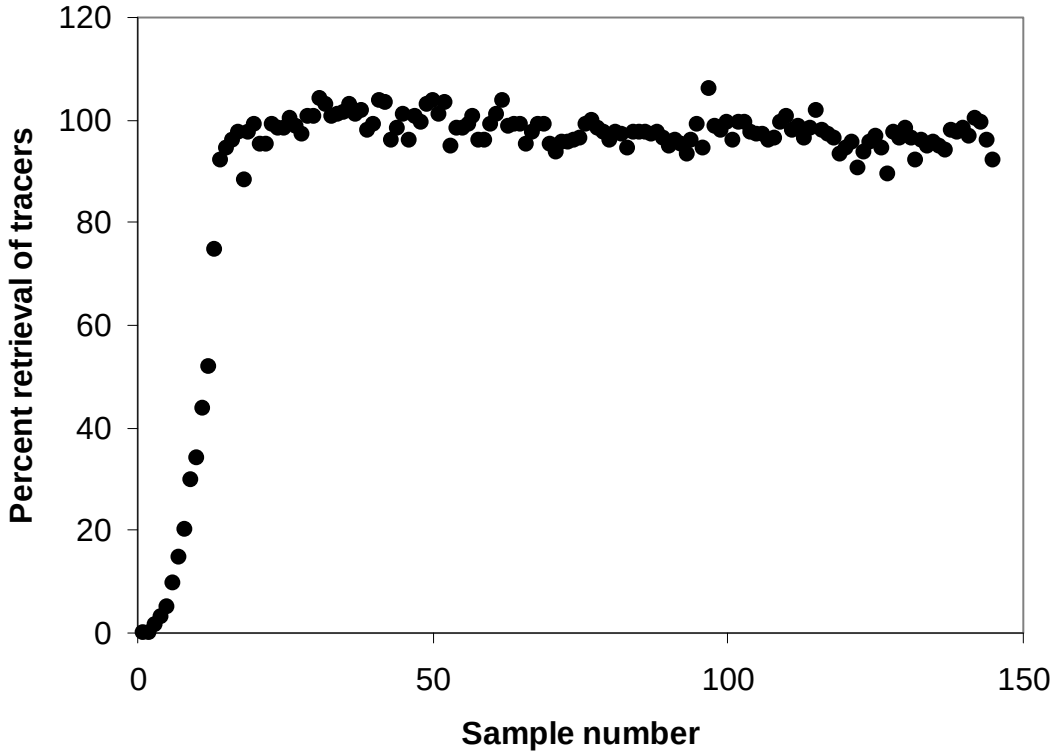

Figure A2.2 – Retrieval of tracers in samples

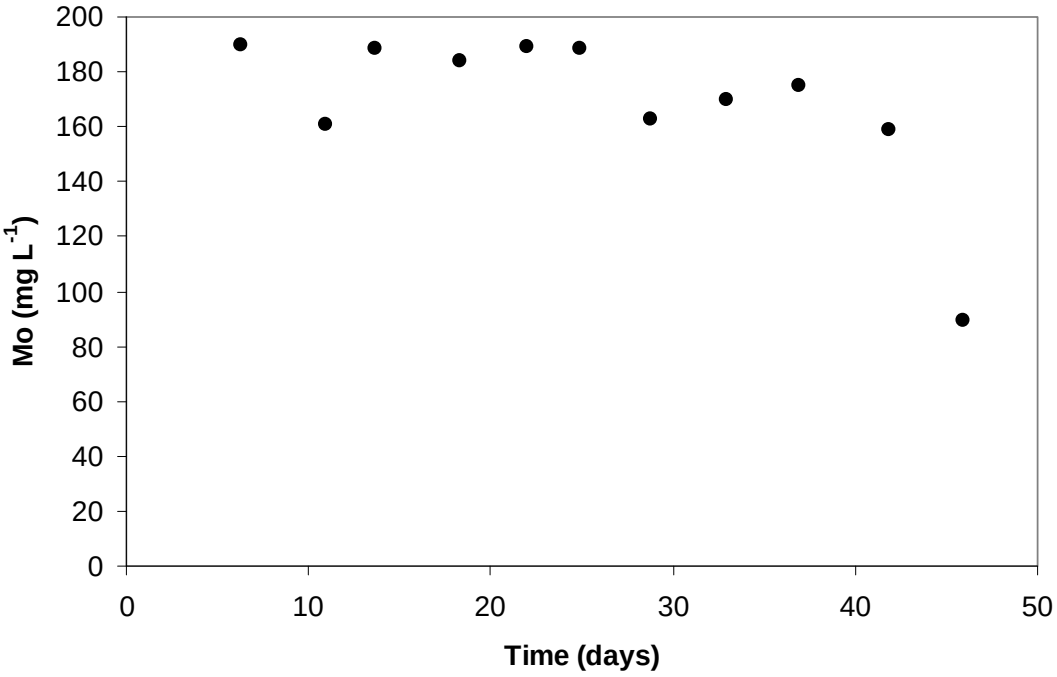

Figure A2.3 – Mo concentrations at the bottom of the column with time

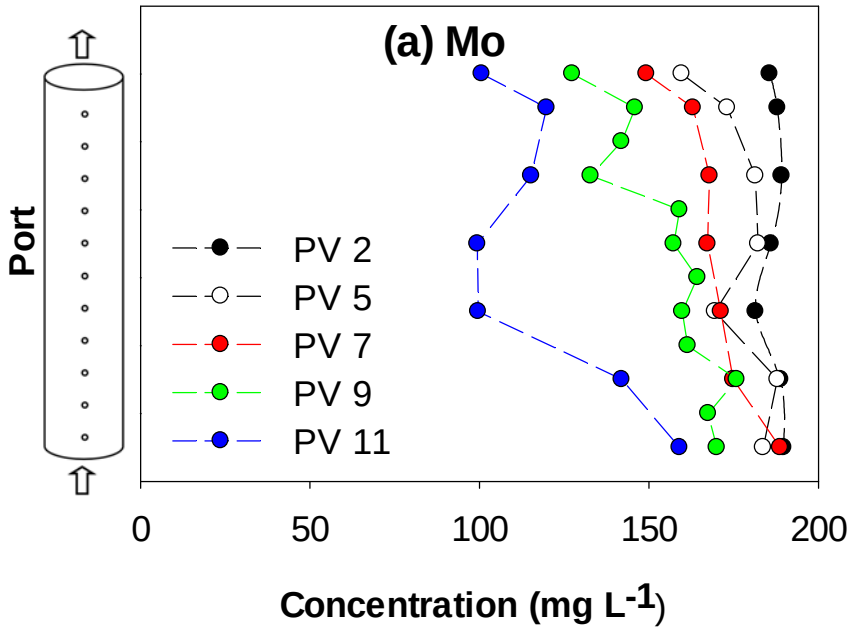

Figure A2.4 – Mo vertical profiles. Each line represents a pore volume with time

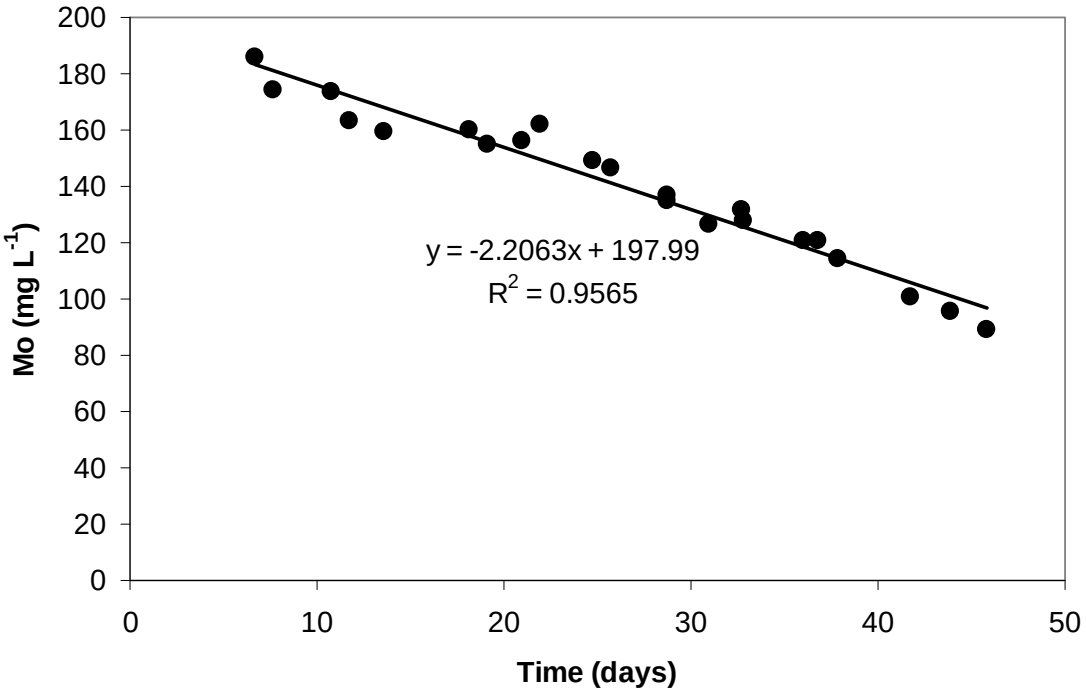

Figure A2.5 – Mo concentrations at the top of the column with time

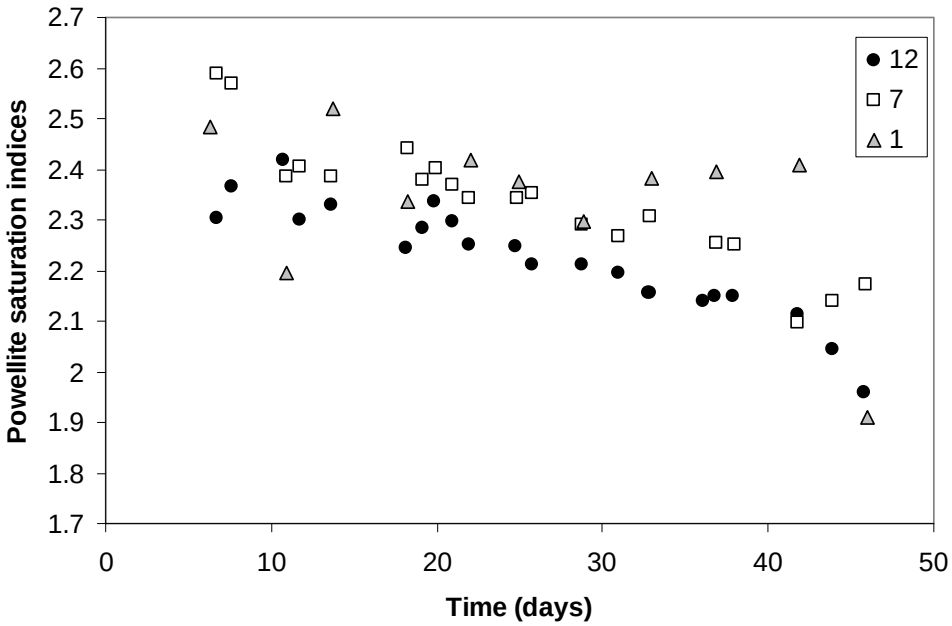

Figure A2.6 – Powellite saturation indices for the top (12), middle (7), and bottom (1) ports of the column with time

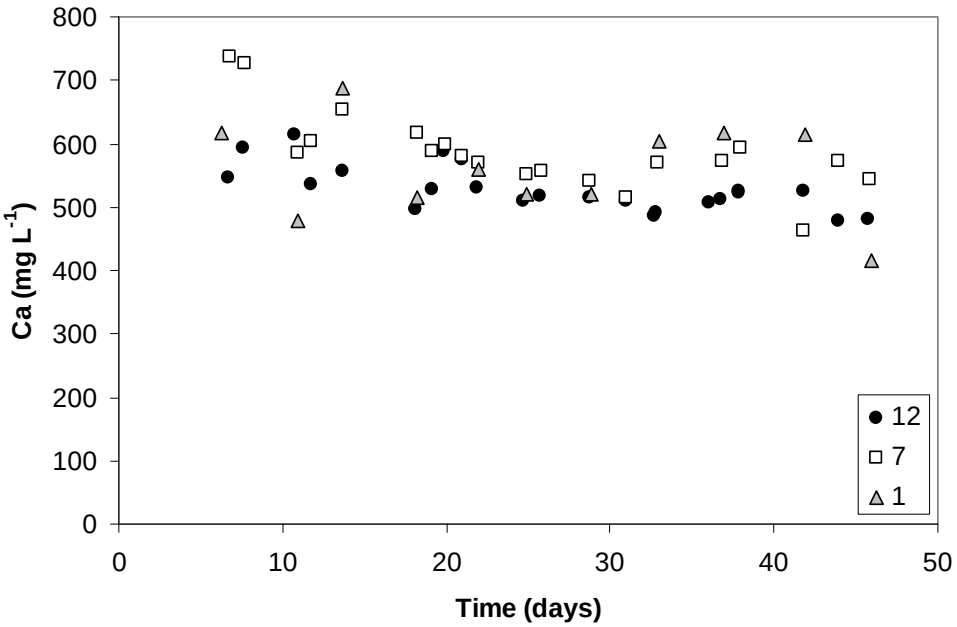

Figure A2.7 – Calcium concentrations for the top (12), middle (7), and bottom (1) ports of the column with time

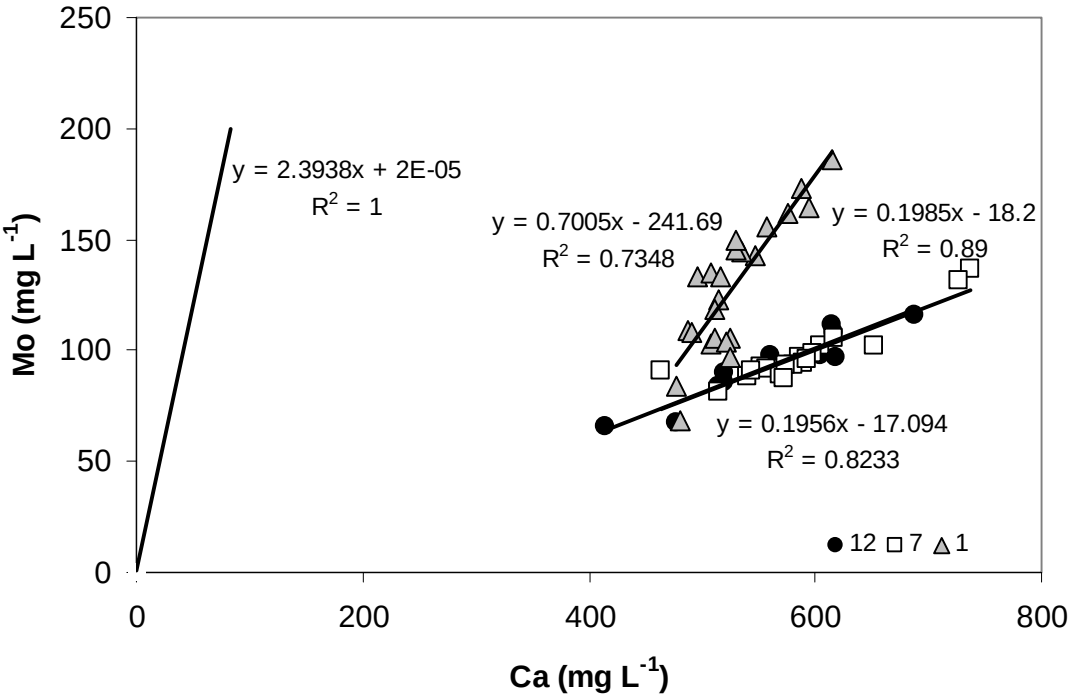

Figure A2.8 – Correlation between Mo and Ca for top (12), middle (7), and bottom (1) ports of column. Left line is 1:1 ratio of Mo:Ca for powellite precipitation

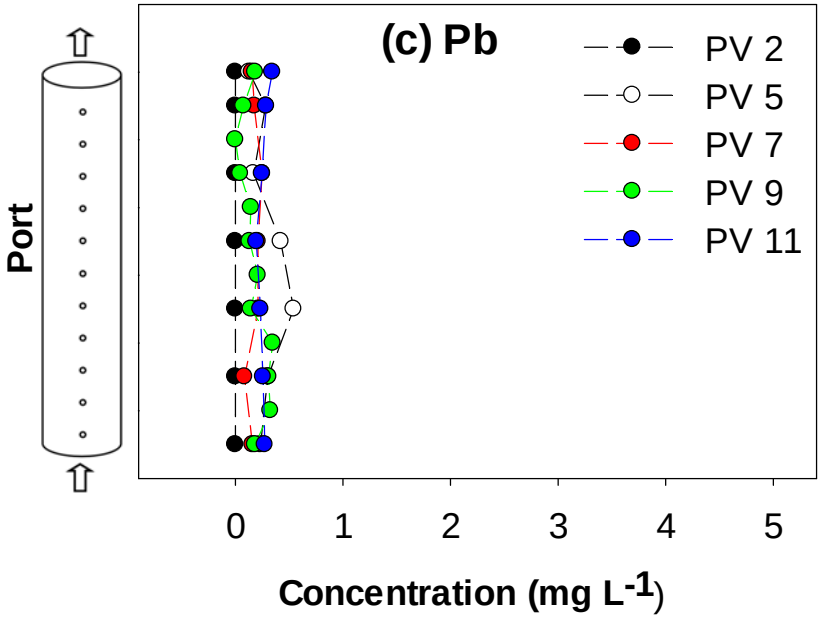

Figure A2.9 – Lead vertical profiles. Each line represents a pore volume with time

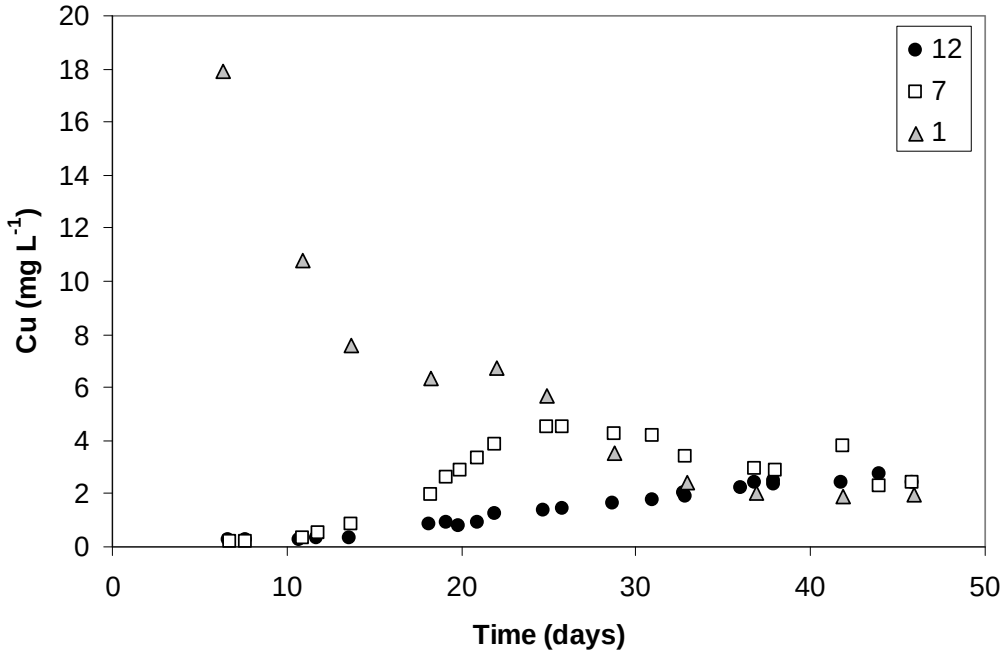

Figure A2.10 – Copper concentrations for the top, middle, and bottom ports of the column with time

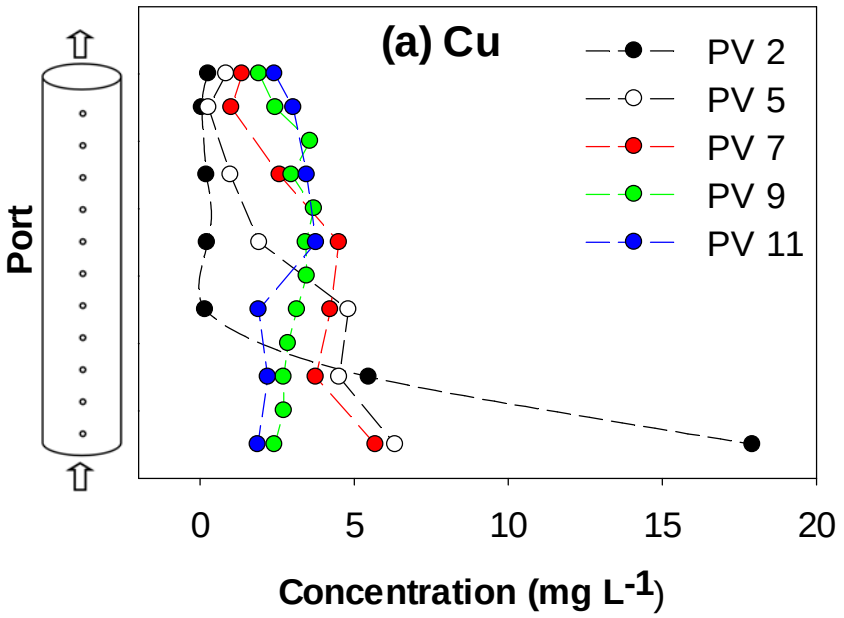

Figure A2.11 – Copper vertical profiles. Each line represents a pore volume with time

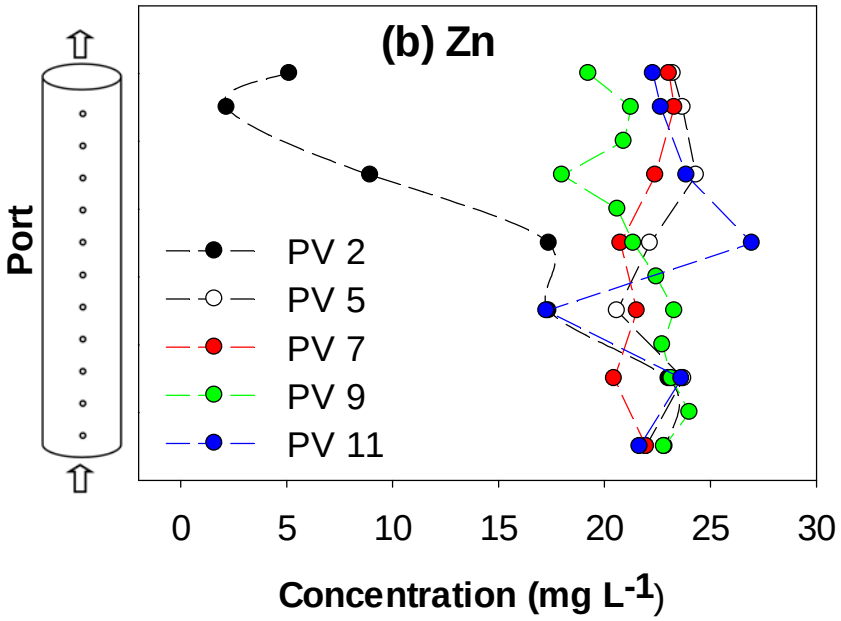

Figure A2.12 – Zinc vertical profiles. Each line represents a pore volume with time

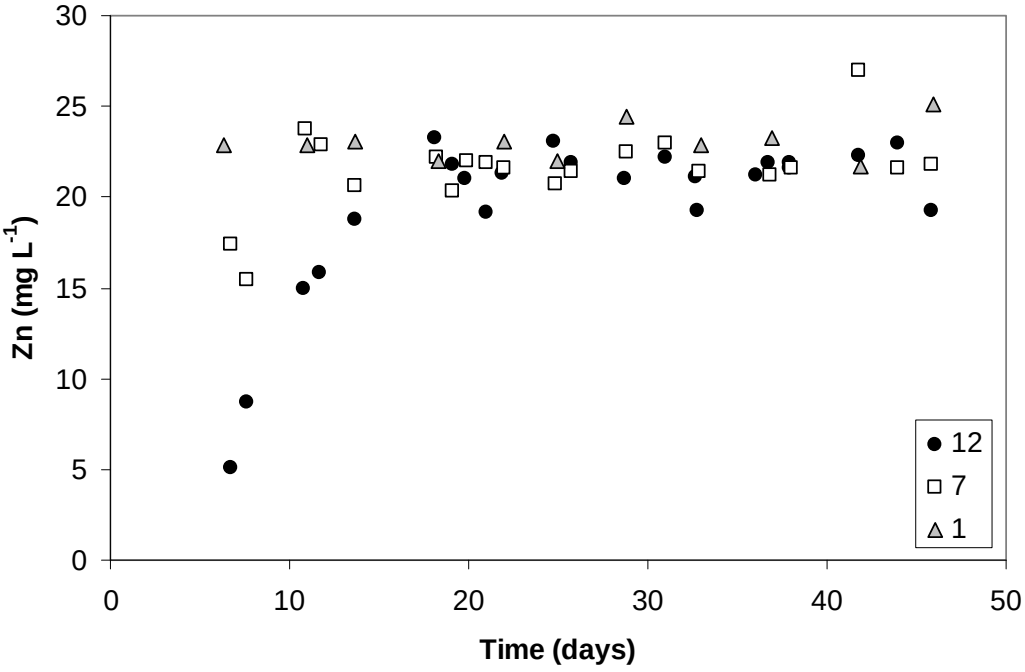

Figure A2.13 – Zinc concentrations for the top, middle, and bottom ports of the column with time

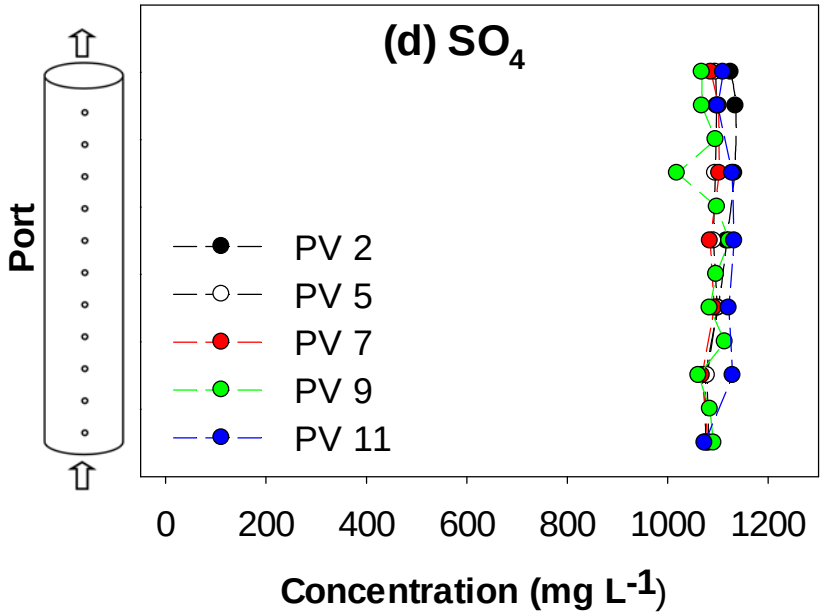

Figure A2.14 – Sulfate vertical profiles. Each line represents a pore volume with time

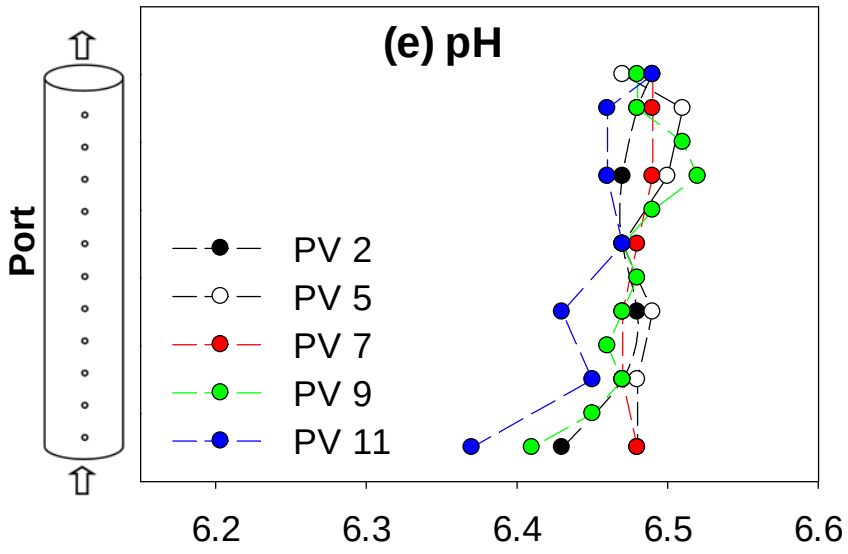

Figure A2.15 – pH vertical profiles for select pore volumes

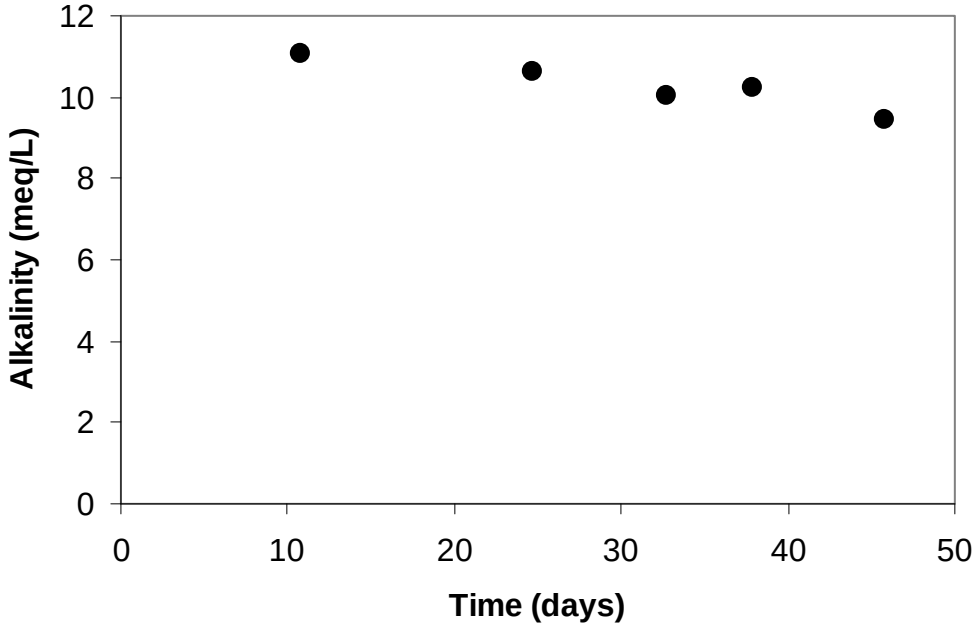

Figure A2.16 – Alkalinity at the column outflow

A2.2.5 References

Kitano, Y., Kanamori, N., Yoshioka, S., 1976. Adsorption of zinc and copper ions on calcite and aragonite and its influence on the transformation of aragonite to calcite. Geochemical Journal 10, 175-179.

Lee, Y.J., Elzinga, E.J., Reeder, R.J., 2005. Cu(II) adsorption at the calcite–water interface in the presence of natural organic matter: Kinetic studies and molecular-scale characterization. Geochimica et Cosmochimica Act 69(1), 49-61.

Zachara, J.M., Kittrick, J.A., Harsh, J.B., 1988. The mechanism of Zn^{+2} adsorption on calcite. Geochimica et Cosmochimica Acta 52, 2281-2291.

Appendix 3 – Zn Adsorption

Zn adsorption was quantified by relating the retarded breakthrough curve with the groundwater velocity of 15.25 cm day^{-1} for the competition column. The end of the breakthrough curves through the middle and end port are observed in the following plot:

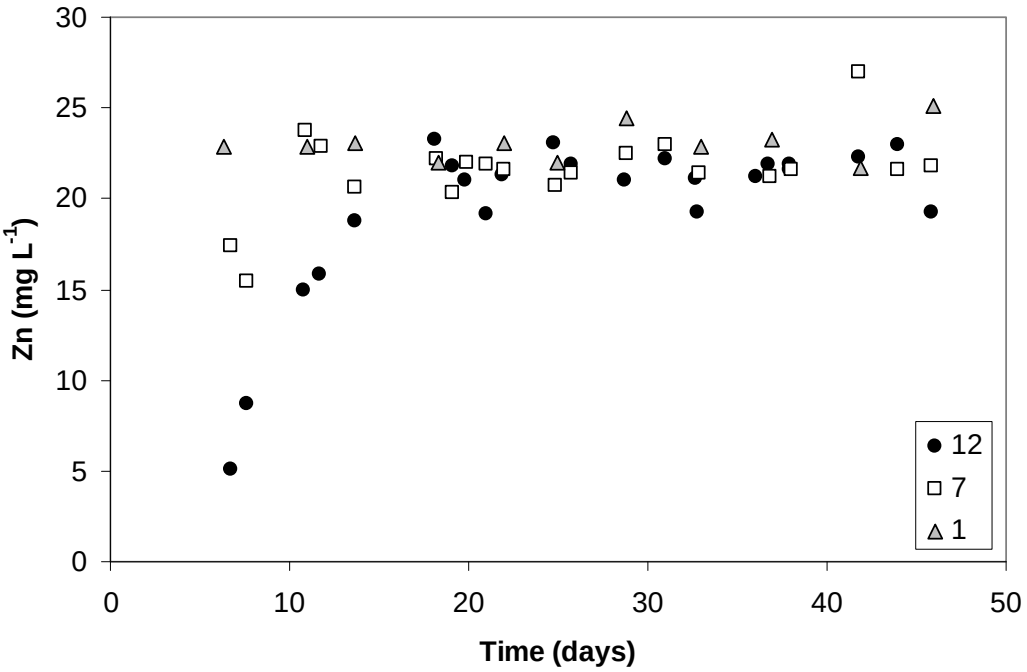

Knowing the start time of the column, the time breakthrough is complete, and the distance from the start of the column and the measured port, the calculations are as follows:

Zn retardation

PORT 12			**PORT 7**		
hits max:	~July 20th		hits max:	~July 13th	
start time:	July 3, 5pm		start time:	July 3, 5pm	
time:	17 days		time:	10 days	
distance:	61 cm		distance:	35 cm	
Velocity (v_{nc}):	3.588235	cm/d	Velocity (v_{nc}):	3.5	cm/d
water vel (v_c):	15.25	cm/d	water vel (v_c):	15.25	cm/d
R =	4.25		R =	4.36	

Where $R = \frac{v_c}{v_{nc}}$

(v_c = velocity of conservative tracer and v_{nc} = velocity of non-conservative tracer)

The distribution coefficient (K_d) is then calculated by relating the retardation factor with the dry bulk density (ρ_b) and porosity (n) of the column medium as follows:

$$R = 1 + \frac{\rho_b}{n} K_d$$

bulk density:	1.39	g/cm3
porosity:	0.4	
R = 1 + (pb/n)*Kd		
Kd =	0.935252	cm3/g

bulk density:	1.39	g/cm3
porosity:	0.4	
R = 1 + (pb/n)*Kd		
Kd =	0.966084	cm3/g

Therefore, an effective retardation factor of 4.3 was calculated with an associated distribution coefficient of 0.95 mL g^{-1}.

Appendix 4 – Photos of Ascorbic Extraction Method

Figure A4.1 – Field cell samples of the <2mm fraction

Figure A4.2 – Samples being degassed with nitrogen gas

Figure A4.3 – Experimental setup

Figure A4.4 – Filtration of sample with 0.22 μm syringe filter

Figure A4.5 – Filtered, acidified samples ready to be stored at 4^{o}C

Appendix 5 – Accounting for Evaporation

Evaporative trends were observed in all batch experiments that lasted longer than approximately one week. Parafilm was placed on all experiments in order to reduce this, but small holes were still left open so that the experiments could equilibrate with atmosphere. It was initially thought that these trends would be relatively easy to fix since the conservative tracer Na was present in all systems, but it proved to not be as easy as expected.

Both Na and SO_4 are expected to be conservative tracers based on PHREEQC analyses and XRD results. The data obtained from ICP-OES for the Pow 6 experiment is present in Table A5.1. Evaporative trends are apparent (Figure A5.1) and would also affect the non-conservative species Ca and Mo (Figure A5.2). In order to try to account for this, Na was normalized to the expected value and all other species were normalized accordingly. This was done as follows:

The expected Na concentration was 95 ppm based on the addition of 200 ppm Mo from $Na_2MoO_4 \cdot 2H_2O$. Each measured Na value was therefore divided by 95 to set a factor of how far off that sample is from the expected value. The first measured sample is used as an example:

$$\text{Evaporation factor} = \frac{95}{100.3} = 0.948$$

$$\text{New Ca} = 479.1 \times 0.948 = 454.0 \text{ ppm}$$

This was completed for all samples, and results are seen in Figure A5.3. The data indicates that this method is not an ideal way of account for evaporation, or SO_4 would also be flat. It also indicates that Ca decreases with time, whereas it is unknown if this is actually the case since calcite saturation indices are above 0. Since there are potentially other processes affecting the data, it was decided that not trying to normalize for evaporation was the best option. All data should still be analyzed knowing that evaporation plays some sort of role in the data, though.

Table A5.1 – Data for Pow 6 (all concentrations mg L^{-1})

Time (hrs)	Ca	Mo	Na	SO_4
0:10	479.1	203.6	100.3	994.8
5:15	481.2	206.6	99.4	997.3
23:55	481.0	204.7	98.4	1001.9
46:50	461.0	161.0	97.5	993.1
52:45	453.0	144.6	98.6	993.8
72:53	437.7	100.1	99.8	1000.5
98:26	425.0	69.9	97.5	998.0
119:25	419.3	56.5	98.9	1000.1
143:52	415.0	45.8	95.3	1005.2
169:25	415.2	39.7	98.8	1008.4
191:20	411.7	34.6	97.4	1010.3
215:03	416.4	32.3	100.0	1018.4
266:15	417.0	28.3	98.7	1038.4
290:50	418.6	26.4	100.0	1018.0
311:50	417.0	25.1	98.3	1034.1
336:40	422.0	23.7	100.7	1044.0
387:42	417.2	21.2	99.8	1042.2
457:11	422.6	18.6	102.0	1040.9
515:41	424.5	17.7	103.5	1066.2
605:35	429.2	16.2	105.1	1080.9
776:03	440.4	14.2	111.7	1205.6
1057:15	456.7	11.7	116.9	1234.8
1329:16	466.1	12.9	122.4	1329.4

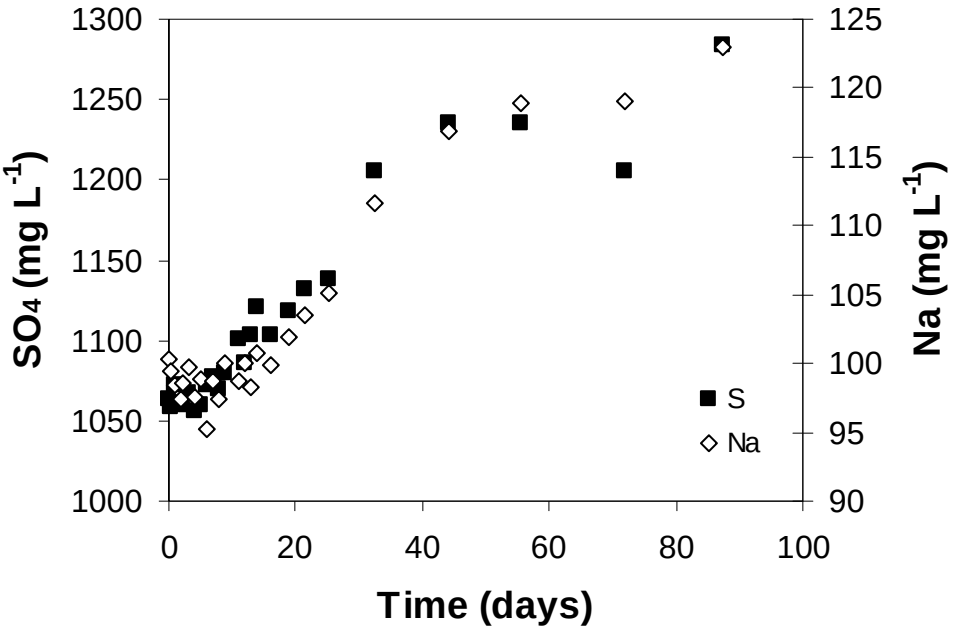

Figure A5.1 – Evaporative trends of conservative species

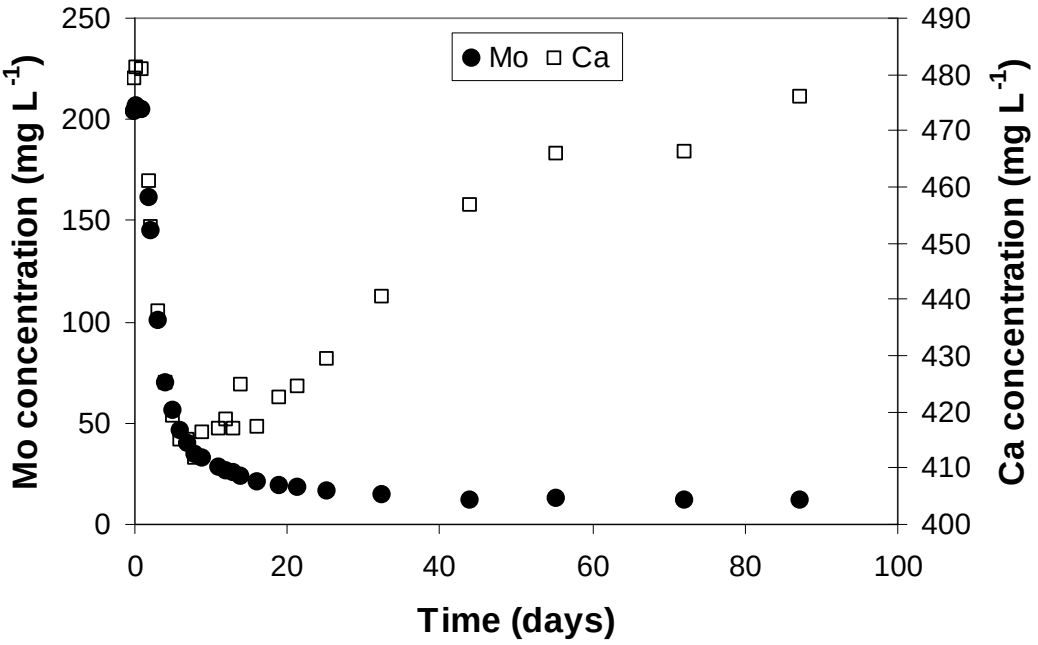

Figure A5.2 – Trends of non-conservative species

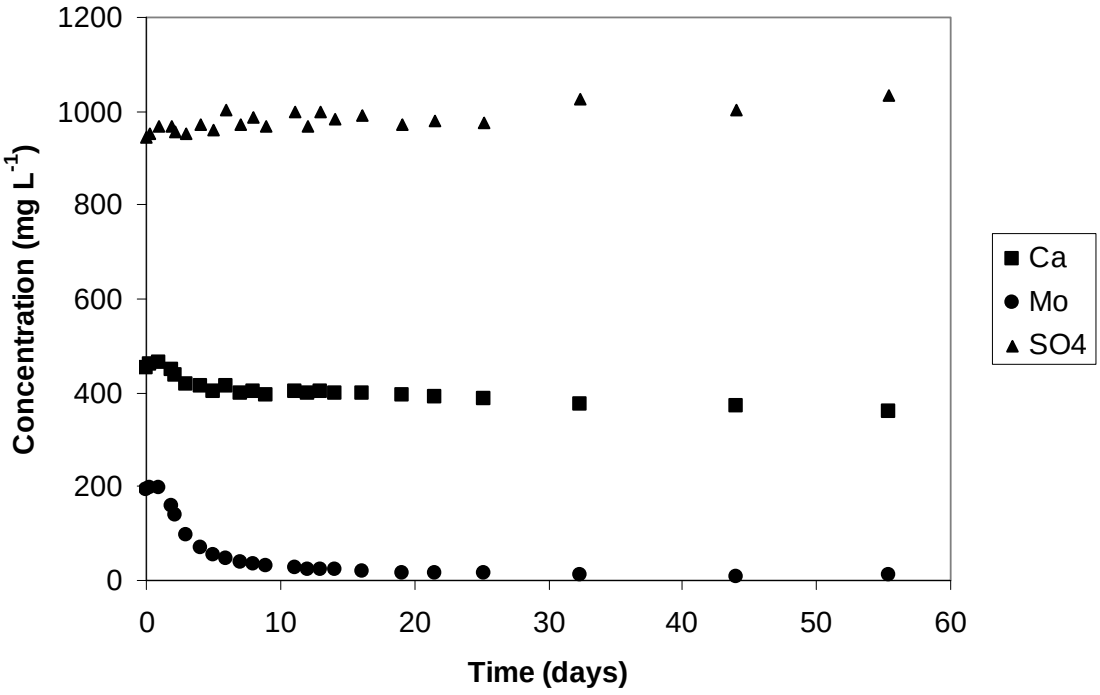

Figure A5.3 – Ca, Mo, and SO_4 Data normalized to Na concentrations

Appendix 6 – PHREEQC Analyses

The modelling code PHREEQC (Parkhurst and Appelo, 1999) was used to perform many geochemical analyses during the extent of this research. It was initially used to predict the outcome of the batch and column experiments. It was subsequently used to determine saturation indices of solid phase material in the experiments using multiple methods.

The database used was an edited version of the wateq4f. This database did not include Mo species, so they were added separately. The prominent reactions of species added are present in Table A6.1.

Table A6.1 – Molybdenum reactions added to the PHREEQC database

Aqueous Reactions	**log *K***	**Reference**
$MoO_4^{-2} + H_+ = HMoO_4^-$	4.24	Smith and Martell (1976)
$MoO_4^{-2} + 2H^+ = H_2MoO_4$	6.85	Kaback and Runnells (1980)
$3H^+ + MoO_4^{-2} = MoO_2OH^+ + H_2O$	7.89	Kaback and Runnells (1980)
$4H^+ + MoO_4^{-2} = MoO_2^{+2} + 2H_2O$	8.34	Kaback and Runnells (1980)
$MoO_4^{-2} + e^- + 4H^+ = MoO_2^+ + 2H_2O$	20.95	Kaback and Runnells (1980)
$MoO_4^{-2} + 3e^- + 8H^+ = Mo^{+3} + 4H_2O$	29.52	Kaback and Runnells (1980)
$Ca^{+2} + MoO_4^{-2} = CaMoO_4$	2.57	Essington (1990)
$Na^+ + MoO_4^{-2} = NaMoO_4^-$	1.66	Essington (1990)
Powellite Precipitation Reaction		
$Ca^{+2} + MoO_4^{-2} = CaMoO_4$	8.05	Essington (1990)

A6.1 Batch Experiment Simulations

The batches were simulated as realistically as possible to the experiments performed. All species were added as the phase of the initial material using Equilibrium Phases. The only exception was sulfate, which was added as sulphuric acid using the Reaction keyword. This was initially conducted in order to simulate the titration experiment and to allow for a comparison of results with different SO_4 concentrations. A typical simulation is as follows:

```
SOLUTION 1
    temp      24
    pH        7 charge
    pe        4
    redox     pe
    units     mg/l
    density   1
    -water    1 # kg
EQUILIBRIUM_PHASES 1
    Calcite   0 0.299739526
    CO2(g)    -3.5 10
    Na2MoO4:2H2O 0 0.002084636
    O2(g)     -0.6778 10
    CaMoO4     0 0
    Gypsum     0 0

SAVE Solution 1

REACTION 1
    H2SO4      1
    0.020819757 moles in 50 steps
# 0.2084 moles is the 21.84mL of 5M I added
```

As seen, atmospheric oxygen and carbon dioxide concentrations are entered, as the batch systems were all exposed to atmosphere. The pH of the system was initially set to DI water and was allowed to change to reach equilibrium. This was conducted for all batch experiments in order to predict the likely outcome of the experiments. It of course does not take kinetic limitations into affect though, which were observed in the batches.

A6.2 Competition Column

PHREEQC was used to set up the column experiment by determining whether species would remain dissolved in the influent solutions. It was also used to predict the equilibrium results. However, the simulation was set up identically to the batch experiment except under closed system conditions. Therefore the results of the simulation only describe what would occur with an endless column, instead of one with a 4 day residence time, which was the case with the experiment.

A6.3 Saturation Indices

The data obtained from the batch and column experiments was input into PHREEQC to determine the saturation indices of potential solid phases. This was conducted in two ways for the batch systems due to the fact that alkalinity was only

obtained at the end of the experiment and therefore could not be applied to each sample taken. The method in obtaining saturation indices for all samples was to say that there was an excess of C^{4+} in solution and let the solution equilibrate in respect to it. Since the batches are open systems with atmospheric oxygen present, C^{4+} is present as $CO2_{(g)}$ and will equilibrate accordingly, similar to alkalinity. An example simulation is as follows:

```
        SOLUTION    1

        pe    11          # assumed
        units mg/L
        density     1
        Temp  20
        pH    7.8
#       Alkalinity  0
        S(6)  1063.84           as SO4
        Ca    479.124
        Cu    0
        C(4)  10 charge
        Li    0
        Mo    203.6245
        Na    100.262
        Pb    0
        Zn    0
        -water      1 #   kg
        EQUILIBRIUM PHASES      1
        O2(g) -0.68     10.0
        # CO2(g)    -3.5     10.0
```

With this method, saturation indices can be obtained for all samples of every batch experiment. The saturation indices were still obtained for the final sample of every batch where alkalinity was also measured, and compared. All major phases not containing carbonate showed negligible change between the two methods. Calcite and pCO_2 were the only species that differed depending on the method. Results are available in Table A6.2.

Table A6.2 – Calcite and pCO2 saturation indices using different modelling methods

	Calcite SI		***pCO_2 SI***	
Batch Experiment	*C^{4+} method*	*Alkalinity*	*C^{4+} method*	*Alkalinity*
Pow 7	0.7	0.3	-2.8	-3.2
Competition	1.1	0.3	-2.6	-3.3
Ca and Mo	-0.0	-3.3	0.4	-3.0
Pb and Mo	-0.1	No alkalinity	-4.1	No alkalinity
Pb, Mo, CaCO3	-0.0	0.3	-3.4	-3.1

The two methods used provide relatively similar results for most of the experiments. Saturation indices of the two methods both predict that phases are either supersaturated or undersaturated for all batches except for Ca and Mo. The pCO_2 using alkalinity values indicate open system conditions whereas the C^{4+} method indicates an excess of CO_2. Due to this large amount of predicted CO_2, calcite is near saturation. This ultimately is not the case, indicating that using the alkalinity value is much more practical. However, the fact that all other tests show similar results indicates that the saturation trends found using the C^{4+} method for all samples of each batch experiment are realistic.

It is interesting to note that the saturation indices of calcite and pCO_2 are almost identical for batch systems containing calcite. Three of the systems were stirred but the competition batch was not, indicating that the energy level of the system does not greatly affect its degassing ability.

Appendix 7 – ICP-OES Analyses

A7.1 Methodology

An inductively coupled plasma optical emission spectrometer (ICP-OES) was used to analyze the chemistry of most of the samples obtained. Although an ICP-OES can handle very high concentrations, dilutions were still applied for most of the samples due to the fact that the standards available were not concentrated enough. All samples were therefore diluted to between 0 and 24 ppm for all elements except for SO_4, which fell in a range between 0 and 150 ppm. This required anywhere from a 2 to 35 times dilution for the samples.

Samples were diluted using a mass balance rather than by volume, as mass is a more precise method with the equipment available. An Eppendorf Repeater Plus pipette was used to add DI water to the ICP test tubes, after the tubes were tarred (Figure A7.1). The mass of DI water was recorded and then sample was added to the test tube using an Eppendorf 100-1000 μL pipette. The final mass was recorded and the dilution factor was calculated as the total mass divided by the sample mass. Between 5 and 10 μL nitric acid was then added in order to create a 1% nitric matrix. Each test tube was then covered with a small piece of Parafilm and vortexed for approximately 10 seconds to ensure a thorough mix. Samples were stored at 4^oC until the day of analysis to prevent evaporation, which was typically 24 hours later.

Blanks, duplicates, and standards were mixed with the analyses to ensure the validity of the results. Typically, one blank, one duplicate, and one standard were analyzed for every 10 samples.

A 0, 1, and 24 ppm standard was made for the ICP-OES. The 24 ppm standard was created by adding 6 mL of 100 ppm multi-element standard and 25 uL concentrated nitric acid to 25 mL of DI water in a volumetric flask. The 1 ppm standard was created in the same fashion, and the blank only contained the nitric acid since this was the set matrix for all standards and samples. After everything was prepared, the Varian ICP-OES was used to analyze the samples (Figure A7.2). The internal standards were re-analyzed every 20-30 samples in order to account for drift and small variations within the machine.

After receiving the data (Figure A7.3), wavelengths were compared and averaged to produce the final results. This took some practice to determine which wavelengths produced the best results. It was ensured that the same wavelengths were used for all samples between each runs. Duplicates, standards, and blanks were analyzed to ensure that the machine was running properly. There were very few instances when results were erroneous.

A7.2 Example Analysis

An example analysis is now discussed. The sample procedure was first created and included both blanks and duplicates. Blanks were sometimes strictly DI water whereas other times they were procedural blanks, so they followed the same filtration procedure as the other samples. All other samples required dilution in order to fall within the standards. Example calculations of dilution factors are seen below.

	DI water (g)	Total mass (g)	Sample mass (g)	Dilution Factor
blank 1				1
blank 2				1
Zn2-1	5.9592	6.2058	0.2466	25.16545012
Zn2-1 dup	6.02	6.2666	0.2466	25.41200324
Zn3-1	5.4914	6.0874	0.596	10.21375839
Zn3-2	5.4744	6.0694	0.595	10.20067227
Zn3-2 dup	5.4879	6.0795	0.5916	10.27636917

Once the samples were ready, the standards were prepared. A multi-element standard (MES) was used, as it included most of the species present in the samples. Its composition was as follows:

MES	**ppm**
Ca	100.3
Cu	100.3
Fe	99.9
Mo	100.5
Na	99.3
Pb	100.5
Zn	100.6

Three standard solutions were produced for the analysis: a 24, 1, and 0 ppm standard. Sulfate is not included in the MES, so it required separate addition, and was added as 150, 20, and 0 ppm concentrations since SO_4 was much more concentrated in the samples than the other species. The standards were created in 25 mL volumetric flasks as follows:

24 ppm, 150 ppm SO4	**1 ppm, 20 ppm SO4**	**Blank**
in 25 mL:	in 25 mL:	in 25 mL:
6 mL MES	0.25 mL MES	25 uL nitric acid
7.81 uL 5M sulfuric	1.04 uL 5M sulfuric	
25uL nitric acid	25 uL nitric acid	

0.5-10, 10-100, and 100-1000 μL pipettes were used for the addition of standards. At this point, samples and standards are ready to be analyzed. Multiple wavelengths are used to analyze each species and then compared and typically averaged to produce the final concentrations. For this example, the molybdenum wavelengths will be analyzed:

	Mo 202.032	**Mo 203.846**	**Mo 204.598**	**Mo 281.615**
blank 1	-0.000518 uv	-0.000276 uv	-0.007349 uv	0.001139
blank 2	-0.003879 uv	-0.008937 uv	-0.006248 uv	0.003039
Zn2-1	212.814	211.396	210.985	210.914
Zn2-1 dup	209.6	209.384	209.214	207.971
Zn3-1	205.996	205.74	204.914	205.702
Zn3-2	216.682	216.34	216.331	215.3
Zn3-2 dup	218.409	218.442	217.84	218.715

As seen above, the blanks produce values below detection limit, as expected. As well, each wavelength of Mo produces almost identical results, indicating that each wavelength is worth using in the final concentration value. They will therefore all be averaged to produce the final value. This is not always this straightforward though. An example is with the wavelengths for sulphur:

	S 181.972	**S 182.562**	**S 189.965**
blank 1	-1.01647 uv	2.03667	uncal
blank 2	-1.02839 uv	1.76526	uncal
Zn2-1	990.029	580.281	uncal
Zn2-1 dup	991.77	585.963	uncal
Zn3-1	126.472	uncal	uncal
Zn3-2	134.458	uncal	uncal
Zn3-2 dup	141.575	uncal	uncal

There is a great amount of variability with the wavelengths. The 'uncal' indicates that the computer program was unable to calibrate the wavelength while staying within the maximum error allowed, ultimately deeming it useless. There is even a large difference between the two wavelengths that produce results, with the 181.972 wavelength producing SO_4 concentrations almost twice that of the 182.562 wavelength for Zn2-1 and other samples with high concentrations. When this is the case, it is good to understand your sample so that you can determine what the true concentration is. Fortunately, it is known that the Zn2 samples contained 1000 ppm SO_4 and that the Zn3 samples contained approximately 150 ppm SO_4, meaning that the 181.972 wavelength is the most correct.

The duplicates of Zn2-1 and Zn3-2 are both relatively close, although Zn3-2 shows a difference of 2 ppm for Mo and 7 ppm for SO_4. This is acceptable due to the fact that both concentrations are high, calculating to a percent error of less than 1%. If this variability was found in a sample that had very low concentrations, then the percent error would be far greater, meaning the samples would have to be analyzed again.

The above procedure is performed for each species analyzed. Once the high-quality wavelengths have been determined, they are averaged to produce the final concentrations of the sample.

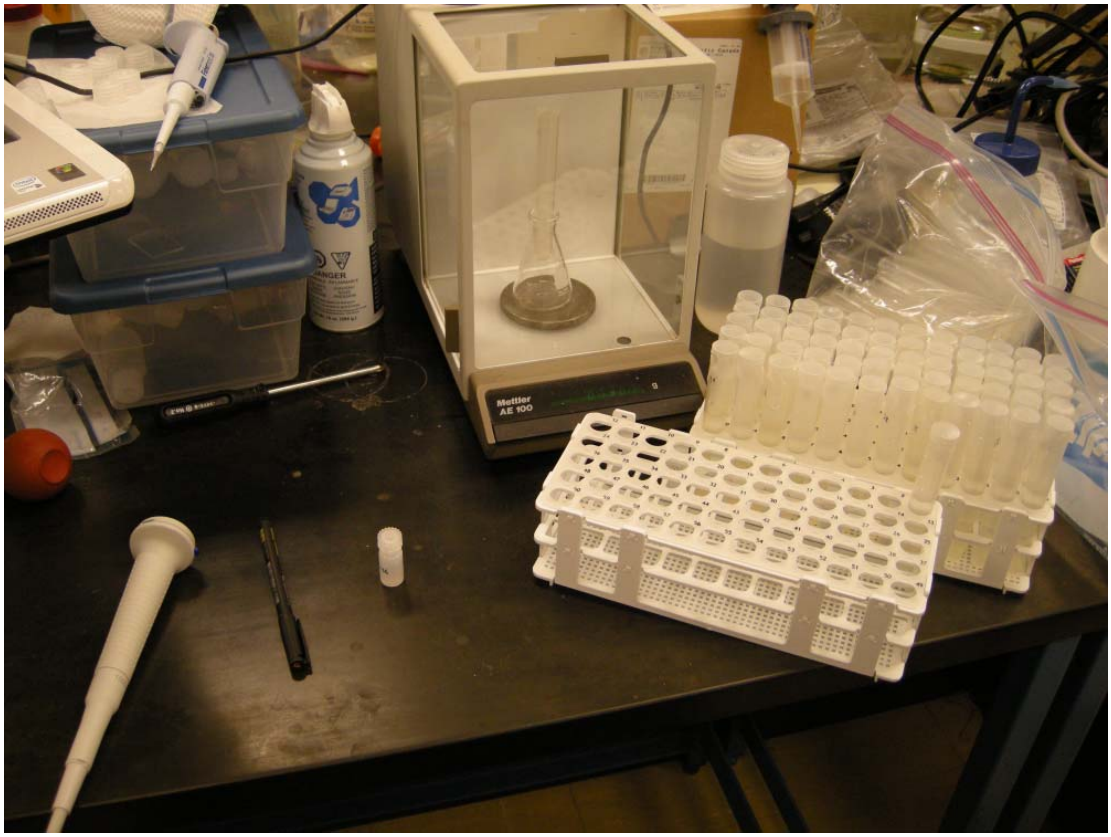

Figure A7.1 – Preparing samples for ICP. Samples were diluted using the mass balance and acidified to 1% nitric using the volumetric pipette

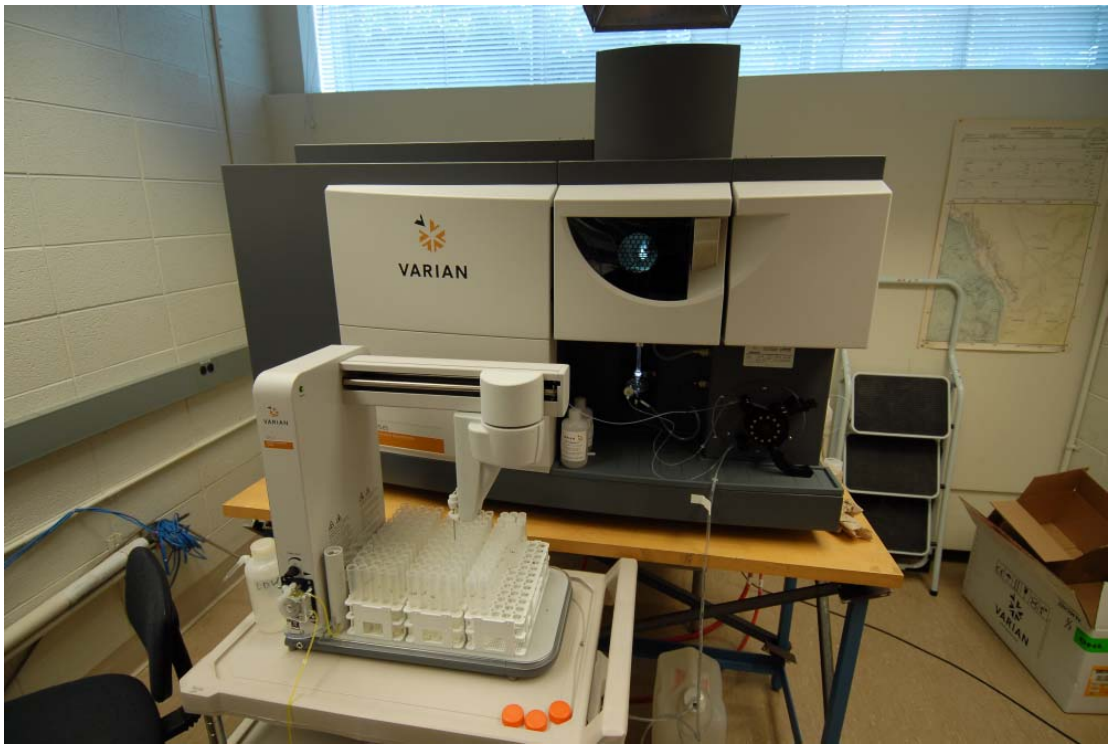

Figure A7.2 – Varian ICP-OES with autosampler

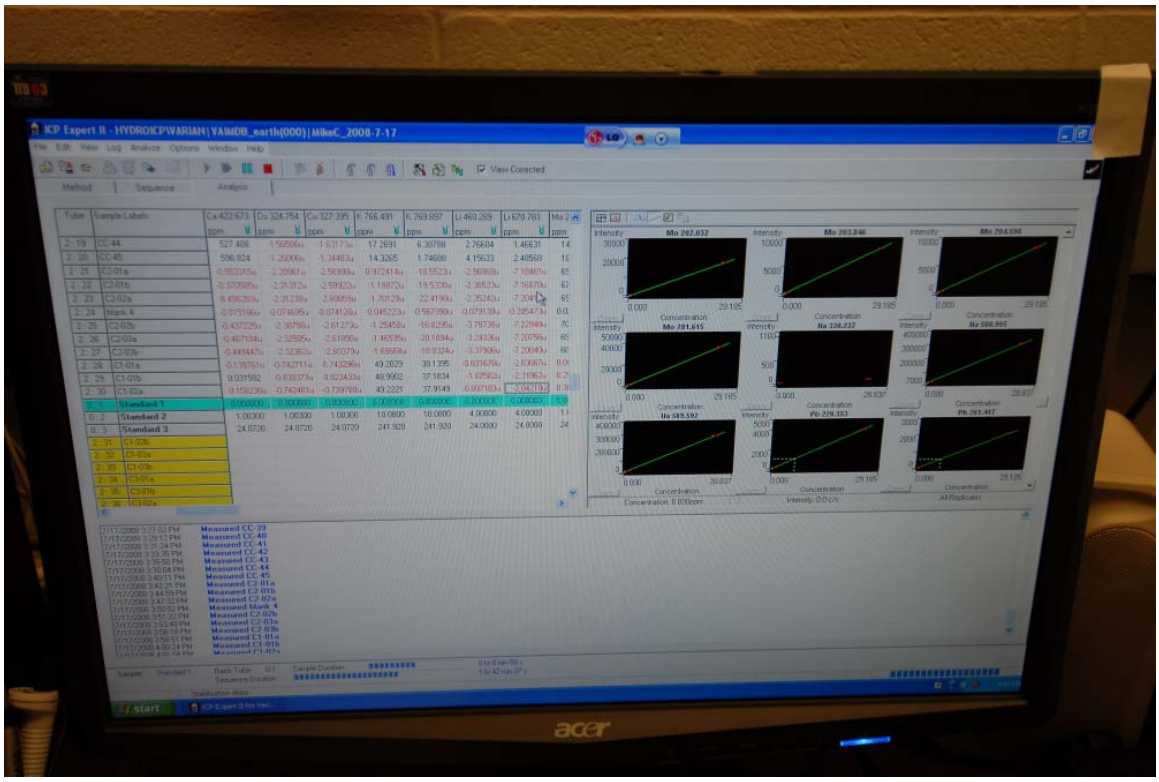

Figure A7.3 – Sample display screen of ICP-OES results

Appendix 8 – XRD and SEM Analyses

A8.1 XRD

X-Ray Diffraction was used to analyze the precipitates at the end of batch and column experiments. The samples were ground into a fine powder and smeared with ethanol onto a glass slide for the majority of the samples. Samples with little material were smeared onto a zero-diffraction quartz plate. Data was collected using step-scan X-ray powder-diffraction over a range of 3-80°2θ with CoKα radiation on a standard Siemens (Bruker) D5000 Bragg-Brentano diffractometer equipped with an Fe monochromator foil, 0.6 mm (0.3°) divergence slit, incident- and diffracted-beam Soller slits and a Vantec-1 strip detector. The long fine-focus Co X-ray tube was operated at 35 kV and 40 mA, using a take-off angle of 6°.

International Centre for Diffraction Database PDF-4 and Search-Match software by Bruker was used to analyze the data. An example of the data is seen in Figure A8.1. All of the results are present in Tables A8.1 and A8.2.

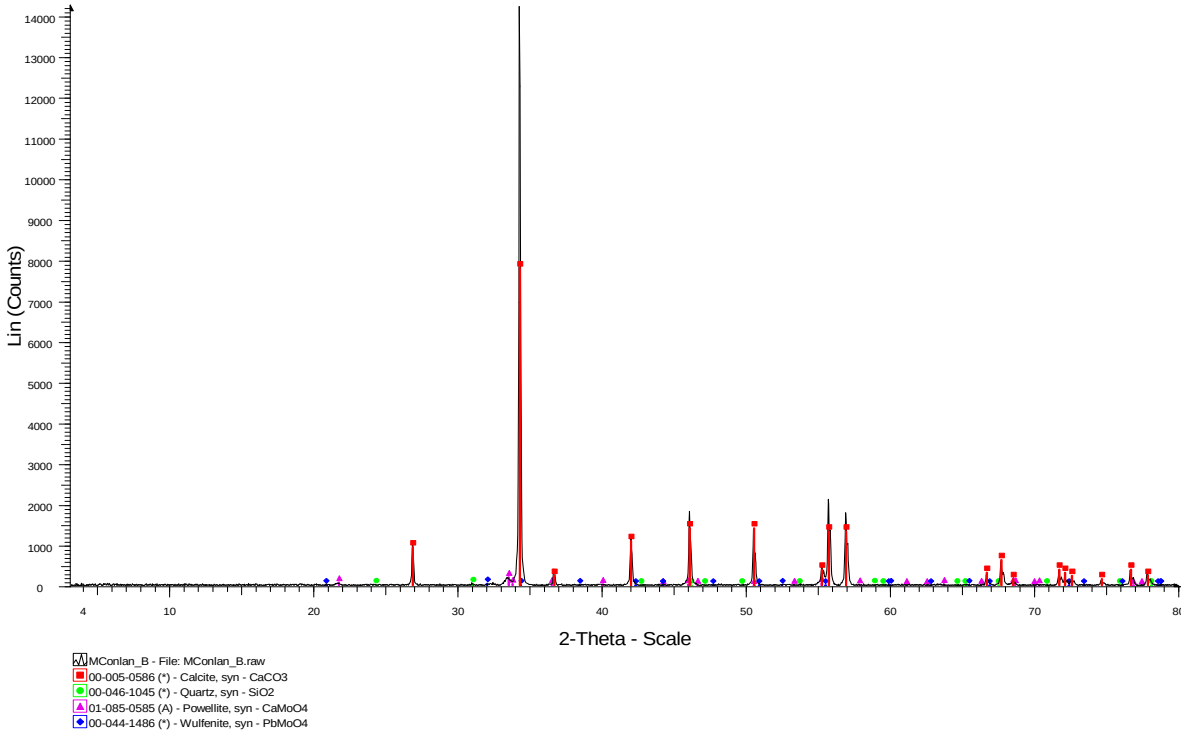

Figure A8.1 – XRD Results for batch test Pb, Mo, $CaCO_3$

Table A8.1 – Column precipitate results

	0a	*0b*	*1*	*2*	*2a*	*3*	*3a*	*3b*	*4*	*Column 1 fine*	*Column 2 fine*
Calcite	X	X	X	X	X	X	X	X	X	X	X
Wulfenite	X	X									
Powellite		X	X	X	X	X	X	X	X		X
Quartz	X	X	X	X	X	X	X	X	X	X	X
Gypsum			X							X	X
Talc	X	X	X	X	X	X	X	X	X	X	X
Montmorillonite	X	X	X	X	X	X	X	X	X	X	
Malachite		X									
Anglesite	X										
Cerussite	X										

Table A8.2 – Batch precipitate results

	Cu1	*Zn1*	*Pb1*	*pow 5*	*CT-1*	*pow 6a*	*pow 6b*	*B*	*D*
Calcite	X	X	X	X	X	X	X	X	
Wulfenite								X	
Powellite	X	X	X	X	X	X	X	X	X
Quartz	X	X	X	X	X			X	
Gypsum				X	X	X			
Talc					X				
Montmorillonite					X				
Malachite									
Anglesite									
Cerussite									
Devilline					X				

A8.2 SEM

A Philips XL-30 scanning electron microscope was used to try to determine the phases that were undetectable using the XRD, due to detection limits. Crystals of unknown precipitate were analyzed using elemental scans. Unfortunately, the SEM detected every element within the batch solution so specific phases could not be determined. For example, the marble sand grains were analyzed from the competition column (Figure A8.2). As seen, the white precipitates show that they contain Mo, Pb, and S, so it is therefore difficult to predict whether it is a lead molybdate or a lead sulfate.

Another example shows malachite well though, with both Cu and O being found within the white spherical precipitates (Figure A8.3).

The images provided interesting information of where the phases precipitate. Figure A8.4 shows spherical malachite on the rough surfaces of the crushed marble sand. Malachite is also present in Figure A8.5 along with smaller powellite. It is interesting to note that there is no precipitation on the cleavage face of the grain, indicating that the medium plays an important role in nucleation and subsequently mineral formation. Figure A8.6 shows powellite covering a marble sand grain. With time, powellite may protect this grain and prevent calcite dissolution. Powellite is also found in Figure A8.7 on fine-grained calcite powder.

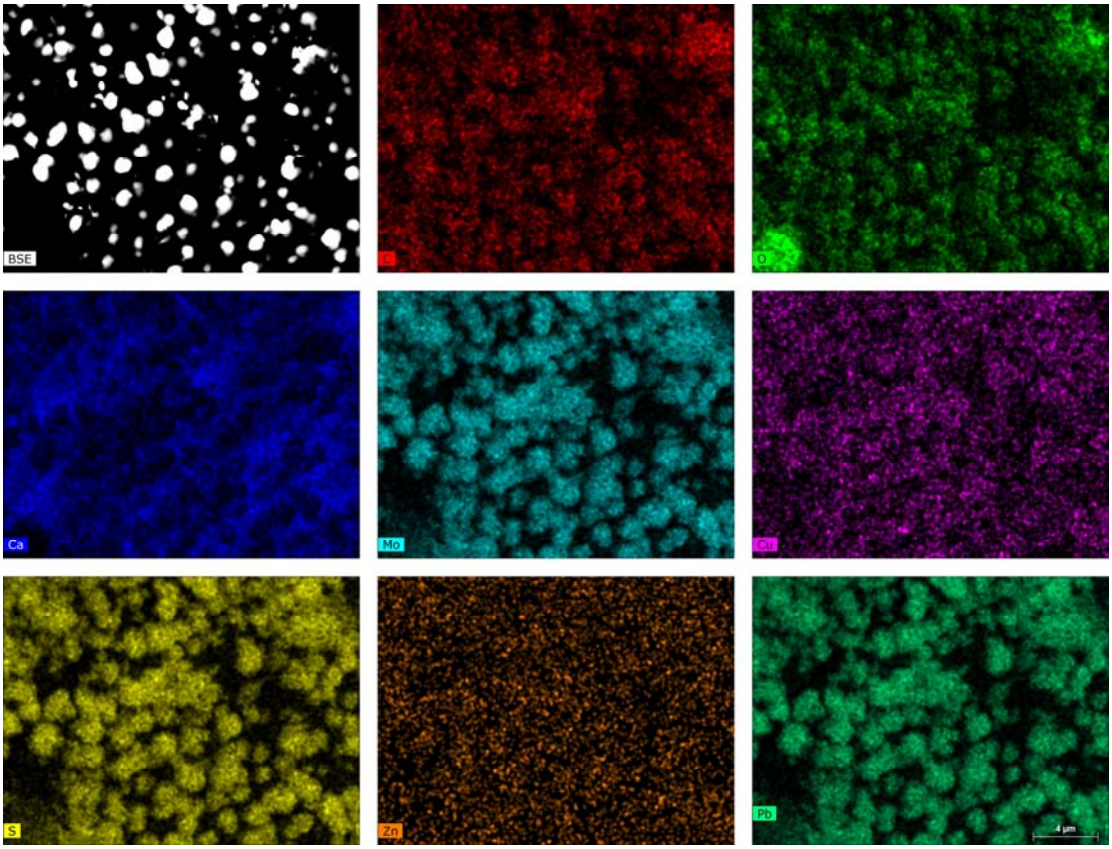

Figure A8.2 – Element scan on marble sand grains from the competition column

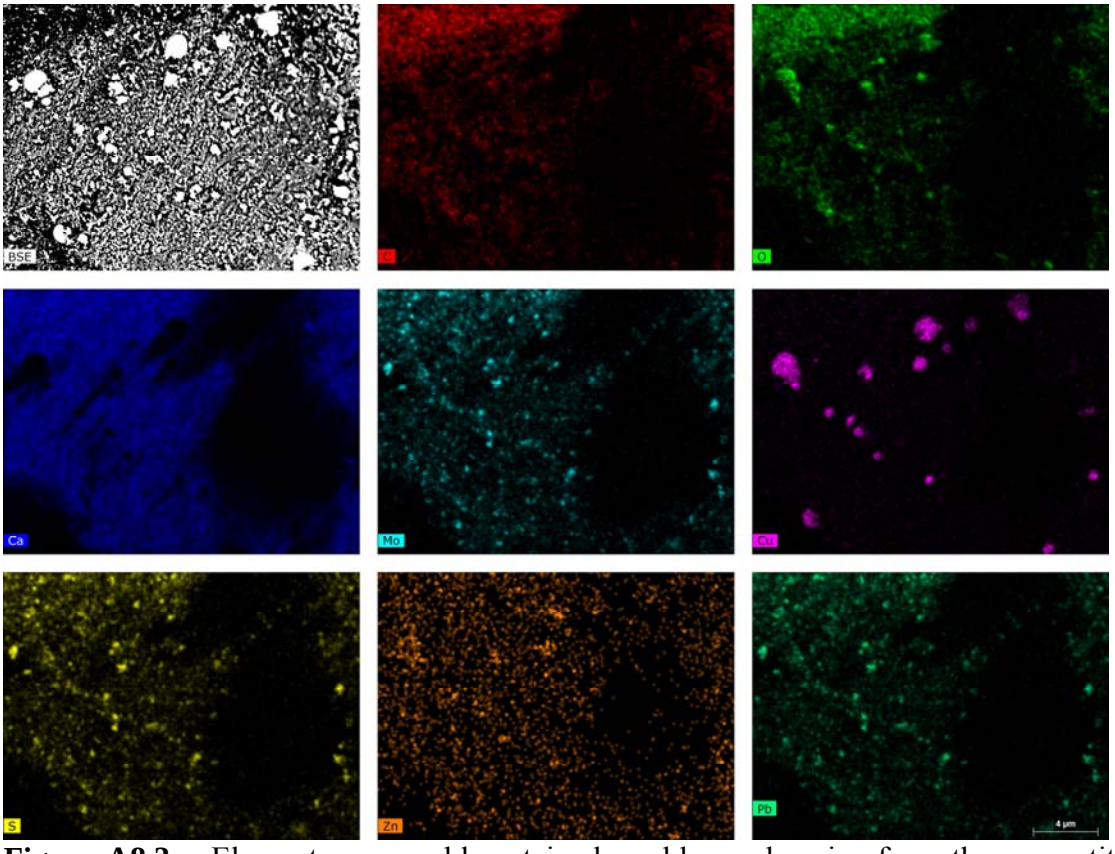

Figure A8.3 – Element scan on blue-stained marble sand grains from the competition column

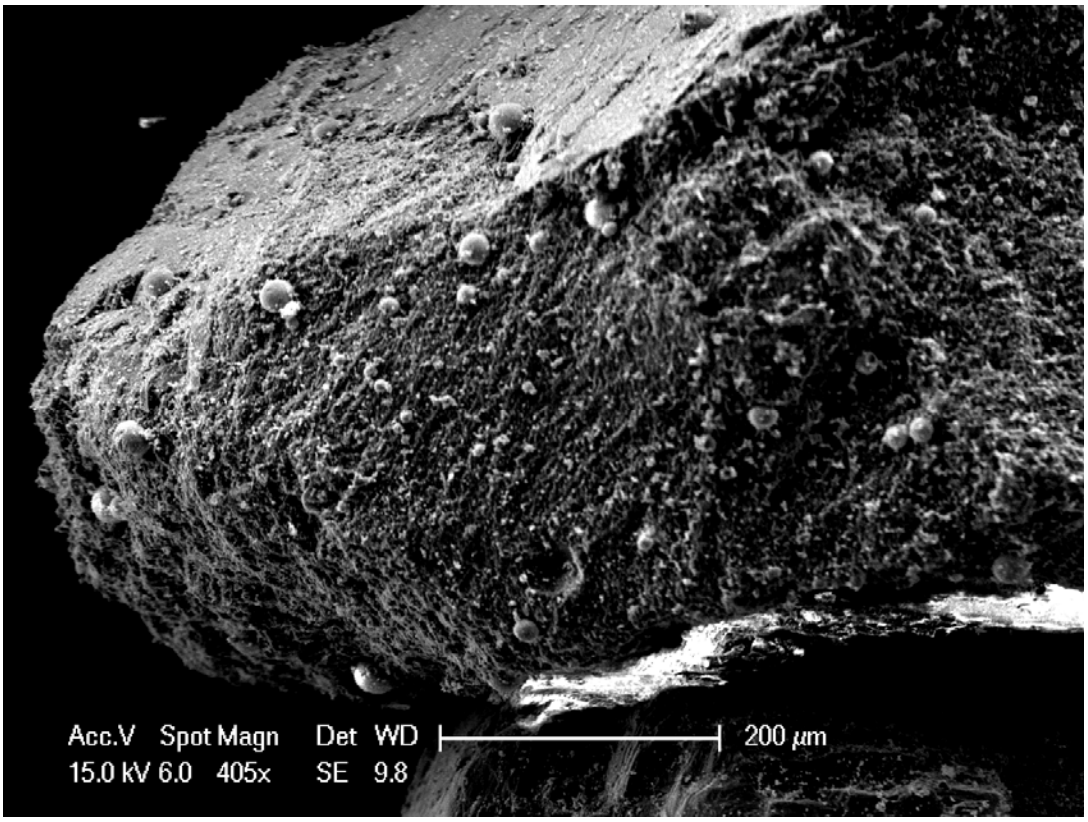

Figure A8.4 – Spherical malachite precipitate on a marble sand grain

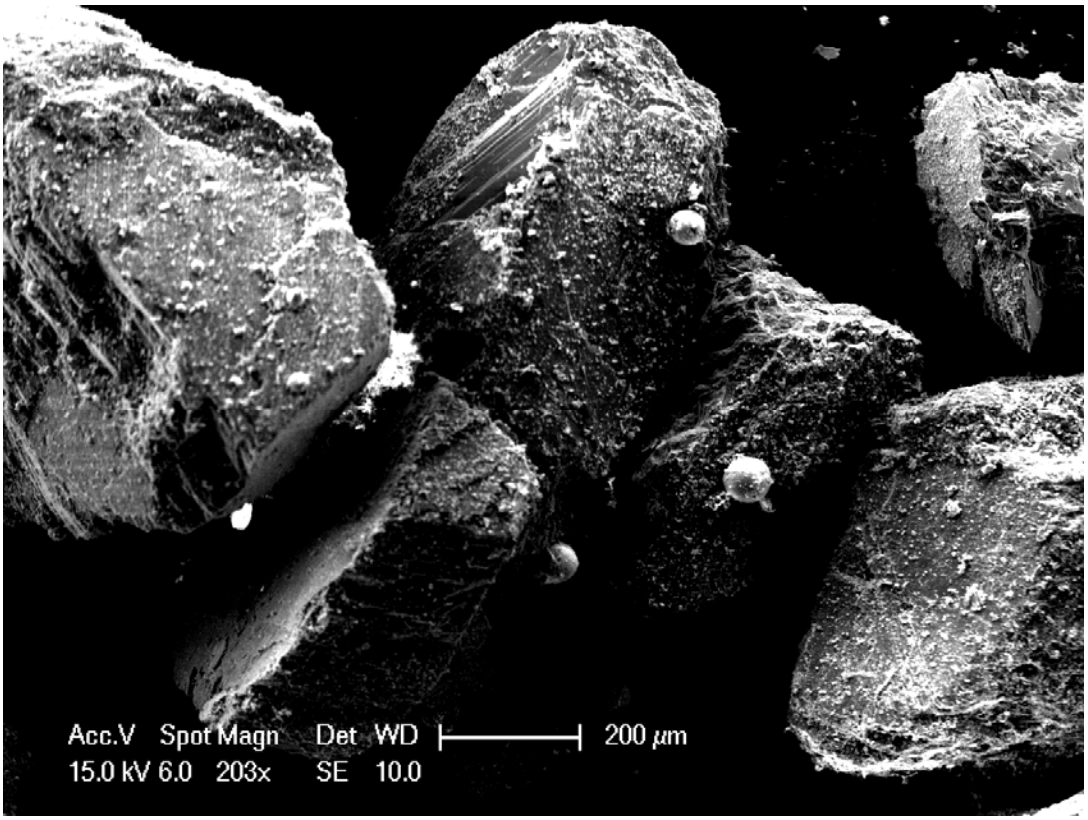

Figure A8.5 – Spherical malachite (large) and powellite on marble sand grains

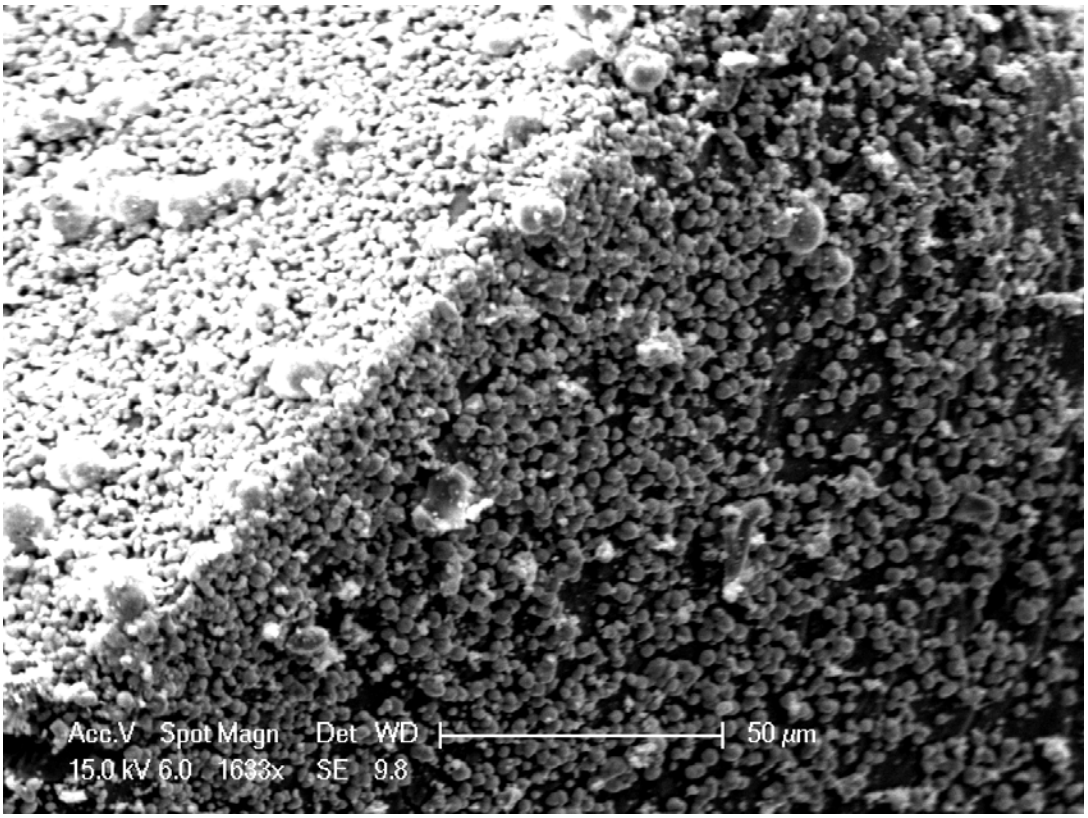

Figure A8.6 – Powellite on marble sand grain

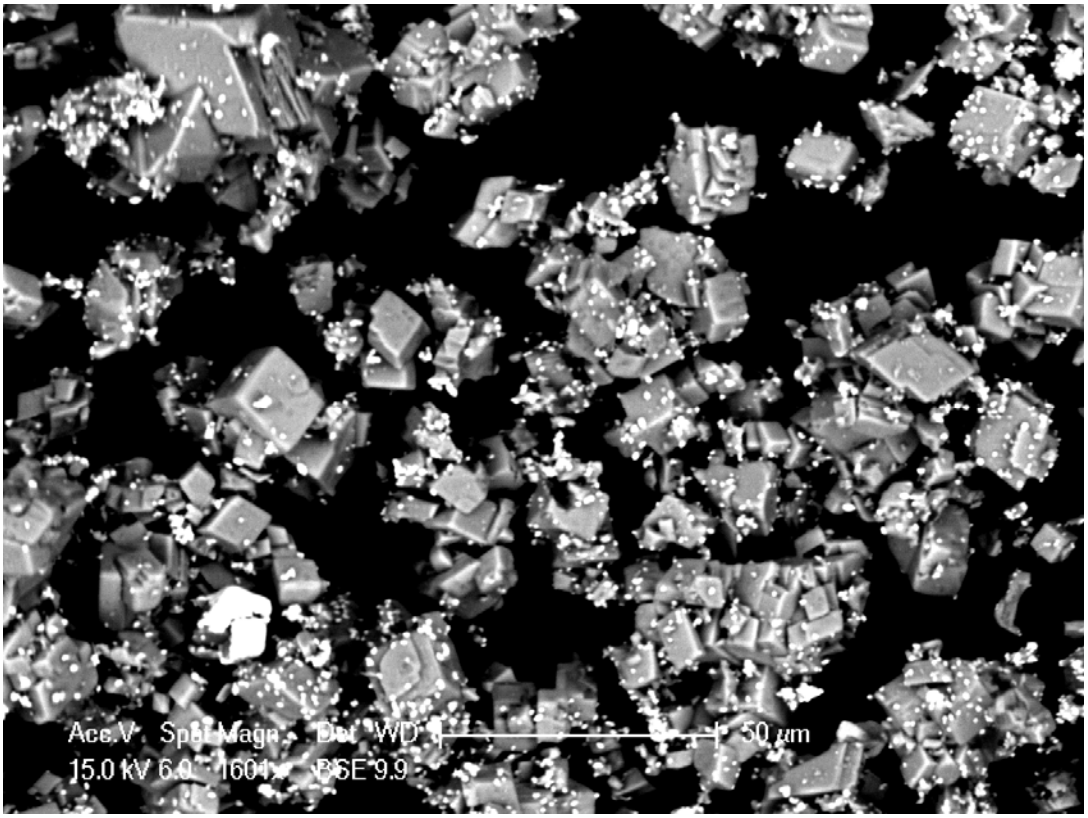

Figure A8.7 – Powellite (white) on fine-grained calcite powder

Appendix 9 – Chemical Inventory

Chemical Name	Chemical Formula	Gram Formula Weight (g/mol)	Provider	Catalog Number
Sodium molybdate dihydrate, minimum 99.5%	$Na_2MoO_4 \cdot 2H_2O$	241.95	Sigma-Aldrich	M1003-500G
Calcium carbonate, powder 99+%, A.C.S. reagent	$CaCO_3$	100.09	Sigma-Aldrich	239216-100G
Copper(II) sulfate pentahydrate, ReagentPlus, ~99%	$CuSO_4 \cdot 5H_2O$	249.68	Sigma-Aldrich	C7631-250G
Zinc sulfate heptahydrate, 99%, A.C.S. reagent	$ZnSO_4 \cdot 7H_2O$	287.54	Sigma-Aldrich	221376-100G
Lead(II) Nitrate ACS reagent, >99%	$Pb(NO_3)_2$	331.2	Sigma-Aldrich	228621-100G
Sodium citrate	$C_6H_5Na_3O_7 \cdot 2H_2O$	294.10	Sigma-Aldrich	S1804-500G
Sodium bicarbonate	$NaHCO_3$	84.007	Sigma-Aldrich	S6014-500G
L-Ascorbic Acid	$C_6H_8O_6$	176.12	Fluka	95210-250G
Environmental Grade Nitric Acid	HNO_3	63.012	Anachemia	62764-320
Sulfuric acid 5 mol/l volumetric solution	H_2SO_4	98.08	Riedel-deHaën	35347
Calcium Chloride Certified A.C.S. Dihydrate	$CaCl_2$	110.99	Fisher Scientific	C79-500
Sodium Hydroxide Certified A.C.S	NaOH	39.997	Fisher Scientific	S318-500
Potassium Chloride	KCl	74.55	Fisher Scientific	P217-500
Lithium Bromide	LiBr	86.845	Sigma-Aldrich	213225-500G

Appendix 10 – Photos of Laboratory Experimental Methods and Results

Figure A10.1 – The batch experiments consist of beakers covered with Parafilm and placed on magnetic stirring plates

Figure A10.2 – Acid baths used to clean equipment. 10% HCl followed by 5% nitric acid and then DI water

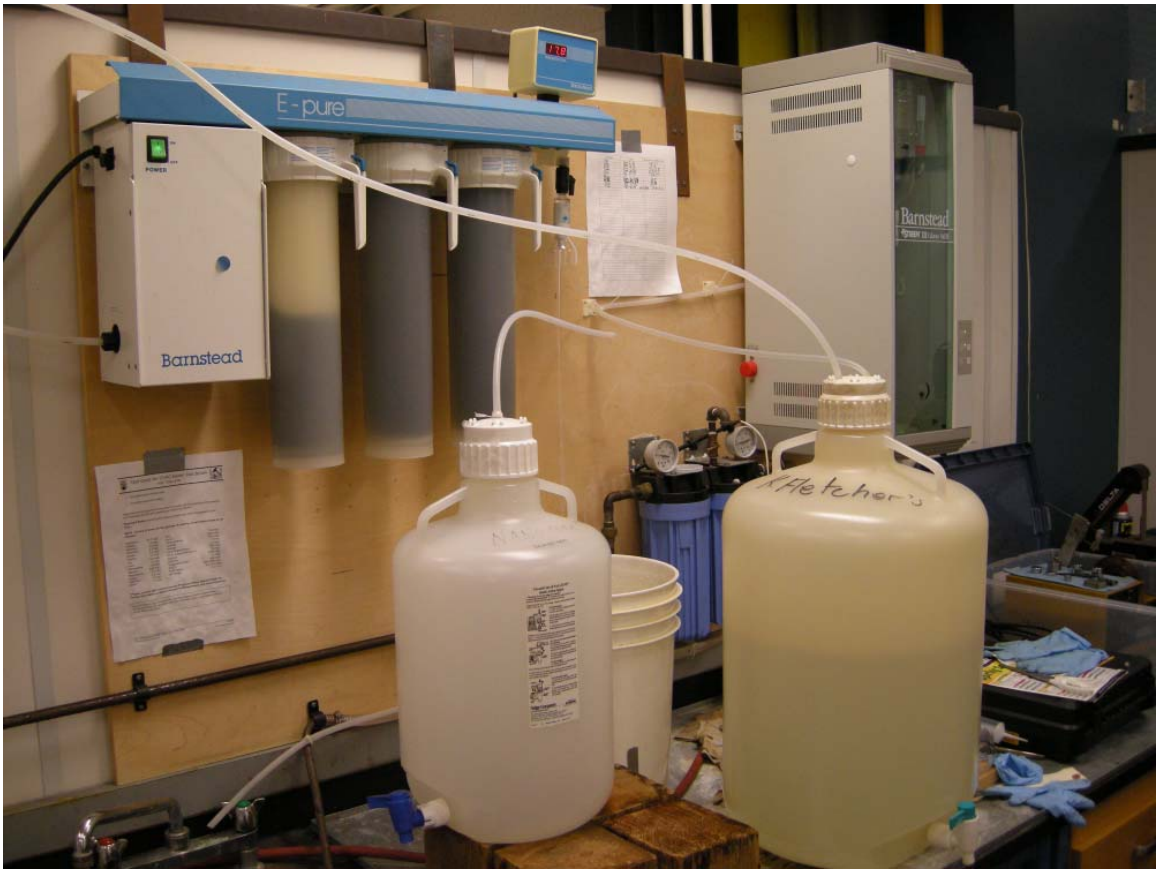

Figure A10.3 – Water purification systems. Distilled water (right) followed by DI water (left)

Figure A10.4 – Mass balance used to make standard solutions (left) and pH probe (right)

Figure A10.5 – Empty acrylic column

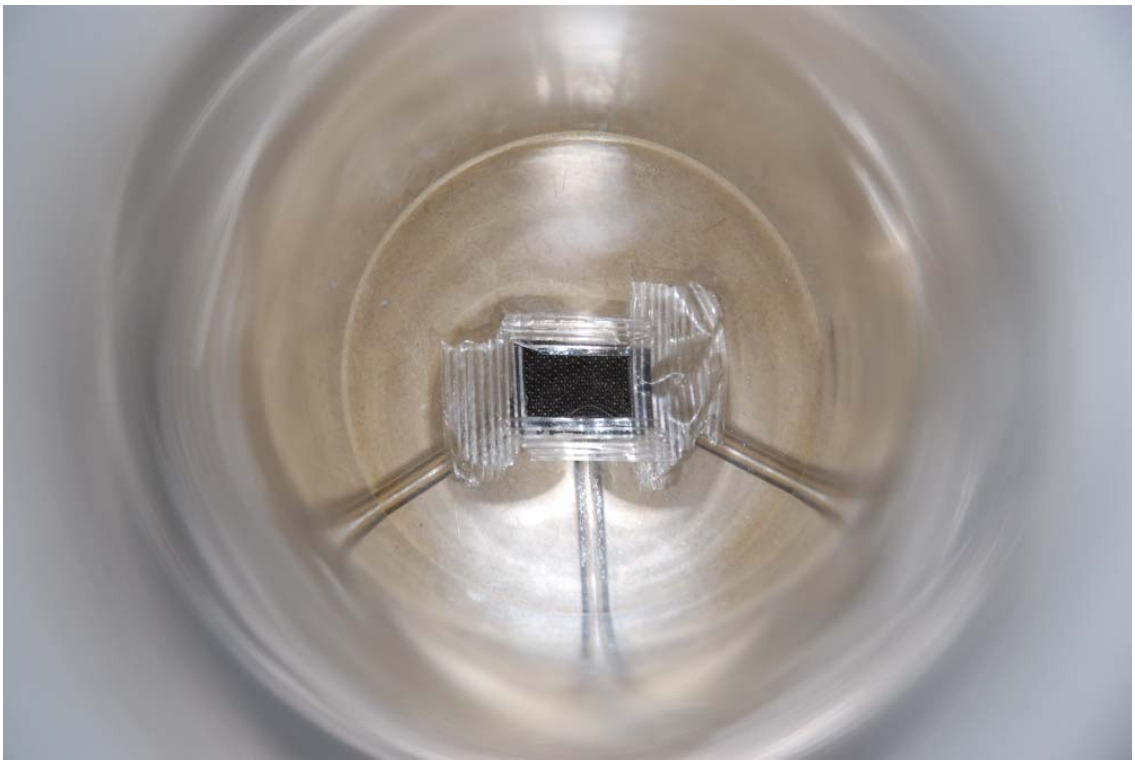

Figure A10.6 – Bottom of the column with the influent ports screened off to prevent clogging. A plastic mesh was used instead of wire due to the corrosive characteristics of the influent with the presence of sulphuric acid.

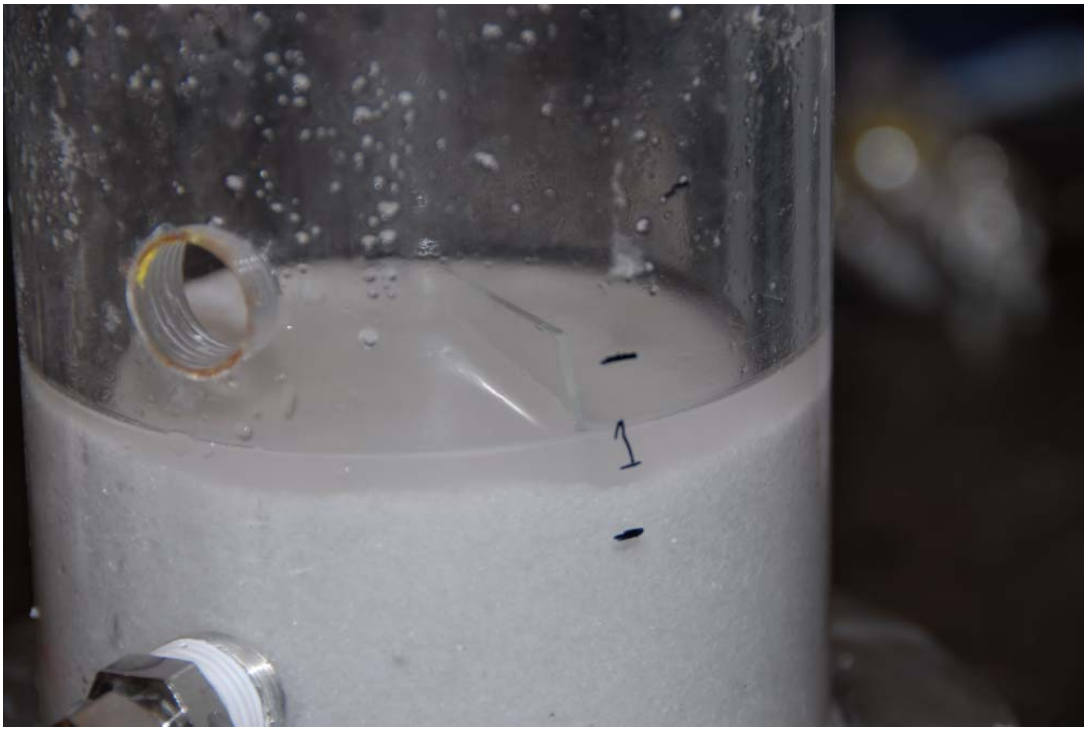

Figure A10.7 – One of the glass plates installed in the column, which proved to be useless as negligible crystals precipitated on it

Figure A10.8 – Packing method

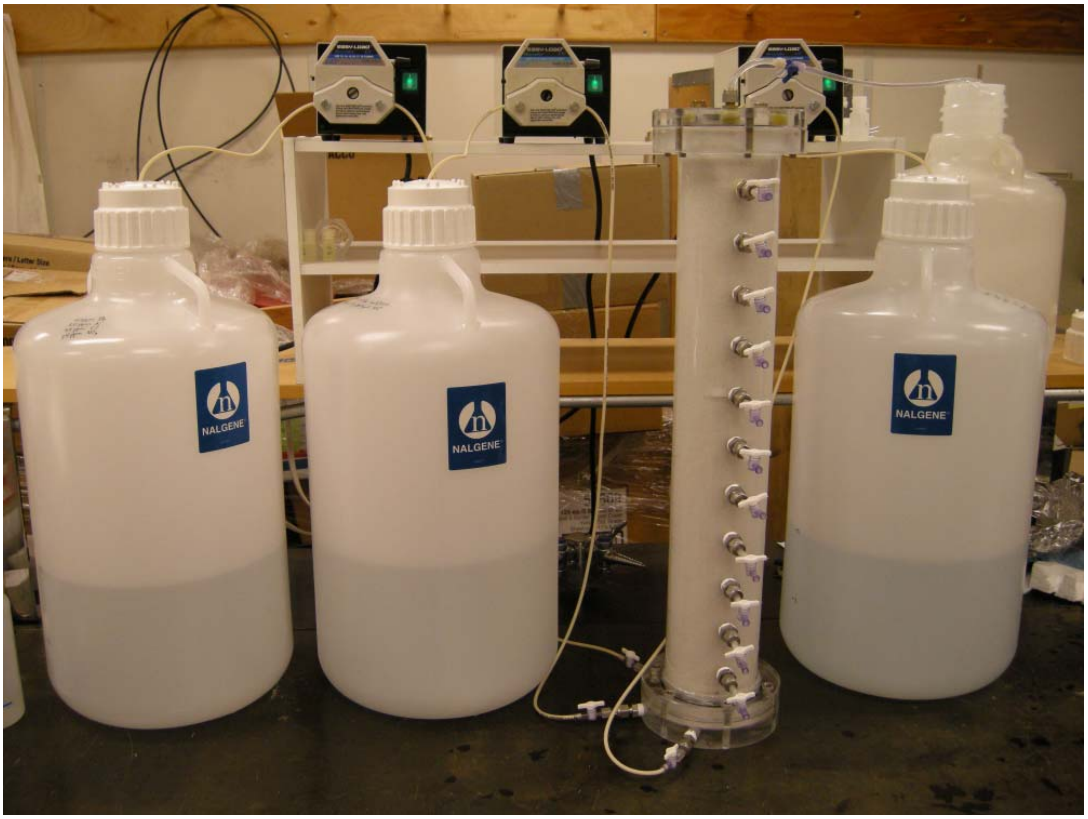

Figure A10.9 – The column set up with three separate carboys and peristaltic pumps

Figure A10.10 – Pipettes used to extract sample from the carboys to ensure the inflow solution remained constant

Figure A10.11 – Final setup of the column experiment with everything covered in aluminium foil to prevent bacterial growth

Figure A10.12 – Method of obtaining pH samples without oxygen ingress

Figure A10.13 – Sample collection method

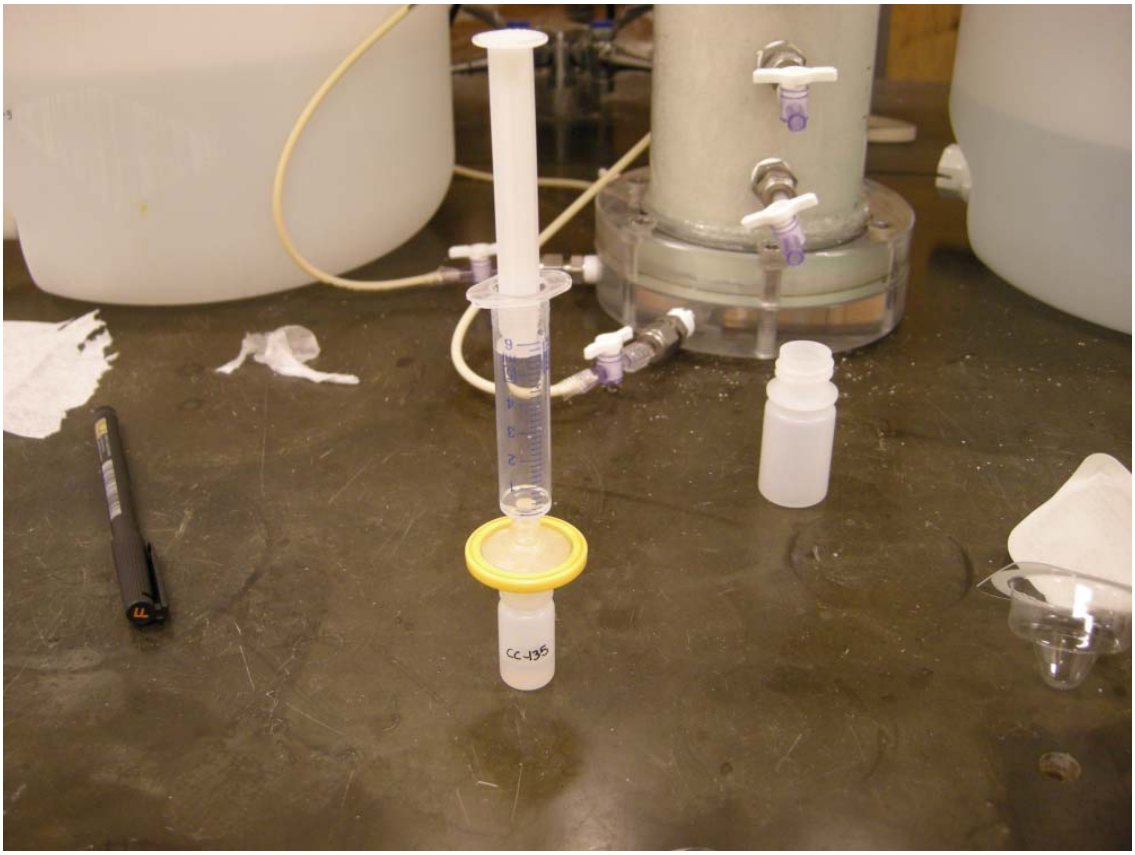

Figure A10.14 – Filtration of samples

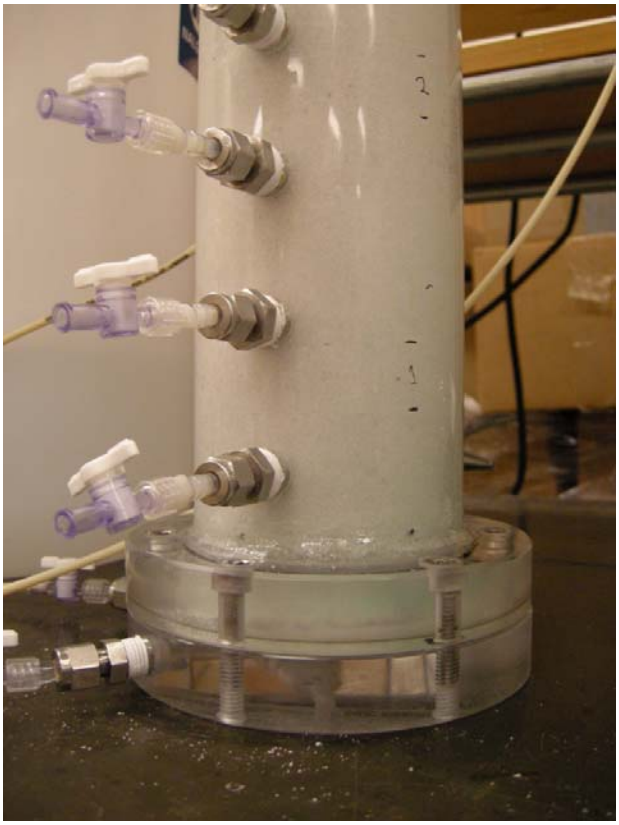

Figure A10.15 – Distinct green-blue copper precipitate near the bottom of the column

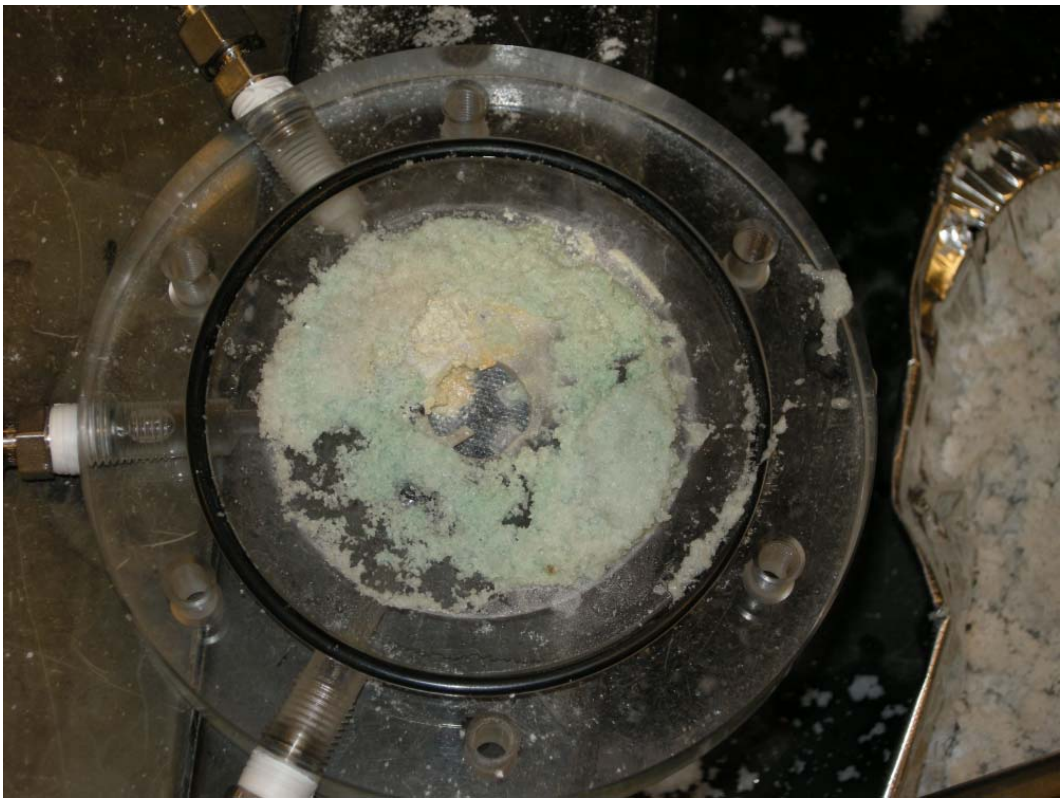

Figure A10.16 – Copper precipitate and yellowish wulfenite directly at the inflow mixing zone

Figure A10.17 – Column marble and precipitates

Figure A10.18 – Sieved precipitate for XRD analysis